Cape Peninsula University of Technology

Investigation of some scale-up conditions on the synthesis of faujasite zeolites from South African coal fly ash

By

James Philip Brassell

Dissertation submitted in fulfilment of the requirements of the degree

Master of Engineering: Chemical Engineering

In the FACULTY OF ENGINEERING

At the Cape Peninsula University of Technology

Supervisor: Prof. T.V. Ojumu

Co-Supervisor: Prof. L.F. Petrik

Cape Town Campus

2017

DECLARATION

I, James Philip Brassell, declare that the contents of this thesis represented my own unaided work, and that the thesis has not previously been submitted for academic examination towards any qualification. Furthermore, it represents my own opinions and not those of the Cape Peninsula University of Technology.

Signed: _____ **Date:** _____

ABSTRACT

Coal fly ash waste produced from the coal combustion process is becoming an ever increasing concern. It is produced in such abundance due to not only South Africa, but the whole of the world relying mainly on coal combustion for the main source of energy production. With the growing rate of the human population this energy production is ever increasing. The current methods of disposal of this fly ash is not sustainable, it is being dumped in ash dumps, and poses a risk to the surrounding environment and human population. Therefore, processes need to be developed to take this waste and turn it into useful materials. This would not only solve the problem of its disposal but also create useful products that can be applied to further protect the environment. It was discovered that one of the useful materials that can be synthesised from fly ash are zeolites. These nano-porous structures have a wide variety of uses. Therefore, many studies have been conducted around optimising the synthesis of various zeolites from coal fly ash. More recently these studies have focused on the scale-up conditions needed to synthesise these zeolites on the large industrial scale, regarding the sheer volume of fly ash produced annually. The most robust and widely used technique for zeolite synthesis involves a pre-synthesis fusion of the fly ash with sodium hydroxide at a temperature of 550 ^{0}C. This would not be feasible to scale-up to industrial scale because of the energy intensity. Therefore, alternative pre-synthesis techniques have been proposed. One of those techniques involves using a sonochemical treatment as a pre-synthesis. It can be argued that this technique may not be able to be easily scaled. To solve this problem, another alternative technique was investigated within this study. It involves the use of a jet loop pilot plant mixing system, which can be scaled-up very readily to industrial scale. This study began with the synthesis of a hierarchical zeolite X from the existing fusion pre-synthesis process. It was found that by using fusion as a pre-synthesis step that 26% of the silicon within the starting fly ash could be extracted. The fusion pre-synthesis involved fusing the fly ash with NaOH in a 1:1.2 mass ratio of fly ash:NaOH at 550 ^{0}C for 1.5 hours. Afterwards the fused fly ash was aged in water by adding it to water in a 1:2.5 mass ratio of fused fly ash:water and stirred for 2 hours before filtering. The faujasite zeolite X was successfully synthesised from the fused fly ash filtrate produced with hydrothermal synthesis conditions of 8 hours at 90^{0}C and a phase crystallinity of 66.85% of zeolite X. This was an improvement time wise on previous studies. The study then focused on using the jet loop pre-synthesis coupled with a curing process instead of the fusion step. Coal fly ash, NaOH and water were fed into the jet loop pilot plant in a 1:1:5 mass ratio of fly ash:NaOH:water. It was shown that jet loop mixing for 30 minutes followed by curing the slurry obtained for 1 day at 80^{0}C followed by 4 days at room temperature allowed 31% of silicon to be extracted from the starting fly ash. This was a 5% improvement on silicon extraction compared to the fusion pre-synthesis, and was also an improvement on the sonochemcial pre-synthesis which extracted only 24% of silicon. Therefore, a realistic alternative pre-synthesis silicon extraction technique that is readily scalable was elucidated. The study, however, could only synthesise a sodalite zeolite from the jet loop and cured filtrate, after varying the Si/Al ratio and the synthesis time of the hydrothermal conditions. This was due to the mass ratios between fusion pre-synthesis and jet

loop and curing pre-synthesis differing with regards to sodium content. Due to this the molar regimes within this study were compared to previous studies where the synthesis of hierarchical zeolite X was achieved in order to serve as comparative guide for future research. The study was successful in the essence of providing an alternative process for silicon extraction needed for the up-scale of zeolite synthesis from coal fly ash. It also recommended the use of the pre-synthesis jet loop and curing process to not only synthesise zeolites but also using the solid residue waste remaining after filtering in geopolymer production. This would lead to a zero waste process and produced large amounts of value added materials from the significant amounts of coal fly ash waste.

DEDICATION

This thesis is dedicated to my loving parents

Robert James Brassell

And

Carol Anne Brassell

For all their support and dedication to my upbringing

ACKNOWLEDGEMENTS

- My supervisor, Professor T.V. Ojumu, for his support throughout my research. He offered valuable insight into my research and continues to be someone to look-up to in the field of chemical engineering research. I would like to highlight his exceptional knowledge, support and guidance throughout my studies.

- My co-supervisor, Professor L.F. Petrik, for her support and guidance throughout my research and welcoming me into her research group with open arms. She truly was always there for queries and provided deep insight into my research topic.

- I would like to thank the ENS research group for welcoming me into their midst and creating an environment that was very conducive to learning.

- Etienne Beya Nkongolo for his assistance with lab work.

- Roland Missengue for his help with analysis and great insight into the research topic.

- Grant Sedres for his help with UV – Vis analysis.

- Vanessa Kellerman, Ilse Wells and Rallston Richards for administrative assistance as well as ICP analysis.

- Hannelene Small for her assistance with acquiring equipment.

- Alwyn Bester for his technical insight.

- Stuart Moir from Scientific Services for his help with XRF analysis

- Remy Bucher from iThemba Labs for his help with XRD analysis

- Adrian Josephs from the Physics department at UWC for his help with SEM analysis.

- My fellow postgraduate colleagues from CPUT for their support and guidance.

- The Maueberger foundation for supplying me with a bursary which made my studies possible.

- The NRF which also supplied me with bursary funds.

- My close family for their love and support throughout my studies.

- My group of friends for their encouragement and support throughout my studies.

LIST OF PUBLICATIONS

Book Chapters

1. Brassell, J.P., Ojumu, T.V. & Petrik, L.F. 2016. Upscaling of Zeolite Synthesis from Coal Fly Ash Waste: Current Status and Future Outlook. In *Zeolites - Useful Minerals*. C. Belviso, Ed. InTech, DOI: 10.5772/63792. 3 – 23. Available: http://www.intechopen.com/books/zeolites-useful-minerals/upscaling-of-zeolite-synthesis-from-coal-fly-ash-waste-current-status-and-future-outlook

TABLE OF CONTENTS

LIST OF FIGURES

LIST OF TABLES

LIST OF SYMBOLS AND ABBREVIATIONS

Symbol	Description	Units
English symbols		
A	Metal cation	-
$A_{\tilde{\nu}}$	Absorbance	%
c	Concentration	mol/L
d	Inter planar spacing	nm
d_l	Pathlength	cm
I	Intensity of entering light	cd
I_o	Intensity of exiting light	cd
m	Degree of hydration	-
M	Molarity	mol/L
n	Valence	-
$T_{\tilde{\nu}}$	Transmittance	%
Greek symbols		
$\varepsilon_{\tilde{\nu}}$	Molar decadic extinction coefficient	L/mol/cm
η	Integer	-
γ	X – ray wavelength	nm
θ	Diffraction angle	Degrees
Abbreviation meaning		
A	Zeolite A	
Al	Aluminium	
AMD	Acid mine drainage	
As	Arsenic	

B	Boron
Ba	Barium
Be	Beryllium
BFD	Block flow diagram
Cd	Cadmium
CEC	Cation exchange capacity
CFA	Coal fly ash
cm	centimetre
Co	Cobalt
Cr	Chromium
Cu	Copper
EDS	Energy dispersive spectrometry
Fe	Iron
FTIR	Fourier-transform infrared spectroscopy
Ge	Germanium
Hr	Hour
Hg	Mercury
ICP – AES	Inductively coupled plasma atomic emission spectroscopy
IZA	International zeolite association
JCPD	Joint committee on powder diffraction
K	Potassium
KOH	Potassium hydroxide
Li	Lithium
LOI	Loss on ignition
M	Mullite

Mg	Magnesium
Mn	Manganese
Mo	Molybdenum
Na	Sodium
NaOH	Sodium hydroxide
Ni	Nickel
nm	Nanometre
P	Zeolite Na-P1
Pb	Lead
PBU	Primary building units
PFD	Process flow diagram
ppm	Parts per million
Q	Quartz
Rb	Rubidium
rpm	Revolutions per minute
S	Sodalite
Sb	Antimony
SBU	Secondary building units
Se	Selenium
SEM	Scanning electron microscopy
Si	Silicon
Sn	Tin
Sr	Strontium
Th	Thallium
Ti	Titanium

U	Uranium
UV – Vis	Ultraviolet visual spectroscopy
V	Vanadium
XRD	X – ray diffraction
XRF	X – ray fluorescence
Zn	Zinc
ZW	Zero water

CHAPTER 1

1. Introduction

1.1. Background

Coal fly ash (CFA) is produced on a global scale and its disposal is fast becoming of concern world-wide. Coal combustion by-products (CCB) are the inorganic residues which result from the coal combustion process. The most abundant CCB is fly ash and it has important economic and environmental applications (Querol et al., 2002). Fly ash is generally grey in colour, it is abrasive, mostly alkaline and refractory in nature (Ahmaruzzaman, 2010). Fly ash from coal combustion process is categorised as a pozzolan, in that it is a siliceous and aluminous material that can form cementitious products when mixed with water and calcium hydroxide. Eskom produces 95% of South Africa's power mainly through the combustion of coal, which produces an estimate of 32.6 million tons of fly ash in per annum (Eskom, 2016). Only 8% of this fly ash is reused, mainly in the cement industry while the remaining 92% is disposed in ash dumps. Eskom also has nitrogen oxide (NO_x) emissions of approximately 893 kilotons per annum (Eskom, 2016). NO_x emissions are mainly nitrogen oxide and result from thermal fixation of atmospheric nitrogen in the combustion flame and from the oxidation of nitrogen bound in the coal (EPA, 2016). Bituminous and subbituminous coals usually contain from 0.5 to 2 weight percent of nitrogen and fuel nitrogen can account for up to 80 percent of the total NO_x emissions from the coal combustion process (EPA, 2016). South African coals have been shown to contain various trace elements such as As, Pb, Sb, Ba, V etc. and these elements are concentrated in the fly ash during the combustion process (Du Plessis et al., 2014). Therefore, the disposal of the fly ash raises environmental concerns. Another factor is the growing cost of disposal in that in the future ash may be too costly to dispose or could be altogether forbidden. Therefore it is important to maximise the reuse of CFA, for example, by optimising the reuse applications of the CFA such that the production of zeolites more affordable, the potential damage to the environment can be lessened, if not stopped altogether (Ahmaruzzaman, 2010).

It is reasonable to infer that, the fact that CFA possess the required constituents for zeolites production; namely silicon and aluminium, presents a solution to the disposal problem. Zeolites are crystalline aluminium-silicates, which have group I or II elements as counter-ions. Their structure consists of a framework of $[SiO_4]^{4-}$ and $[AlO_4]^{5-}$ tetrahedra linked to each other by sharing their oxygen atoms at the corners (Ahmaruzzaman, 2010; Blissett and Rowson, 2012). The tetrahedra make up a 3 dimensional network with many voids and open spaces. These voids define many properties of the zeolites, such as adsorption of molecules etc. The substitution of Si (IV) with Al (III) in the tetrahedra produces the negative charge for the structure which can give rise to a high cation exchange capacity (CEC) when the open spaces or voids allow for the access of cations (Querol et al., 2002). Due to the

peculiar nature of their structural properties zeolites have a wide range of industrial applications, namely ion exchange; gas adsorption; catalysis and the treatment of water such as de-fluoridation (Querol et al., 2002). There are a number of synthetically produced zeolites which fall into groups pertaining to their structure; these groups are represented by 3 letter codes by the IUPAC commission, some codes being: Faujastie (FAU); Gismondine (GIS); Gmelinite (GME); Boggsite (BOG); and Mordentie (MOR) (Musyoka, 2012). South African coal fly ash is class F fly ash and it is established that this class of fly ash is more favourable for zeolite synthesis because of its compositional dominance of aluminosilicate and silicate phases and also due to its relatively low calcium content (Musyoka et al., 2012c).

Another challenge was the inability of developing a process for the optimization before scaling up of the zeolite. There has been research conducted on scale-up options for zeolite synthesis. This included the investigation of agitation during the aging step (Mainganye, 2012; Mainganye et al., 2013) as well as ultrasonication during the aging step (Musyoka et al., 2011b; Musyoka, 2012; Du Plessis, 2014; Ojumu et al., 2016). There has been extensive research concerning the synthesis of zeolites from South African coal fly ash, however it is mainly focused on zeolites A, X and P (Musyoka, 2009; Mainganye, 2012; Musyoka, 2012; Musyoka et al., 2012a; Musyoka et al., 2012c; Du Plessis, 2014). Regarding this research the novel finding of the hierarchical structured zeolite X which was synthesized would be favourable to investigate regarding scale-up options (Musyoka, 2012). The hierarchical pore structure allows the zeolite to have maximum structural functions in a limited volume and space, due to its high diffusion efficiency (Liu et al., 2013). There are generally complicated procedures to synthetically produce the hierarchical structured zeolites, and the procedure formulated in this research could contribute to its mass production from the coal fly ash waste. The faujasite zeolite group contains the zeolites X and Y. The two zeolites are isostructural, with type X being the aluminate rich zeolite and type Y being the silicate rich zeolite, relating to their Si/Al ratios (Rayalu et al., 1998).

The process used to synthesize faujasite zeolites is a fusion method with a high temperature fusion step (550^0C) which is very intensive and may not be feasible to scale up regarding the purpose built furnaces that would be required. Therefore, investigations need to be conducted on the synthesis of faujasite zeolites with respect to replacing the fusion step with a jet loop pilot plant system used in recent studies (Madzivire et al., 2013; Nyale, 2014). In a recent study by Ojumu et al. (2016) the 90 minute fusion pre-synthesis was replaced by a high intensity 10 minute ultrasonication process for the synthesis of zeolite A. Although the authors reported an improved synthesis time and energy input, the possibility of scaling-up a high intensity ultrasonication process to industrial scale is very much in doubt (Moholkar et al., 1999). However, a jet loop pilot plant may provide a more feasible process regarding scale-up operation for zeolite synthesis. Jet loop pilot plant uses hydrodynamic cavitation and impingement techniques to thoroughly mix the fly ash and sodium hydroxide with water. It is thought this form of cavitation could resemble the acoustic cavitation produced during the ultrasonication process with a probe. Indeed Nyale (2014) showed that the amorphous content could be enhanced by jet loop mixing of the fly ash, which favours geopolymer synthesis. It should be noted

that the amorphous content also serves as a precursor for the zeolite synthesis regarding reducing the synthesis time and increasing the yield of zeolite (Querol et al., 2002).

Also a study was performed regarding the fate of elements during the two well-known routes for zeolites synthesis, namely the two step process for zeolite P and the fusion process for zeolite A (Du Plessis et al., 2014). Building on this study a material balance would need to be conducted around the fusion process to produce the hierarchical zeolite X and in comparison the jet loop reactor process to synthesis the same zeolite. This comparison can serve to quantify the yield of zeolite X obtained for each process route. Also with additional characterisation analysis of the zeolites obtained the purity of the zeolite for each process route may also be compared.

1.2. Problem statement

Synthesis of zeolites from coal fly ash has received much attention in the past as a solution to the disposal problem of fly ash. The problem lies in scaling up the process to industrial scale. This is concerning replacing the laboratory process with a larger pilot plant process that can be readily scaled-up. The laboratory scale process is the fusion process, which is an energy intensive process that may be problematic to scale-up. This process is used to break up the quartz and mullite phases in the CFA and render them soluble to release silicon and aluminium. There needs to be an investigation in replacing this process with a pilot plant scale jet loop process coupled with a low temperature curing process to see if the same extent of silicon and aluminium extraction can be achieved. The problem lies in the refractory nature of the CFA, with the quartz and mullite locking up most of the silicon and aluminium in these insoluble matrices. If the jet loop and curing process can unlock the necessary silicon and aluminium for zeolite synthesis it would be favourable over the energy intensive fusion pre-synthesis. Faujasite zeolites are the most widely employed zeolites on an industrial scale. The faujasite zeolites are used extensively as a component of fluid catalytic cracking catalysts for refining oil and as materials for adsorbing and removing gaseous emissions (Liu et al., 2013). Therefore, it is a very significant value added material to be achieved from fly ash and hence deserves further investigation into its synthesis from South African coal fly ash regarding the scale-up conditions needed.

1.3. Objectives and research questions

The aim of this study is to investigate an alternative method to improve dissolution of Si and Al from a South African coal fly ash for the synthesis of faujasite zeolites with the potential for scale-up of the process. This will be achieved by the following objectives:

- establish a base case of the synthesis of faujasite zeolites that can be synthesised from South African coal fly ash using the existing pre-synthesis fusion method,
- determine the dissolution of silicon and aluminium achieved by replacing the fusion step with a jet loop system during pre-synthesis mixing,
- determine whether curing after jet loop treatment allows for further dissolution of the silicon and aluminium precursors from fly ash feedstock,

- determine whether a high purity zeolite can be produced by replacing the pre-synthesis fusion step with low temperature jet loop and curing as a pre-synthesis alternative,
- perform material balances to determine the distributional fate of elements from the optimal synthesis conditions.

The objectives listed above would be met by answering the following research questions:

- Can the high temperature fusion step be replaced by a jet loop and curing step to produce precursors for preparing a high purity faujasite zeolite by allowing for sufficient dissolution of silicon and aluminium?
- What is the effect of curing the samples produced from the jet loop?
- What is the effect of the optimised synthesis conditions on the distributional fate of elements?
- How does the distribution of the elements in the two pre-synthesis routes compare to one another regarding the waste and product streams produced by fusion and by the jet loop and curing processes?

1.4. Significance of study

The significance of the study relates to the fact that Eskom (2016) only reuses 8% of its coal fly ash with the rest going to ash dumps which is detrimental to the environment. Also the safe disposal and long term management/storage of ash has become a financial burden for Eskom. An investigation into some of the scale-up conditions needed to synthesise faujasite zeolites from coal fly ash would not only alleviate the disposal problem, but also benefit Eskom by decreasing its environmental impact. This alleviation would be two fold in that the environmental impacts of the fly ash disposal would be decreased and the zeolites prepared from the fly ash could be used to treat NO_x gaseous emissions from coal burning. This is due to faujasite zeolites being suitable de-NO_x catalysts if its production can be scaled up to industrial scale, which this study would contribute towards.

1.5. Research approach

The research was based upon the study conducted by Muysoka (2012), using this study as a base case reference for the synthesis of the hierarchically structured zeolite X. Therefore, the study began with the synthesis of the hierarchically structured zeolite X from the fusion method. Given the differing nature of coal fly ash from batch to batch, the hydrothermal conditions optimised by Musyoka (2012) had to be optimised again for this study. Once the optimal results were ascertained abased upon characterisation of the zeolites obtained through XRD, FTIR and SEM analysis the next stage of the research could be undertaken. The raw coal fly ash was also characterised with XRF, XRD, QXRD, FTIR and SEM analysis to conclude on its nature to serve as a feedstock for the zeolite synthesis. The next stage of the experiments involved changing the pre-synthesis method, namely the fusion method, with a jet loop system and low temperature curing. This was performed to compare the amount of silicon and aluminium that could be released from this method compared to what is released through the fusion method. The jet looping time and curing time was varied and the filtrates and residues were analysed through ICP – AES, UV – Vis, XRD, FTIR and SEM techniques. Once

the optimal jet looping and curing time were found the last stage of experiments began. This included using first the same hydrothermal conditions optimised from Musyoka's study using the fusion method and then attempting to synthesize zeolite X through molar regime adjustment from the jet looped and cured filtrate. Material balances were also attempted for each synthesis route to serve as comparisons between the two different processes.

1.6. Delineations

Zeolites can be synthesised from any source containing the necessary silica and alumina feedstock, however this study will be focused on zeolite synthesis from South African class F CFA. More specifically, it will be focused on the conditions needed for preparing faujasite zeolites. The application of faujasite zeolites as de-NO_x catalysts will not be investigated in this study.

1.7. Thesis outline and structure

The thesis is divided into 6 chapters. Chapter 1 introduces the proposed study and lists the aims and objectives of the study. Chapter 2 included an extensive literature review of the study mentioning all current literature to date regarding zeolite synthesis from CFA. Chapter 3 explains all the experimental procedures and analytical techniques used within the study. Chapter 4 deals with the characterisation of the CFA starting material and also with the base case optimised fusion method to synthesize the hierarchical zeolite X based on previous studies. Chapter 5 concerns the replacement of the fusion method in Chapter 4 with a jet loop pilot plant and curing synthesis process. Chapter 6 provides the general conclusions which could be drawn from this study and the comparisons between the two synthesis routes, while also providing recommendations for future work.

CHAPTER 2

2. Literature review

2.1. Coal fly ash

2.1.1. Introduction

Ever since coal combustion was used on a wide spread scale as a source of electricity it has driven and is still driving the greatest amounts of electricity production worldwide. Thus the resulting consumption of coal has increased significantly over this period to the present day. Coal fired electricity generation accounted for 29.9% of the world's electricity supply in 2011, and this is anticipated to increase to 46% by 2030 (Yao et al., 2015). Regarding the top ten major countries in coal consumption South Africa is ranked 6th in the world at 2.4% of the world coal consumption, the greatest being China at 50.2% (Yao et al., 2015).

Approximately 77% of South Africa's energy needs are supplied by coal fired power stations, which is unlikely to change significantly in the next decade (Stone, 2015). South Africa's coal reserves are estimated at 53 billion tonnes which, given the present production rate, should last approximately 200 years (Stone, 2015). According to the latest available report from Eskom (2016) the annual production of CFA is 32 million tonnes per annum of which only approximately 8% is reused, the remaining 92% being disposed in ash dumps. It was also reported by Eskom 2016 integrated report that there is nitrogen oxide (NO_X) gaseous emissions amounting to approximately 893 kilotons per annum.

CFA is the most predominant coal combustion by-product (CCB) resulting from the coal combustion process. Other CCB's include bottom ash, boiler slag, and flue-gas desulfurization by-products, all of which are the inorganic residues resulting from the coal combustion process (Querol et al., 2002). CFA is obtained through the electrostatic or mechanical precipitation of the dust-like particles, which are collected from the flue gases in the furnaces of coal fired power plants with electrostatic precipitators (Querol et al., 2002; Vassilev et al., 2003; Vassilev and Vassileva, 2007). Coal fly ash is mainly grey in colour, abrasive, mostly alkaline and refractory in nature (Ahmaruzzaman, 2010). It is comprised mainly of silicon and aluminium and is thus classified as a pozzolan and can form cementitious products when mixed with water and calcium hydroxide (Ahmaruzzaman, 2010).

The reuse of coal fly ash currently stands at around 39% in the US and 47% in Europe with the global average for ash reuse being around 25% (Blissett and Rowson, 2012). Therefore with current estimates of coal fly ash production ranging in the 500 million tonnes per annum (Blissett and Rowson, 2012) this presents a significant amount of coal fly ash which needs to be disposed.

Traditionally, it has been disposed in landfills or ash lagoons, however these lagoons have been known to breach and cause significant harm to the local communities surrounding them (Blissett and Rowson, 2012).

2.1.2. Mineralogy and chemical nature of coal fly ash

The main components of coal fly ash are silica (SiO_2), alumina (Al_2O_3), ferrous oxide (Fe_2O_3) and calcium oxide (CaO) with varying amounts of unburned carbon (Ahmaruzzaman, 2010; Blissett and Rowson, 2012). The chemical properties of CFA are greatly influenced by the type of coal being burned to produce it, as well as the handling and storage procedures (Kruger, 1997; Vassilev and Vassileva, 2007; Ahmaruzzaman, 2010; Blissett and Rowson, 2012; Yao et al., 2015). It is a result of this that the composition of fly ash varies considerably from region to region, as well as within regions themselves (Blissett and Rowson, 2012). It was also shown by Mainganye (2012) that fly ash varies significantly from batch to batch, even when sampled from the same power station. The composition of fly ash constitutes major (>1%), minor (1-0.1%) and trace (<0.1%) elements, with the major and minor elements expressed as oxides in the order O>Si>Al>Ca>Fe>C>K>Mg>H>Na>Ti>P>Ba and in some cases also Mn, Sr, F, and Cl (Vassilev and Vassileva, 2007; Blissett and Rowson, 2012). Some of the trace elements found in coal fly ash include As, B, Ba, Be, Cd, Co, Cr, Cu, Ge, Hg, Li, Mo, Ni, Pb, Rb, Sb, Se, Sn, Sr, Th, U, V and Zn (Blissett and Rowson, 2012). The major phases found in coal fly ash are in the order of glass>mullite>quartz>char>hematite-magnetite>anhydrite-gypsum>feldspars>lime-portlandite>clay and mica minerals>cristobalite-tridymite>calcite-ankerite>corundum>jarosite>and some Ca and CaMg silicates (Vassilev and Vassileva, 2007; Blissett and Rowson, 2012).

2.1.3. Morphology of coal fly ash

The morphology of coal fly ash particles is dependent on the parameters of the coal burning process, namely combustion temperature and cooling rate (Kutchko and Kim, 2006; Blissett and Rowson, 2012). Through Scanning Electron Microscopy (SEM), it has been revealed that coal fly ash consists of mainly spherical particles i.e. solid spheres and hollow spheres (cenospheres) and irregular unburned carbon (Kutchko and Kim, 2006; Ahmaruzzaman, 2010; Blissett and Rowson, 2012; Yao et al., 2015). The apparent colour of the fly ash is influenced by the iron and unburned carbon contents and ranges from water-white to yellow, orange to deep red, or brown to opaque (Fisher et al., 1978; Yao et al., 2015).

2.1.4. Classification of coal fly ash

CFA is one of the most complex anthropogenic substances that can be classified based on the variety of its components (Blissett and Rowson, 2012; Yao et al., 2015). This is highlighted in that approximately 316 individual minerals and 188 mineral groups have been identified in different CFA's (Vassilev and Vassileva, 1997; Vassilev et al., 2003; Vassilev and Vassileva, 2005; Blissett and Rowson, 2012; Yao et al., 2015). The American Society for Testing Materials (ASTM C618) states that ash containing greater than 70% SiO_2+Al_2O_3+Fe_2O_3 and having a low lime (CaO) content (about 5%) is defined as class F fly ash, while ash containing between 50 – 70 % of SiO_2+Al_2O_3+Fe_2O_3 and

high in lime content (10 – 35%) is classified as class C (Ahmaruzzaman, 2010; Blissett and Rowson, 2012). Based on these compositions, it is reported that Class C fly ash is generated from lignite and sub-bituminous coals while class F is generated from bituminous and anthracite coals (Vassilev and Vassileva, 2007; Blissett and Rowson, 2012).

2.1.5. Environmental impacts of coal fly ash

The environmental effects of CFA relate to the toxic trace elements and heavy metals which have the ability to leach into groundwater systems as well as the immediate impact on mine workers and the surrounding population. There have been many studies concerning the leachability of CFA to the surrounding ecosystems (Wadge and Hutton, 1987; Khanra et al., 1998; Wang et al., 1999; Choi et al., 2002; Iyer, 2002; Praharaj et al., 2002; Ugurlu, 2004; Jegadeesan et al., 2008; Dutta et al., 2009; Izquierdo and Querol, 2012; Xiang et al., 2012; Nyale et al., 2014; Belviso et al., 2015; Komonweeraket et al., 2015). There is also the possibility of CFA to pose an inhalation hazard where it can leach genotoxic compounds, such as polycyclic aromatic hydrocarbons, inside the lungs after inhalation (Borm, 1997; León et al., 2007).

2.1.6. Applications of coal fly ash

There are numerous applications for the reuse of CFA, with some presented here, however the scale required to meet the production of CFA regarding its reuse has not yet been met. Eskom (2016) only reuses approximately 8% of the CFA produced, which will not be sustainable given the ever increasing need for energy. Therefore, there is a need to scale-up some of the following applications of fly ash.

2.1.6.1. Agriculture

Currently there are no clear guidelines or regulations for CFA use in agriculture which is a major barrier regarding using CFA for soil improvement (Ahmaruzzaman, 2010; Shaheen et al., 2014). The use of CFA for soil improvement has received a lot of attention in the past three decades due to the fact that it contains some beneficial nutrients (Ukwattage et al., 2013; Shaheen et al., 2014). CFA application in soil improvement provides beneficial factors such as water infiltration, soil water holding capacity, hydraulic conductivity, bulk density and soil aggregation regarding the improvement of the soil conditions (Ukwattage et al., 2013; Ram and Masto, 2014; Shaheen et al., 2014). Caution is needed however for the correct utilisation of CFA for soil improvement as applying too large an amount of CFA or using acidic CFA with acidic soil can lead to phytotoxicity (Ukwattage et al., 2013; Ram and Masto, 2014; Shaheen et al., 2014).

2.1.6.2. Construction

One of the more predominant uses of CFA in large volumes is in the cement industry for the production of concrete (Ahmaruzzaman, 2010; Yao et al., 2015). There are beneficial factors relating to using CFA for cement production namely reducing the water demand, enhancing the workability of concrete and reducing production costs and greenhouse gas emissions (Ahmaruzzaman, 2010; Yao et al., 2015). There are also unwanted factors such as reducing the compressive strength of the

concrete at early stages especially when there are cold weather conditions or when more than 40% of CFA is used (Siddique, 2004; Yao et al., 2015).

2.1.6.3. Wastewater treatment

There have been many studies on the use of CFA as an adsorbent of various heavy metals from wastewater streams. An extensive review of all these studies can be found in an article by Ahmaruzzaman (2011). However, there are certain economic barriers which have to be overcome regarding using high volumes of CFA. This is due to the low adsorption capacity of CFA depending mainly on the origin of the CFA and the chemical treatment used (Ahmaruzzaman, 2010; Ahmaruzzaman, 2011; Yao et al., 2015).

2.1.6.4. Recovery of rare earth elements

Recent studies have been investigating the extraction of rare earth elements from coal fly ash (Seredin and Dai, 2012; Kashiwakura et al., 2013; Mayfield and Lewis, 2013; Seredin et al., 2013; Franus et al., 2015). Rare earth elements are the group of elements known as the lanthanides plus yttrium and scandium and are used in new technologies such as green energy devices, hi-capacity batteries, magnets for wind power generation, fuel cells and also used by the aerospace industry (Mayfield and Lewis, 2013; Franus et al., 2015).

2.1.6.5. Geotechnical applications

It has been shown in studies that CFA can be potentially used in geotechnical applications (Pandian, 2004; Bose, 2012; Butt, 2015). This is due to certain characteristics of CFA such as its low specific gravity, freely draining nature, ease of compaction, insensitiveness to changes in moisture content and good frictional properties (Pandian, 2004; Bose, 2012). It can be used in the construction of embankments when mixed with soil (Santos et al., 2011) and sand (Kumar et al., 2014), in successive layers of soil and CFA for load bearing structures (Saha and Pal, 2012), reclamation of low lying areas and fill behind retaining structures (Pandian, 2004; Bose, 2012).

2.1.6.6. Synthesis of geopolymers

Joseph Davidovits first introduced the technology known as geopolymerisation in the 1970's which involves the alkali activation of aluminosilicates, and termed the resulting product 'geopolymer' (Blissett and Rowson, 2012; Nyale et al., 2013). A geopolymer consists of amorphous to semi-crystalline three dimensional aluminosilicate polymers of which the chemical composition resembles that of zeolites (Jha and Budhamagar, 2013; Böke et al., 2015). The novelty of geopolymers is that they exhibit good chemical and mechanical properties such as low density, micro and nano porosity, low shrinkage, high mechanical strength, good thermal stability, durability, surface hardness, and fire and chemical resistance (Blissett and Rowson, 2012; Jha and Budhamagar, 2013). It is for these reasons that they find applications in areas such as ceramics, cements, matrices for hazardous waste stabilisation, fire-resistant materials, asbestos free materials, high tech materials (Nyale et al., 2013) in industries such as construction, aerospace, mining and metallurgy (Blissett and Rowson, 2012).

2.1.6.7. Synthesis of zeolites

There has been significant research into the synthesis of zeolites from coal fly ash around the world since the pioneering work in 1985 (Holler and Wirsching, 1985; Shigemoto et al., 1993; Querol et al., 1995; Querol et al., 1997b; Steenbruggen and Hollman, 1998; Hollman et al., 1999; Querol et al., 2002; Tanaka et al., 2003; Musyoka, 2009; Musyoka, 2012; Musyoka et al., 2012a). The synthesis of zeolites is a focus of this study especially concerning the scale-up of the process.

2.2. Zeolites

2.2.1. Introduction

The first natural zeolites were discovered in 1756 but it was only during the 19th century that the microporous nature of these natural zeolites was fully recognised and this led to their use in ion exchange and adsorption (Xu et al., 2007). Zeolites are crystalline aluminosilicates which contain pores and cavities on the molecular scale (Cundy and Cox, 2003). As previously mentioned, they occur as natural minerals but the most widely used kind are the synthetic zeolites, utilised mainly as sorbents, catalysts and ion exchange materials (Cundy and Cox, 2003). The natural zeolites are formed as crystals in small cavities of basaltic rocks or as volcanic tuffs or glass altered by the interaction with saline water over the timeframe of many years (Jha and Singh, 2011). However the more predominant synthetic zeolites are produced by chemical processes resulting in a more pure mineral form and more uniform regarding its lattice structures, size of pores and cages in its framework (Jha and Singh, 2011). The empirical formula of a zeolite according to Xu et al. (2007) is given below:

$$A_{x/n}\,[Si_{1-x}Al_xO_2]\blacksquare mH_2O \qquad \text{…Equation 2-1}$$

- Where A is a metal cation of valence n, m is the degree of hydration and x is an integer

Due to the nature of the zeolite structure consisting of SiO_4 and AlO_4 tetrahedra it possesses an anionic framework of which the negative charge on Al is compensated by extraframework cations such as Na^+, K^+, Ca^{2+}, Mg^{2+} and others (Xu et al., 2007). The internal voids are generally occupied by water, the sorbed phase, however the water and extraframework cations can be removed by thermal or ion exchange treatment respectively allowing for the pores to be opened (Auerbach et al., 2003). This means the pores can discriminate against molecules that have a dimensional difference of less than 1 angstrom, which gives rise to the name and idea of molecular sieves (Auerbach et al., 2003). Some common frameworks and their pore sizes are given below in Figure 2-1. The framework structures will be explained in detail in section 2.2.2. However, there is a database of frameworks available at the International Zeolite Association (IZA) (Baerlocher et al., 2007).

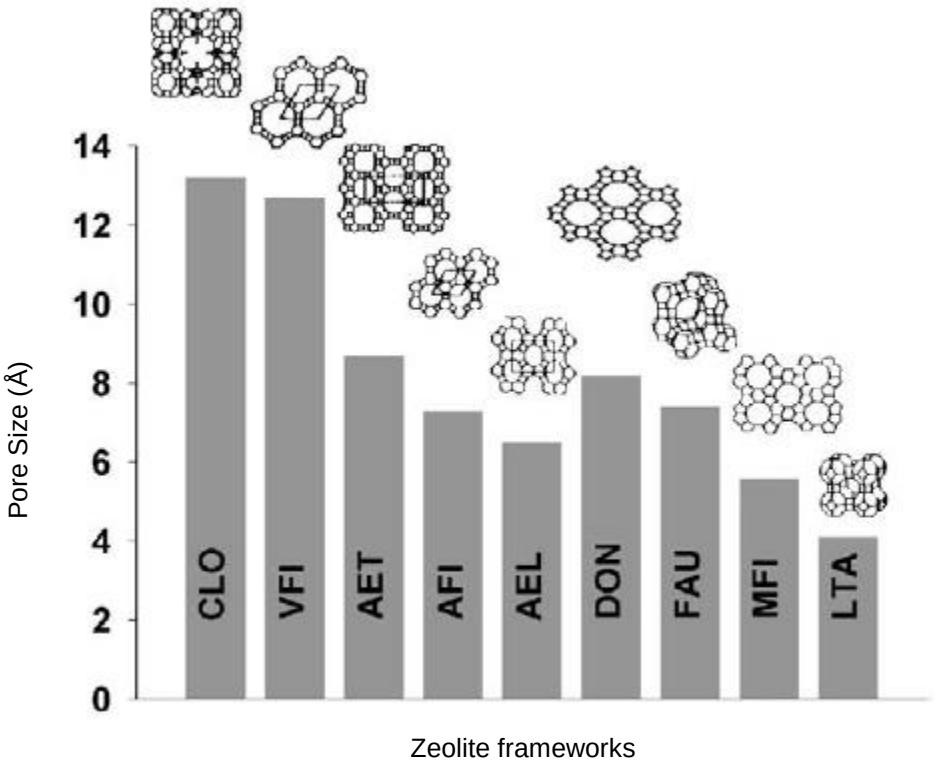

Figure 2-1: A comparison of the different framework pore sizes (Auerbach et al., 2003)

2.2.2. Structural framework of zeolites

The pores and cavities in the form of cages and channels of zeolites are created by a framework of TO_4 tetrahedra (T=Si, Al) with oxygen atoms connecting the neighbouring tetrahedra. With the addition of Al into the Si framework the 3+ charge of the Al creates a negative charge in the framework which then requires extraframework cations such as Na^+, K^+, Ca^{2+}, Mg^{2+} to name a few, to keep the framework neutral (Auerbach et al., 2003) as depicted in Figure 2-2 and Figure 2-3.

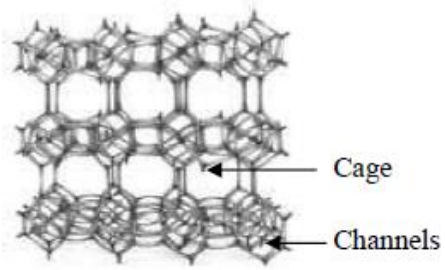

Figure 2-2: Typical zeolite structure showing cages and channels (Jha and Singh, 2011)

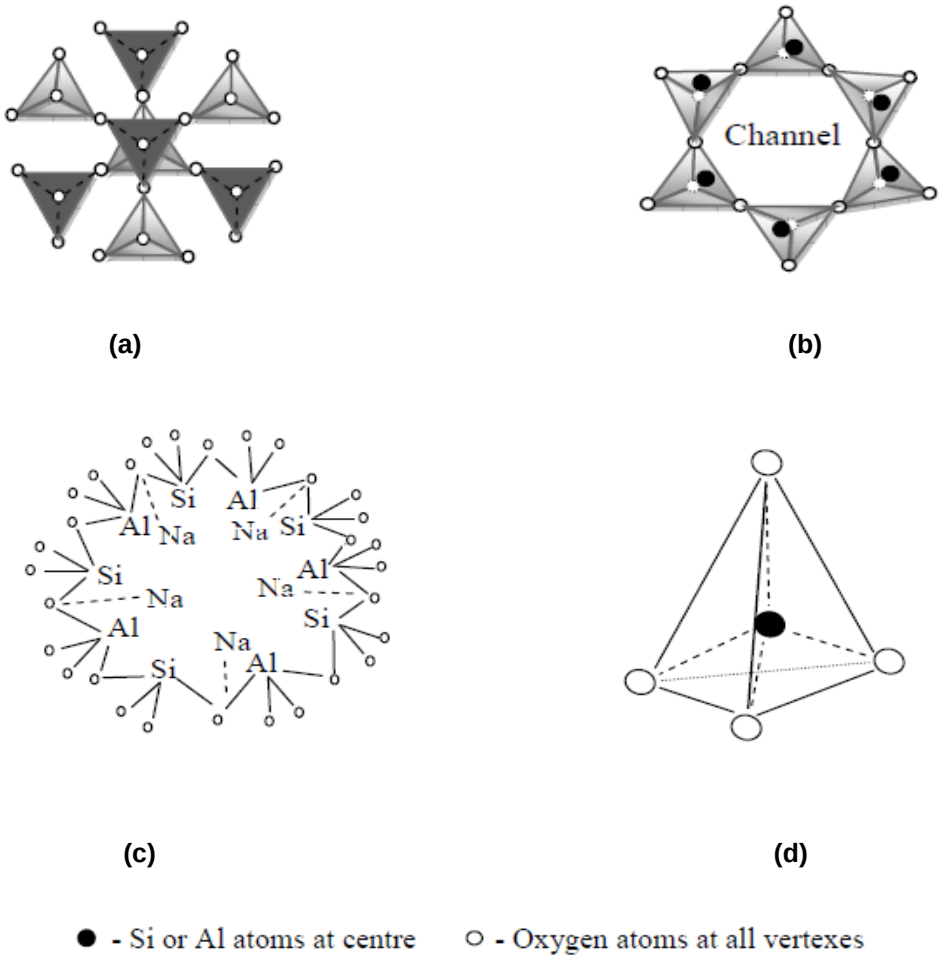

Figure 2-3: (a) Basic tectosilicate structure (b) Single ring tetrahedron structure and framework of a zeolitic mineral (c) SiO_4^- and AlO_4^- in a ring of sodium zeolite and (d) Pictorial representation of a 3-D view of a tetrahedra (Jha and Singh, 2011)

Figure 2-3 (a) shows the basic tectosilicate structure of the zeolite where the dark (vertex in) and light (vertex out) shades to add the 3-dimensional (3-D) effect and upside down orientation of the tetrahedra for vertex sharing between the two rings of the zeolite structure in its 2-D view on a picture plane. The TO_4 tetrahedra seen in Figure 2-3 (d) represented by a 3-D view of a tetrahedra with the centrally located Si or Al atoms are known as the primary building units (PBU's) of the zeolite structure (Xu et al., 2007). The secondary building units (SBU's) are a concept of infinite component units due to the zeolite framework being thought to be made up of finite component units or infinite component unit-like chains or layers (Xu et al., 2007) some of which can be seen in Figure 2-4. SBU's can have single and double rings each consisting of four-, five-, six- or eight- interlinked tetrahedra, this includes the silicon and aluminium atoms (Jha and Singh, 2011). These varying framework structures give rise to the 3 letter code system used to name each unique framework type, of which there are 176 unique zeolite framework structures (however they have currently reached 218 unique types) (Bukhari et al., 2015). This coded system can be found in the Atlas of Zeolite

Framework Types currently in its sixth edition (Baerlocher et al., 2007). Some common codes are given below:

Table 2-1: Zeolite framework codes

Code	Zeolite
FAU	Faujasite
GIS	Gismodine
GME	Gmelinite
BOG	Boggsite
MOR	Mordenite

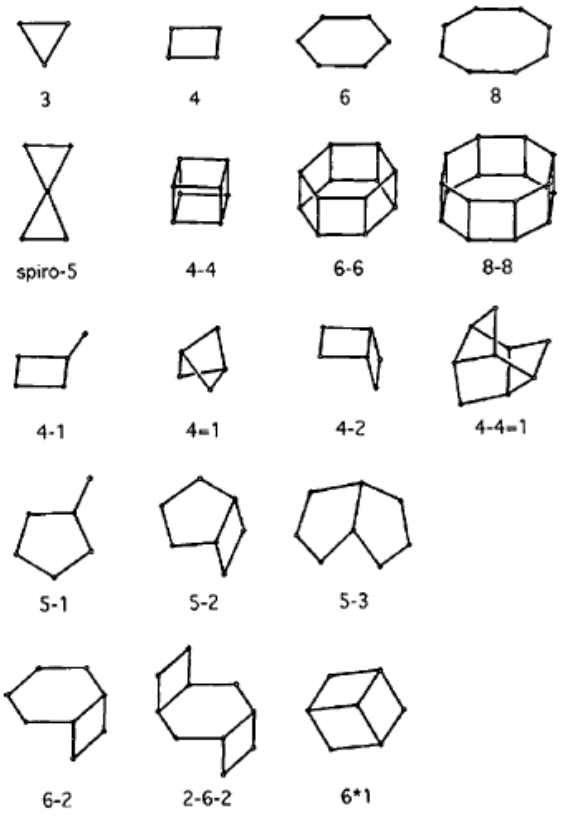

Figure 2-4: Secondary building units (SBU's) with SBU codes below figures (Xu et al., 2007)

Figure 2-5 shows how a sodalite unit can be assembled to form more common zeolitic frameworks such as those of zeolite A (LTA), zeolites X and Y (FAU) and EMT. A pair of TO_4 tetrahedra is linked to a single sodalite cage by T-O-T bonds. In a less cluttered representation, the oxygen atoms are omitted and straight lines are drawn connecting the tetrahedral (T) atoms. The sodalite cage unit is found in SOD, LTA, and FAU, EMT frameworks (Auerbach et al., 2003).

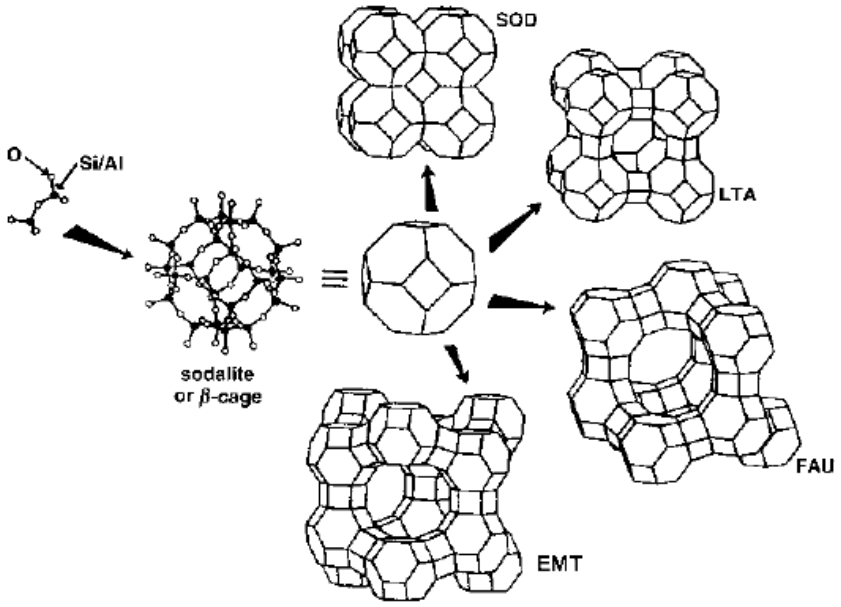

Figure 2-5: The construction of four different zeolite frameworks with sodalite or β cages (Auerbach et al., 2003)

2.2.3. Properties and applications of zeolites

The three main uses or applications of zeolites are namely adsorption, ion-exchange and catalysis. Also natural zeolites find use in bulk mineral applications because of their lower cost (Auerbach et al., 2003). This section will give some examples of these three primary uses as well as some of the properties of zeolites. The zeolite type has a significant impact on its potential industrial application. For example zeolite X with its large pore size and high cation exchange capacity (CEC) would be more favourable as a molecular sieve and in ion-exchange than hydroxysodalite, which has a much smaller pore size (Jha and Singh, 2011).

2.2.3.1. Properties of zeolites

Some of the physical properties of zeolites relate to bulk density and specific gravity which can correlate with their porosity and their most dependant parameter: CEC (Jha and Singh, 2011). The most general physical property of common zeolites, for example an analogue of the natural zeolite faujasite (Na-X or zeolite X or Linde X or molecular sieve 13X) is their particle size, which has been reported to vary from 2 µm for bulk-NaX to 800 nm for micro NaX and from 20 to 100 nm for nano NaX zeolite (Jha and Singh, 2011). Regarding the chemical properties of zeolites they are known to consist of the oxides of aluminium, calcium, iron, magnesium, silicon and sodium within their structure while having water molecules inside their pores or cages (Jha and Singh, 2011). The properties which depend on the chemical composition of the zeolite are the CEC, adsorption properties, pH, and loss on acid immersion (Jha and Singh, 2011). As will be explained further in section 2.2.4 regarding the synthesis of zeolites there are high silica zeolites and low silica zeolites. It has been found that the decomposition temperature for low silica zeolites is approximately 700^0C while a completely siliceous zeolite such as silicalite is stable up to approximately 1300^0C (Auerbach et al., 2003). Another factor related to thermal stability is the crystallinity of the zeolite with higher crystallinity

resulting in greater thermal stability. Also a higher SiO_2/Al_2O_3 ratio and CEC of zeolites can result in higher temperature resistance (Jha and Singh, 2011).

High silica zeolites are unstable in basic solutions, however they are stable in boiling mineral acids whereas low silica zeolites are unstable in acid (Auerbach et al., 2003). The angle between the Si-O-Al bonds in the zeolite crystal plays an important role in its resistance to corrosion in an acidic medium(Jha and Singh, 2011). Therefore in high silica zeolites there is a greater T-O-T bond angle, where T is silicon or aluminium atoms, whereas in low silica zeolites the bond angle has been found to be lower (Jha and Singh, 2011). In zeolites the total surface area is composed mainly (98%) of the internal surface area of the porous zeolite, with surface areas being typically in the range of 300-700 m^2/g (Auerbach et al., 2003). The favourable properties of zeolites which make them suitable for industrial applications are illustrated in Table 2-2.

Table 2-2: Example of common zeolites and applications (Musyoka, 2009)

Framework Code	Zeolite type	Si/Al Ratio	Application
FAU	Zeolite X	1-1.5	Gas drying in industries Removal of CO_2 from industrial flue gases
FAU	Zeolite Y	1.5-5.6	As an acid catalyst in fluid catalytic cracking
LTA	Zeolite A	1-1.7	Softeners in detergent industrial gas drying
MFI	ZSM-5	>10	As an acid catalyst in fluid catalytic cracking Use in $DeSO_x$ and $DeNO_x$ processes
GIS	Zeolite P	2-8	Waste water treatment Softeners in detergent industrial

2.2.3.2. Adsorption applications

Table 2-3 lists some of the more common adsorption applications of zeolites relating to removal of small polar or polarizable molecules by more aluminous zeolites and bulk separations based on the molecular sieve process (Auerbach et al., 2003).

Table 2-3: Adsorption applications of molecular sieve zeolites (Auerbach et al., 2003)

Purification		**Bulk separations**
Drying:	natural gas (including LNG)	Normal/iso-parrafin separation
	cracking gas (ethylene plants	
	insulated windows	Xylene separation
	refrigerant	
		Olefin separation
CO_2 removal:	natural gas, flue gas (CO_2 + N_2)	
		Separation of organic solvents
	cryogenic air separation plants	
Sulfur compound removal		O_2 from air
Sweeting of natural gas and liquefied petroleum gas		Separation of CO_2, SO_2, NH_3
Pollution abatement:	removal of Hg, $NO_{x,}$ SO_x	Sugar separation
Removal of:	organic and inorganic iodide compound from commercial acetate acid feed streams	Separation of amino acids, n-nitrosoamines

2.2.3.3. Ion-exchange applications

The extraframework cations mentioned previously have the ability to exchange with other cations within the zeolite, giving rise to ion-exchange properties of zeolites (Jha and Singh, 2011). The major use in this field is found as ion-exchange agents for water softening applications as substitute for phosphates, using zeolites synthesised from fly ash (Hui and Chao, 2006; Cardoso et al., 2015). Another major application is in the removal of phosphates, ammonium and various heavy metals from wastewaters, also using zeolites synthesised from fly ash (Chang and Shih, 2000; Moreno et al., 2001; Somerset et al., 2008; Wang et al., 2008; Guan et al., 2009; Jha et al., 2009; Izidoro et al., 2013; Ji et al., 2015). Natural zeolites are also favourable for the removal of Cs^+ and Sr^+ radioisotopes from radioactive waste streams (Auerbach et al., 2003) however there are also studies of Cs^+ removal with coal fly ash (CFA) zeolites (Shih and Chang, 1996; Chang and Shih, 1998; El-Naggar et al., 2008).

2.2.3.4. Catalysis applications

Zeolites find a wide application in the field of catalysis including various inorganic reactions, hydrocarbon conversion and dehydration to name a few (Auerbach et al., 2003). Due to the strong activity of zeolites prepared via certain pathways, including NH_4^+ and multivalent cation exchange and also steaming, the hydrocarbon transformations using zeolites are promoted (Auerbach et al., 2003). There is another unique characteristic of zeolites known as the concentration effect of the reactants within the various pores and channels which promotes molecular reactions, such as efficient

intermolecular hydrogen transfer (Auerbach et al., 2003). Zeolites from fly ash have recently been applied as heterogeneous catalysts for biodiesel production (Babajide et al., 2012; Bhandari et al., 2015; Volli and Purkait, 2015).

2.2.4. Synthesis of zeolites

The founding fathers of zeolite synthesis science are R. M. Barrer and R. M. Milton, with Barrer beginning his studies in the 1940s, synthesising the first synthetic zeolite in 1948 (Cundy and Cox, 2003; Cundy and Cox, 2005). Robert Milton began his work in the Linde corporation laboratories in 1949 and with the use of more reactive starting materials it allowed for milder reaction conditions (Cundy and Cox, 2003; Cundy and Cox, 2005). Progress was significant and by 1950 a pure form of zeolite X had been synthesised which was isostructural with the natural mineral faujasite (Cundy and Cox, 2003). By 1953 Milton and his co-workers, including D. W. Breck had synthesised 20 zeolites with the patents of zeolite A and X being filed in that same year (Cundy and Cox, 2003; Cundy and Cox, 2005). However due to a battle with patent examiners the official publication date was set as 1959 (Cundy and Cox, 2003). These zeolites fall into the group of low-silica or Al-rich zeolites with zeolite A and X having the highest cation contents as well as being excellent ion-exchange agents (Auerbach et al., 2003).

The next advancement was made in producing intermediate silica zeolites, such as Breck synthesising zeolite Y in 1964, having a Si/Al ratio of 1.5-3.8 and a framework similar to zeolite X and the mineral faujasite (Auerbach et al., 2003; Xu et al., 2007). From then a variety of intermediate silica zeolites with Si/Al ratios of 2 – 5 were synthesised such as mordenite, zeolite L, erionite, chabazite etc. (Xu et al., 2007). With the addition of organic species to the aluminosilicate and silicate gels high silica zeolites were then synthesised during the 1960s and 1970s, the best known example being ZSM-5 (Auerbach et al., 2003).

2.2.5. Synthesis of zeolites from coal fly ash

2.2.5.1. History and referenced work

The synthesis of zeolites from fly ash began with the pioneering work of Holler and Wirsching (1985). This was after it was found that CFA contains significant amounts of silicon and aluminium that are necessary in zeolite synthesis. Since then there has been significant research into the synthesis of zeolites from CFA (Shigemoto et al., 1993; Zhao et al., 1997; Steenbruggen and Hollman, 1998; Hollman et al., 1999; Rayalu et al., 2000; Murayama et al., 2002b; Tanaka et al., 2003; Ojha et al., 2004; Adamczyk and Białecka, 2005; Inada et al., 2005a; Rungsuk et al., 2006; Fotovat et al., 2009; Belviso et al., 2010; Kazemian et al., 2010; Kondru et al., 2011; Zou et al., 2015) as well as zeolite synthesis from South African CFA (Hendricks, 2005; Somerset et al., 2005; Musyoka, 2009; Musyoka, 2012; Musyoka et al., 2012a). There has also been studies investigating the scale-up of zeolite synthesis from coal fly ash (Querol et al., 2001; Moriyama et al., 2005; Chareonpanich et al., 2011; Wdowin et al., 2014) again including recent studies conducted regarding South African fly ash. These studies included the investigation of the impact of agitation on zeolite synthesis during the aging step

(Mainganye et al., 2013), as will be further explained in section 2.2.5.2 on methods of synthesis. Du Plessis et al. (2014) also investigated aspects of zeolite up-scaling which included a study on the distributional fate of elements during the two main synthesis methods, as well as waste minimisation protocols for the synthesis methods (Du Plessis et al., 2013). There have also been investigations into alternative and more economical methods of zeolite synthesis including using alternate solutions instead of water such as molten salt (Park et al., 2000) as well as seawater (Belviso et al., 2010; Belviso et al., 2012) and even mine waters (Musyoka et al., 2011a; Musyoka et al., 2011b; Musyoka et al., 2013). Other more economical methods included replacing the high energy fusion step in zeolite synthesis with processes such as ultrasound (Belviso et al., 2011; Musyoka et al., 2011b; Bukhari et al., 2016; Ojumu et al., 2016) or microwave treatment (Querol et al., 1997a; Inada et al., 2005b; Tanaka et al., 2008) of which there is a recent comprehensive review published (Bukhari et al., 2015).

2.2.5.2. Synthesis methods

The International Zeolite Association (IZA) formed a synthesis commission at the 9th International Zeolite Conference in Montreal in 1992 and information can be found online at http://www.iza-online.org/synthesis/default.htm (IZA, 2013). The website lists all the known synthesis routes for easy access and serves as a forum for zeolite synthesis discussion. In the following sections i - iv some of the most common synthesis routes will be discussed.

i. 2-Step method of synthesis

Following the traditional 1-step process route for synthesis which produced zeolites with significant amounts of residual fly ash, Hollman (1999) introduced a 2-step process for zeolite synthesis from CFA. The conventional hydrothermal treatment of the one step synthesis can be seen in Figure 2-6 in comparison to the 2-step process illustrated in Figure 2-7. The direct hydrothermal method involves dissolving the CFA in an alkaline solution, typically NaOH or KOH to extract the aluminate and silicate contents followed by the heat treatment to produce the zeolite crystals from the reaction mixture (Bukhari et al., 2015).

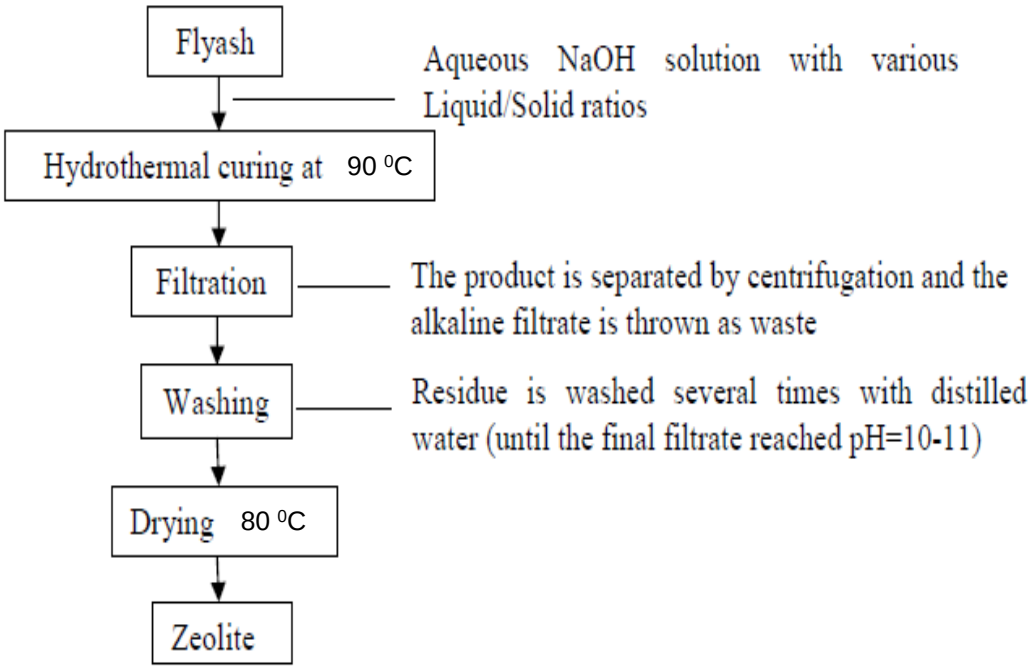

Figure 2-6: Flow chart of the 1-step hydrothermal process for zeolite synthesis from CFA (Jha and Singh, 2011)

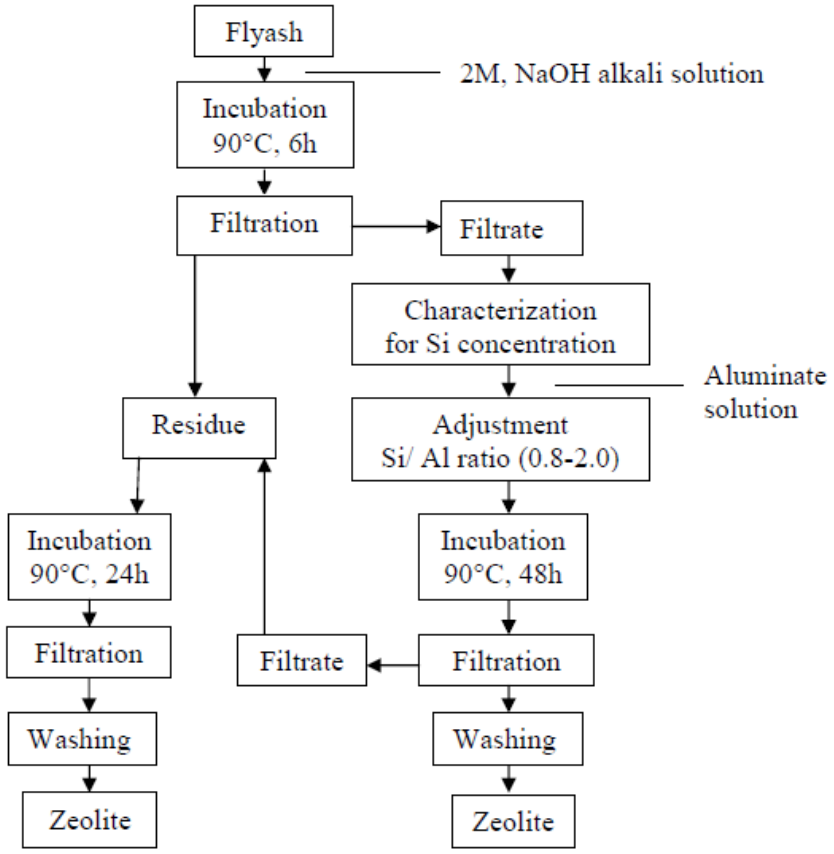

Figure 2-7: Flow chart for the 2-step process of zeolite synthesis from CFA (Jha and Singh, 2011)

The 2-step process was found to be more costly than the traditional 1-step process, however there is an advantage of using the 2-step process because it produces more “pure” zeolites (Hollman et al., 1999).

ii. Fusion assisted method

Shigemoto et al. (1993) were the first to investigate using a high temperature fusion step prior to the conventional hydrothermal treatment by fusing NaOH with CFA. It was found that a NaOH/CFA ratio of 1:1.2 and a fusion temperature of 550 ^{0}C were the optimum fusion conditions for zeolite synthesis, a flow chart of the synthesis method is depicted in Figure 2-8. It was found that by fusion with NaOH the majority of the CFA particles were converted into sodium salts, such as silicate and aluminate from which the proceeding hydrothermal reaction without stirring favoured the formation of Na-X.

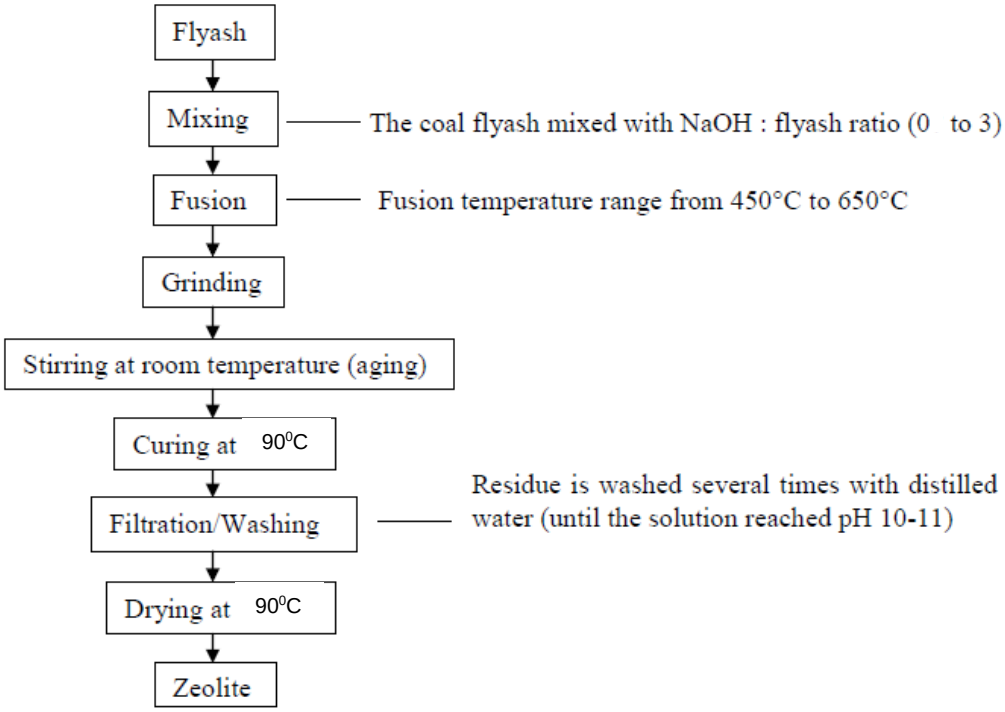

Figure 2-8: Flow chart of fusion assisted synthesis of zeolites from CFA (Jha and Singh, 2011)

The advantages of fusion pertains to factors such as increasing the conversion rate of the CFA, the BET surface area, increased CEC and crystallinity (Bukhari et al., 2015).

iii. Microwave assisted synthesis

Querol et al. (1997a) drastically reduced the activation time needed during hydrothermal conversion of CFA into zeolites using microwave assisted synthesis from 24-48 hours to 30 minutes. Inada et al. (2005b) explained the mechanism effecting zeolite synthesis from CFA, as will be explained further in detail in section 2.2.7. It was concluded that continuous microwave irradiation retards the formation of the zeolite in crystalline form, inhibiting it in the intermediate gel. An early stage of microwave heating however enhances the zeolite formation while heating in the middle stage significantly inhibits zeolite

formation. It was found that early stage microwave heating followed by conventional heating is effective in enhancing the zeolite formation from CFA (Inada et al., 2005b).

iv. Ultrasound assisted synthesis

Studies have been conducted by applying ultrasound after fusing CFA during the aging step of synthesis before hydrothermal synthesis to reduce the crystallisation time (Musyoka, 2012; Ojumu et al., 2016) and the temperature needed (Belviso et al., 2011; Ojumu et al., 2016) in hydrothermal synthesis. Musyoka et al. (2011b) also used mine waters during ultrasonic assisted synthesis namely, acid mine drainage and circumneutral mine water, as a substitute for pure water, also noting a reduction in synthesis time. There have also been studies using ultrasound as an in-situ technique to better understand the mechanism of CFA conversion to zeolites (Musyoka et al., 2012b; Musyoka et al., 2014) as will be discussed in section 2.2.6.

2.2.6. Mechanism of zeolite formation

There is a comprehensive article on the history and formation mechanisms of zeolite synthesis presented by Cundy and Cox (2005). It has been a subject of study for many years and is still not fully understood. The three main steps involved in zeolite formation according to Murayama et al. (2002a) are listed below.

i. the dissolution of Si^{4+} and Al^{3+} in the CFA,
ii. the condensation of silicate and aluminate ions in the alkali solution to make the aluminosilicate gel,
iii. the crystallisation of the aluminosilicate gel to form zeolite crystals.

The above process is presented pictorially in Figure 2-9, where (a) is the initial amorphous structure, (b) areas of local order are established, (c) the local orders grow by acquisition of building units from the solution, (d) the amorphous material dissolves to provide growth units, (e) supplies nutrients to both distant (i) and near (ii) growth sites, (f) all material converted to zeolites (Cundy and Cox, 2005). There has been a lot of effort to understand the zeolite formation process from pure analytical grade sources of silicon and aluminium but not as much effort has been focused on zeolite formation from CFA (Musyoka et al., 2012b). Therefore, the mechanism of zeolite formation will be discussed with reference to literature pertaining to the mechanism related to zeolite formation from CFA.

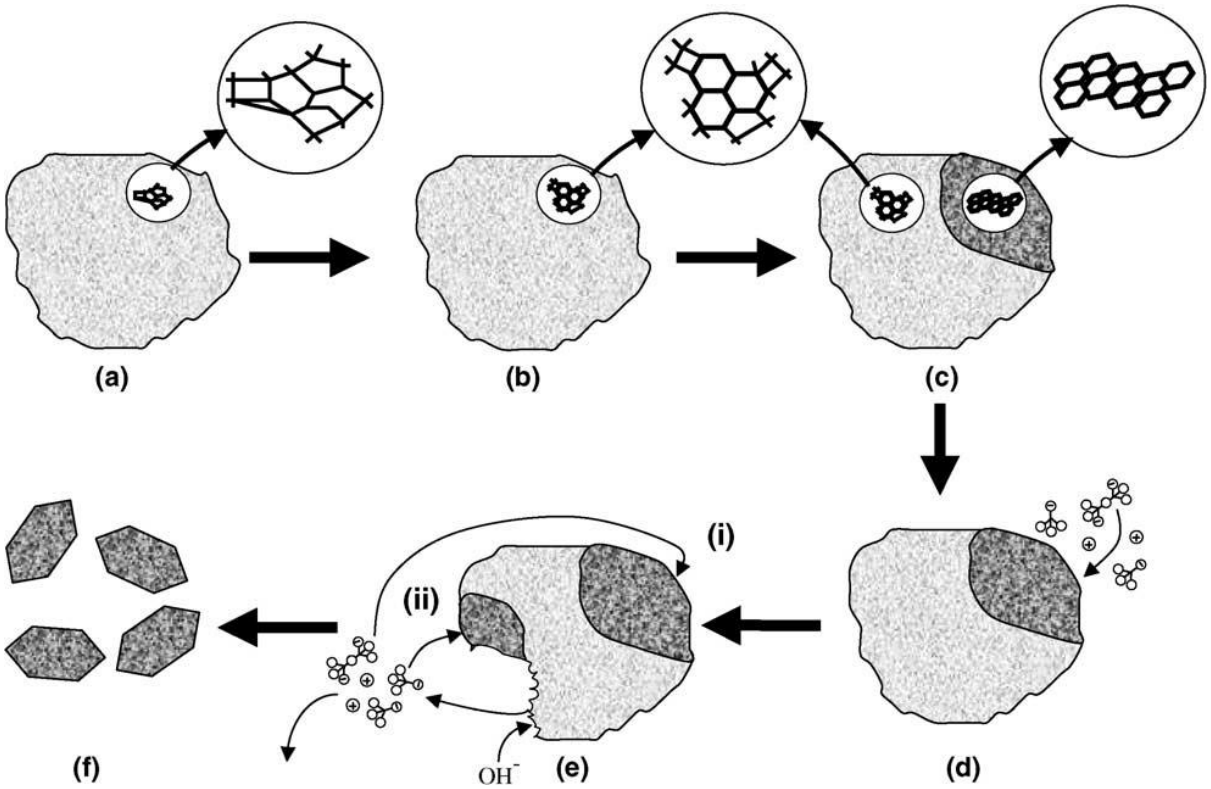

Figure 2-9: The progress from a gel particle to a crystalline zeolite (Cundy and Cox, 2005)

CFA is converted to zeolites by an alkali hydrothermal reaction of the aluminosilicates contained within the CFA, as mentioned previously (Bukhari et al., 2015). After the aluminosilicates have dissolved in the reaction mixture they cluster, nucleate and grow as crystals. The Si/Al ratio may vary locally within a sample but the average ratio can be adjusted to target a certain zeolite by addition of insufficient constituents (Bukhari et al., 2015), as will be explained further regarding one of the factors affecting zeolite formation in section 2.2.7. There are factors which make crystallisation from CFA different from normal zeolite synthesis in that in CFA the Si and Al are generally less reactive and also the presence of other cations can hinder or aid the crystallisation process (Bukhari et al., 2015). Musyoka et al. (2012b) reported that the zeolitization process should be studied for each type of zeolite independently, since, given the complexity of the starting composition of CFA, it is not expected that the process will always follow the same reaction pathways. The synthesis mechanism is also affected by the use of unseparated fly ash slurry in comparison to using a filtered clear solution after aging regarding the morphology of the zeolite formed (Musyoka et al., 2012b), the unseparated slurry contains residual fly ash particles which could be entrapped in growing the zeolite crystals. The Si/Al ratio of the unseparated slurry is expected to change over time given that more dissolution of the undissolved fly ash particles is expected to take place (Musyoka et al., 2012b).

Two recent studies by Musyoka et al. (2012b) investigated the zeolite formation mechanism using an in-situ ultrasound technique complemented by ex-situ techniques, for the formation of zeolite A, and zeolite X with a novel hierarchical morphology (Musyoka et al., 2014). For the synthesis of zeolite X

the clear solution from filtration of the fly ash slurry before hydrothermal synthesis was used in order to study the formation mechanism. Four regions were identified in both in situ studies, relating to the induction, nucleation, crystal growth and crystal stabilisation periods. During the induction period the zeolite precursor species undergo complex structural rearrangements and physiochemical changes leading to supersaturated conditions as the temperature increases (Musyoka et al., 2014). It is during this period that various processes including gel formation, dissolution and/or rearrangement of precursor species take place. The directing structure of the zeolite is found to be the cationic species in the reaction mixture, while the anionic species, such as the hydroxyl ions, help in catalysing the depolymerisation and polymerisation of the aluminosilicate species, regarding the breaking and remaking of the T-O-T bonds (T=Si or Al) (Musyoka et al., 2014). It was also found that gel formation was not a prominent process during the induction period of zeolite X. Regarding the nucleation stage there were minor fluctuations in the ultrasound signal which were ascribed to rapid interfacial changes taking place between nucleation sites in the condensation of the precursor species and their monomeric form however no significant changes in the signal were observed (Musyoka et al., 2014). Zeolite nucleation is a 'discreet chain of events' involving reversible condensation reactions associated with the formation and deconstruction of the T-O-T bonds leading to the establishment of sufficient ordered nucleation sites in preparation to the start of the crystal growth stage (Cundy and Cox, 2005; Musyoka et al., 2014). The period to obtain zeolite X with novel hierarchical morphology was found to be shorter than the time to obtain zeolite A crystals. This is attributed to the fact that zeolite X has a more complex structure with larger structural units (DR6) and a less dense structure than zeolite A, which is composed of DR4 structural units which are more condensed (Musyoka et al., 2012b; Musyoka et al., 2014).

2.2.7. Factors affecting zeolite formation

This section will discuss the physical and chemical factors which can affect zeolite formation from CFA. Some of the chemical factors include the SiO_2/Al_2O_3 ratio of the feedstock, the degree of depolymerisation or state of the precursor species (in solution or solid phase), the concentration of NaOH, the extraframework cations and the water content. The physical factors include the synthesis temperature, the synthesis time period and the effect of agitation.

2.2.7.1. Chemical factors

i. Effect of SiO_2/Al_2O_3 ratio in feedstock

Inada et al. (2005a) demonstrated how the zeolite crystallisation is dependent on the silica-alumina composition and also the alkaline conditions. It was found that zeolite Na-P1 was formed from a silica-rich fly ash, while hydroxysodalite formed from a silica-lean fly ash, the Si/Al molar ratio being controlled by addition of SiO_2 and Al_2O_3 aerosil powders. The Na-P1 zeolite is favoured due to its higher CEC value, therefore a Si-rich fly ash is preferable but if it cannot be acquired the Si/Al molar ratio would need to be controlled.

Querol et al. (1997b) postulated that the synthesis of zeolite NaP1 and analcime depends not on the SiO_2/Al_2O_3 ratio of the bulk fly ash but on the ratio found within the aluminosilicate glass since that phase is the first to be activated, which was also concluded in a later review article (Querol et al., 2002). Quartz was found to be digested after the first activation stage with mullite being digested in the last phase. It was found that, given the activation sequences, if the SiO_2/Al_2O_3 ratio is high in the glass fraction the first zeolite synthesised is analcime, while if it is low Na-P1 is synthesised instead.

ii. Degree of depolymerisation

As mentioned previously in section 2.2.6 concerning the formation mechanism of zeolites, the degree of depolymerisation of the precursor species plays an important role in zeolite synthesis. It is achieved by hydrolysis and dissolution of the silica followed by condensation of the aluminosilicate species which serves as the zeolite precursor (Cundy and Cox, 2005). The degree of depolymerisation concerns the hydrolysis of the most condensed form being the silicon centre bonded to the other T atoms though oxo-bridges, giving $Si(OT)_4$ (T= Si or Al). As depolymerisation takes place the T atoms are replaced by the hydroxyl groups until the least dense silicon centre is produced, known as a monomer, $Si(OH)_4$ with the most terminal hydroxyl groups. These small and soluble species serve as the precursor for the framework for zeolite synthesis through the condensation reactions which follow (Cornelius, 2015).

iii. Effect of NaOH concentration

Murayama et al. (2002b) investigated the synthesis of zeolites from CFA using various alkali sources such as NaOH, Na_2CO_3 and KOH. It was found that the amount of OH^- in an alkali solution makes a great contribution to the dissolution reaction regarding the formation mechanism mentioned previously in section 2.2.6. It was also found that the crystallisation rate of zeolite P was mainly controlled by the amount of Na^+ in the alkali solution.

According to Molina and Poole (2004) the concentration of NaOH affects not only the degree of zeolitisation but also the type of zeolite obtained as a product. It was noted that the difference in the product resulted from the increase in supersaturation achieved due to the higher proportion of soluble species with the rise of the NaOH concentration (Shigemoto et al., 1993; Molina and Poole, 2004). This relates to Ostwald's rule of successive transformation in that the higher the supersaturation the better are the conditions to nucleate metastable phases. For example zeolite X which later redissolves or recrystallizes and is replaced by the more stable and denser zeolite hydroxysodalite (Molina and Poole, 2004).

iv. Effect of extraframework cations

As mentioned previously regarding the effect of NaOH concentration, Murayama et al. (2002b) demonstrated that the crystallisation rate could be controlled by the amount of Na^+ in the alkali solution. It was shown that the cations can significantly alter the reaction to form one crystal over another with Na^+ ions promoting zeolite P and K^+ ions promoting the zeolite chabazite. It was noted in a review by Bukhari et al. (2015) of the intriguing nature that zeolite P and chabazite have completely

different frameworks and extraframework cations, as well as secondary building units and composite building units therefore proving the significance of the choice of cation in producing certain zeolites. It was also demonstrated how zeolite synthesis favours Na^+ ions over K^+ ions regarding enhancing the synthesis (Querol et al., 1995; Ríos et al., 2009). The reason Na^+ ions play such an important role in zeolitisation is because they stabilise the secondary building units of the zeolite frameworks, while K^+ ions act as a suppression factor due to their promotion of slow crystallisation rates and are known as structure breaking cations (Ríos et al., 2009).

v. Effect of water content

It is noted that an increase in water content results in an increase in yield when utilising CFA for synthesis. This is due to the increase in crystalline and amorphous dissolution rates with the increase of the water content (Querol et al., 1995; Querol et al., 2001). This poses disadvantages of high water consumption regarding zeolite synthesis. Therefore, there have been studies investigating the use of alternative sources of water during zeolite synthesis. Mainganye (2012) investigated the use of tap water, distilled water and AMD in replacement of ultra-pure water and found that tap water and distilled water obtained similar products as ultra-pure water. It was concluded however that AMD was not a suitable solvent for zeolite production. Musyoka et al. (2013) found that AMD yielded hydroxysodalite which is not favourable, however circumneutral mine water resulted in similar quality Na-P1 and X zeolites in comparison to ultra-pure synthesis.

Belviso et al (2010) conducted a study using seawater in place of distilled water where it was found that lower temperatures could be used during hydrothermal synthesis to synthesise zeolite X and ZK-5 from seawater. Hydroxysodalite was also formed using seawater however zeolite A could only be synthesised from distilled water. A later study revealed zeolites A and X could crystallise from a solvent of artificial seawater at room temperatures (25^0C) (Belviso et al., 2012).

2.2.7.2. Physical factors

i. Effect of temperature

Zeolite X formation is always competitive with hydroxysodalite, this is with reference to the synthesis temperatures, with zeolite X favouring lower synthesis temperatures due to its metastable behaviour, while the dominant phase at higher temperatures is hydroxysodalite, the higher temperature resulting in the denser phase of zeolite (Belviso et al., 2010; Boycheva et al., 2014). It is also generally accepted that the higher the temperature the larger the particle size of the zeolite (Molina and Poole, 2004). In order to promote and feed crystal growth silicon and aluminium need to be dissolved continuously and it has been found that the aluminium dissolution rate tends to be faster, with the dissolution of silicon being favoured with an increase in temperature (Molina and Poole, 2004). This means at higher temperatures the Si/Al ratio will increase and favour the formation of zeolite X over zeolite A.

Kim et al. (2009) used a step change in the heating source during zeolite synthesis. First conventional heating was used to transform most of the Si and Al species into zeolite A, enhancing the nuclei formation and forming the sodalite structures which further condensed to small zeolite A seeds. Then a second microwave irradiation was applied to increase the small zeolite A nuclei to larger zeolite A crystals, increasing the crystallisation rate.

ii. Effect of synthesis time

The results obtained by Boycheva et al. (2014) revealed a sequence in the thermodynamic stability of the crystallised zeolite forms from the investigated NaOH/FA mixtures at the settled synthesis conditions given as follows: Linde → Faujasite → Chabazite → NaP1 → Hydroxysodalite. It has been reported that the transformation of faujasite into more stable phases such as chabazite and NaP1 occurs at longer retention times of the crystallised phase in the reactant liquor (Ojha et al., 2004; Boycheva et al., 2014). It is also noted that the time needed to obtain a high synthesis yield is inversely proportional to the glass content of the CFA, as high glass contents CFA's are synthesised in short time periods while longer reaction times are needed for the same yield when using high quartz and mullite CFA's as feedstock (Querol et al., 2002).

iii. Effect of agitation

Mixing has an significant effect on zeolite synthesis as explained by Casci (2005), where if the viscous gel produced before the crystal growth step has inadequate mixing then an inhomogeneous reaction mixture could result. This inhomogeneous reaction mixture would have "pockets" of gel each having different compositions and each acting like a "mini-reactor" and generating phases correlating to that "mini-reactor's" composition. It is noted that although many lab scale synthesis of zeolites are carried out without mixing, there would be a need to incorporate mixing in large scale synthesis. This is problematic because the role of agitation in zeolite synthesis is not well understood due to many processes taking place during the course of crystallisation which mixing could affect such as (Casci, 2005):

- reagent dissolution,
- initial gel formation,
- maintaining a homogeneous gel,
- assisting with gel structure break-up,
- maintaining uniform temperature across the reactor,
- transferring "nutrients" to growing crystals,
- keeping the zeolite crystals in complete suspension on completion of the reaction.

A big factor in the above points is of course the drastic change in viscosity that can be experienced during synthesis, with the gel starting out as very viscous but by the end of synthesis having a viscosity closer to water (Casci, 2005). Another aspect of agitation is shearing, which can have a harmful effect on zeolite synthesis regarding the stability of the zeolite and the purity that can be synthesised as explained by Marrot et al. (2001). Different impellers were used by Marrot et al.

(2001) at different agitation speeds and it was found that the Archimedes screw impeller produced the zeolite with the highest crystallinity due to its low rate of shearing with the higher shearing impellers resulting in lower crystallinity. Mainganye et al. (2013) investigated the effect of agitation during the aging step of zeolite synthesis, mentioning that agitation during the hydrothermal treatment step may not be favourable regarding the stability and purity of the zeolite produced (Marrot et al., 2001). It was believed that shearing during the aging step of synthesis to facilitate the dissolution of the fly ash into the alkaline solution may favour zeolite formation thereafter. It was found that a 4-blade impeller was optimum for gel aging and dissolution during the aging step, which releases the precursors from CFA. The nature of the precursors that become available during aging then influenced the outcome of the zeolite synthesis during the hydrothermal step. It is noted however that it would be favourable to determine whether agitation during the hydrothermal step has a significant effect on the yield and purity of the zeolite formed when attempting the up-scale of zeolite synthesis from CFA.

2.2.8. Characterisation techniques

There are a number of characterisation techniques associated with zeolite synthesis. However, for the purposes of this study the relevant methods will be limited to five, namely XRF, XRD, FTIR, SEM and ICP-AES, which each will be discussed in this section. The techniques allow for the characterisation of the zeolite by giving information about the structure and morphology of the zeolite as well as the chemical composition.

2.2.8.1. X-ray fluorescence

X-ray fluorescence (XRF) is not only a well-established analytical technique but is one of the most versatile methods for elemental analysis (Jenkins, 1984). The basis of XRF concerns the relationship between wavelength, λ (or energy, E) of the X-ray photons emitted by the sample element and the atomic number, Z. Bombarding an atom with high energy particles could displace an inner orbital electron, leaving the atom in an excited state. The atom then can regain stability by the rearrangement of the atomic electrons, thus inner shell vacancies may be replaced by electrons from the outer shell, which leads to the emission of X-radiation (Jenkins, 1984). There is however a competing internal rearrangement process known as the Auger effect so not all vacancies result in the production of this characteristic X-radiation. The ratio of the number of vacancies resulting in the characteristic radiation to the total number of vacancies created in the excitation process is called the fluorescent yield (Jenkins, 1984). This can be used to identify an element and quantify it.

2.2.8.2. X-ray diffraction

X-ray diffraction (XRD) is an analytical technique used to identify crystalline structures and may also provide a semi-quantitative value of the structure's crystallinity (Rayalu et al., 2005). It is based upon the diffraction of X-rays off a crystal surface. A beam of X-rays is transmitted onto the crystal surface by a diffractometer and is diffracted by the crystal structure. These beams are always co-planar with the angle between them being 2θ (Cullity, 1956). The relationship may be mathematically represented by Bragg's Law as follows (Cullity, 1956):

$$\eta\gamma = 2dsin\theta \quad \text{…Equation 2-2}$$

Where,

- η is the order of reflection of any integer value,
- γ is the wavelength of the transmitted beam,
- d is the inter-planar spacing,
- θ is the diffraction angle.

The XRD analysis produces diffractograms which have different intensities of peaks at various degrees of 2θ which can be matched to known diffractograms of each unique mineral phase listed by the Joint Committee on Powder Diffraction Standards (JCPDS). A simulated diffractogram is shown in Figure 2-10. Using the diffractograms the percentage of each phase in a mixed phase sample can be calculated. It is done by measuring the area under each XRD peak. The sum of all these areas are then calculated with the total area being assumed to be 100%. Then the percentage of each phase could be calculated as follows (Dyer, 1988):

$$Percentage\ of\ crystalline\ phase\ (A) = \frac{sum\ of\ area\ under\ peaks\ of\ phase\ (A)}{total\ area} \times 100 \quad \text{…Equation 2-3}$$

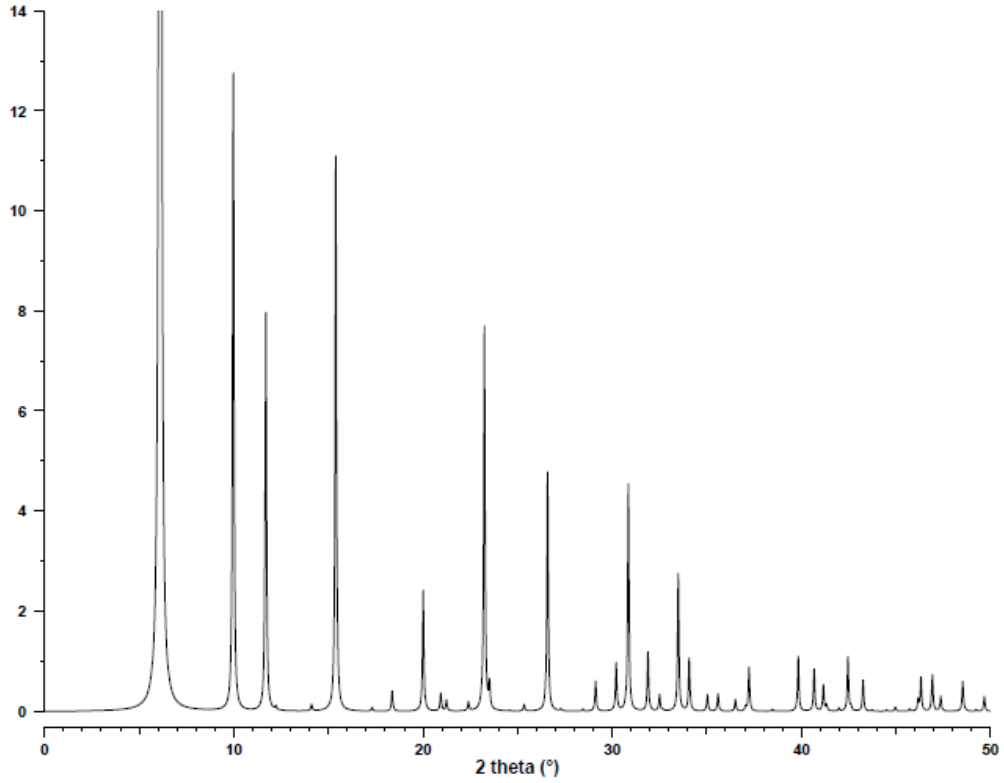

Figure 2-10: Simulated XRD powder pattern of zeolite X (Treacy and Higgins, 2007)

2.2.8.3. Fourier-transform infrared spectroscopy

Infrared spectroscopy is used to identify what functional groups are present in a molecule, giving its molecular structure, achieved through relating the produced infrared spectra to an existing database

of spectra that have been measured (Smith, 2011). Infrared spectra are plotted using the unit of wavenumbers abbreviated as cm^{-1}. The wavenumber measures the number of cycles a wave undertakes per unit length. Most infrared spectra are plotted from 4000 to 400 cm^{-1} on the x-axis with either % absorbance or % transmittance on the y-axis. Absorbance measures the amount of light absorbed by the sample which can quantify the concentration of the sample while % transmittance measures the percentage of light transmitted by the sample (Smith, 2011). An example of the infrared spectra is given in Figure 2-11 for a fly ash-based zeolite X and a commercial zeolite X.

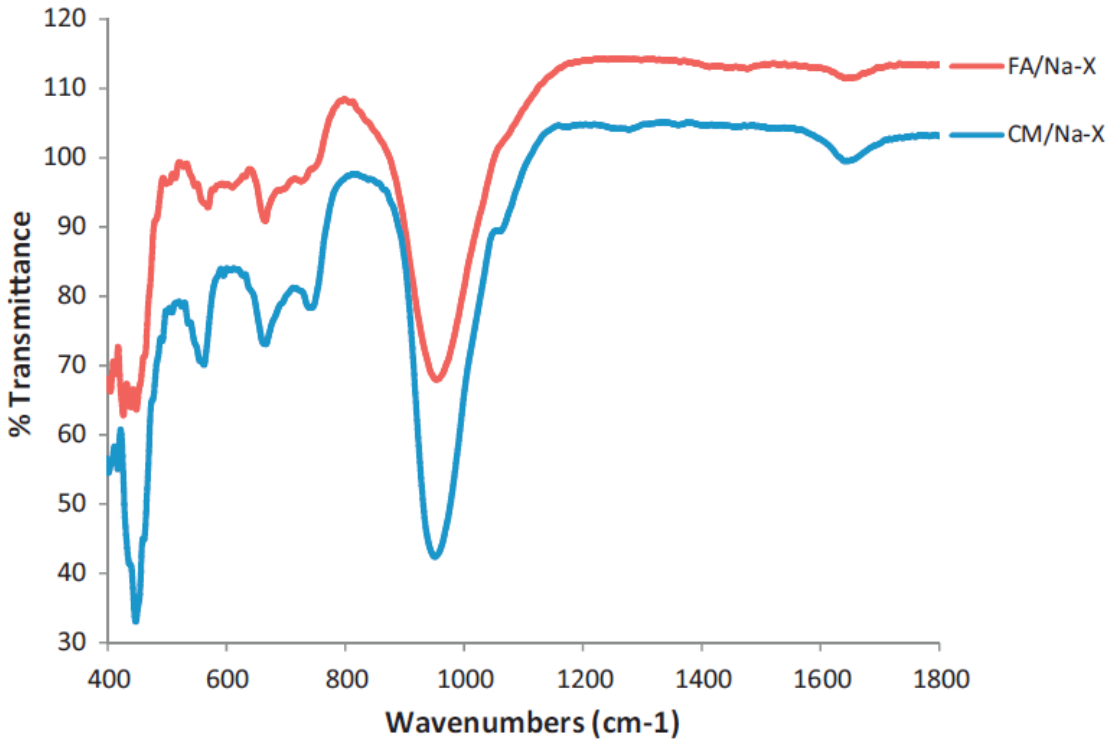

Figure 2-11: IR spectra of commercial zeolite X (CM/Na-X) and a fly ash synthesised zeolite X (FA/Na-X) (Babajide et al., 2012)

The above FTIR spectra relates the molecular structure to features such as TO_4 (where T stands for Si and Al atoms) and hydroxyl, OH^- of water molecules present as hydrate. Based on the size and type of cage, T-O stretching, bending and pore opening modes, each zeolite exhibits a different infrared spectrum which can be attributed to its asymmetrical and symmetrical stretches, broadening and narrowing in bending as well as the presence of distorted double ring (D2R) and six ring (D6R) and/or other vibrations without distortion i.e. 2R, 6R etc. (Jha and Singh, 2011). The IR spectra of common zeolite materials are given in Table 2-4 as well as the spectra specific for zeolite Na-X. The IR spectra of the monomeric species relating to the degree of depolymerisation is given in Table 2-5.

Table 2-4: FTIR frequencies and common modes of vibration for zeolites and zeolite X (Ojha et al., 2004; Fernández-Jiménez and Palomo, 2005; Jha and Singh, 2011)

Locations	**Type of vibration modes**	**Frequency range (cm^{-1})**
Internal tetrahedra	OH^- stretch	3700-3200
	OH^- deform (Bending)	1700-1600
	Assymetric stretch (Si-O-Si), (T-O) stretch	1250-950
	Symmetrical stretch (O-T-O) group	720-650
	(Si-O-Al), T-O bend	500-420
External linkage	Double Ring	650-500
	D6R units	640-630
	D4R units	730-720
	Pore Opening	420-300
	Symmetric stretch	820-750
	Assymetric stretch	1150-1050
Zeolite Na-X spectra		
Locations	**Type of vibration modes**	**Frequency (cm^{-1})**
External linkage	Double Ring	560 m
	Asymmetric stretch	1060 ms 971 s 746 m
	Symmetric stretch	668 m 690 wsh
	T-O bending	458 ms
	Pore Opening	406 w 365 m

s – strong; ms – medium strong; m – medium; w – weak; sh – shoulder

Table 2-5: FTIR frequencies relating to the degree of depolymerisation of the precursor species (Cornelius, 2015)

Degree of depolymerisation	**Frequency (cm^{-1})**
$Si(OH)(OT)_3$	1100-1050
$Si(OH)_2(OT)_2$	1000-950
$Si(OH)_3(OT)$	900
$Si(OH)_4$	850

T = Si or Al atoms

2.2.8.4. Scanning electron microscopy and energy-dispersive spectrometry

Scanning electron microscopy (SEM) is used to observe the morphology of the zeolite and the raw CFA. It allows for the observation and characterisation of heterogeneous organic and inorganic materials on the nanometer (nm) to micrometer (μm) scale using a focused beam of electrons to irradiate the sample (Goldstein et al., 2012). The popularity of SEM is that it gives three-dimensional like images of a wide range of materials. Regarding fly ash particles, SEM micrographs reveal spherical particles of size 50-80 μm with also hollow broken spheres (Jha and Singh, 2011). Figure 2-12 shows the SEM images of the hierarchical zeolite X at varying magnifications. The scanning electron microscope can also be used to obtain an elemental analysis of the sample using characteristic x-rays. This is with the addition of an energy-dispersive spectrometer (EDS) to the SEM. A modern EDS is capable of detecting characteristic x-rays of all elements above atomic number 4 (Goldstein et al., 2012).

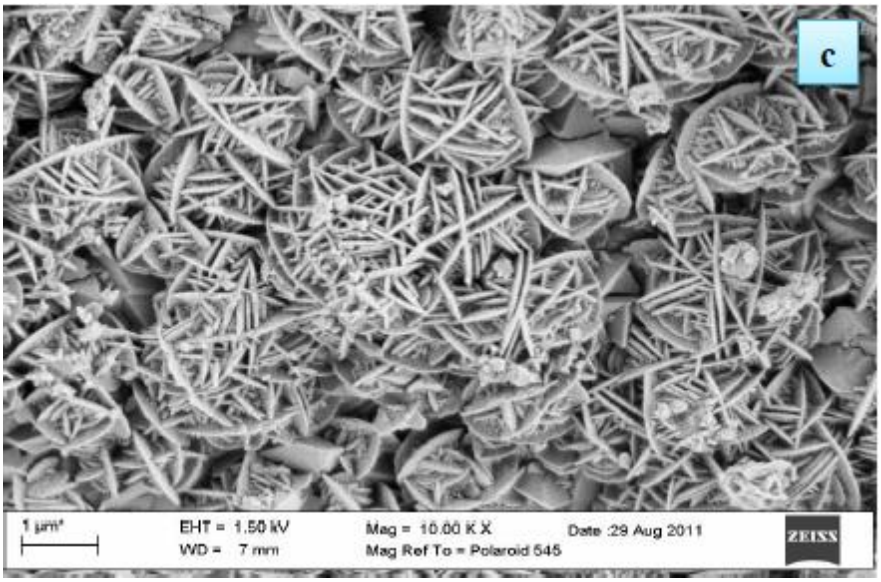

Figure 2-12: SEM micrograph of the hierarchically structured zeolite X

Taken from Musyoka (2012)

2.2.8.5. Inductively coupled plasma atomic emission spectroscopy

Inductively coupled plasma atomic emission spectroscopy (ICP-AES) works on the same principles as XRF except that it is a technique used for liquid samples, while XRF is used for solids, as described in section 2.2.8.1. ICP is based on the principle that excited atoms or ions emit radiation of a characteristic wavelength when electrons return to lower energy orbitals after being excited to higher energy orbitals (Moore, 2012). Therefore with each element having a unique electronic configuration its emission spectrum is unique and can be identified and quantified using ICP-AES (Moore, 2012).

2.2.8.6. Ultraviolet visual spectroscopy

Ultraviolet visual spectroscopy (UV – Vis) concerns the range of the of the light spectrum in the ultraviolet (UV) and visible (VIS) region from 200 nm to 800 nm. It occupies only a very narrow

frequency region with the energy differences corresponding to the electronic states of atoms and molecules (Perkampus et al., 2013). The mathematical basis of the light absorption in the UV – Vis region is given by the Bouguer-Lambert-Beer law:

$$lg\left(\frac{I_0}{I}\right)_{\tilde{\nu}} = lg\left(\frac{100}{T(\%)}\right)_{\tilde{\nu}} \equiv A_{\tilde{\nu}} = \varepsilon_{\tilde{\nu}} \cdot c \cdot d_i \quad \text{…Equation 2-4}$$

Where $A_{\tilde{\nu}}$ is the absorbance, $T_{\tilde{\nu}}$ is the transmittance and $\varepsilon_{\tilde{\nu}}$ is the molar decadic extinction coefficient. I_0 is the intensity of the monochromatic light entering while I is the intensity of the light which emerges from the sample. The concentration of the light absorbing substance is given by c while d_i is the pathlength of the sample in cm (Perkampus et al., 2013).

2.3. Hydrodynamic cavitation

Cavitation is increasingly being studied as an alternative source of energy for chemical processes due to it being able to create high temperatures and pressures or “hot spots” under nearly ambient conditions which provides effective mixing of substances (Moholkar et al., 1999). Until recently only ultrasound was studied relating to acoustic cavitation, in which ultrasound generates, grows and collapses the cavities in a relatively short amount of time (microseconds). There is hardly any process carried out on an industrial scale though due to the lack of expertise required in diverse fields such as material science, acoustics, chemical engineering etc. for scaling up the lab scale processes (Moholkar et al., 1999). A cheaper alternative is hydrodynamic cavitation. In this process cavitation is generated by the flow of a liquid under controlled conditions through obstructions such as venturi tubes and orifice plates. When the pressure at the throat falls below the vapour pressure of the liquid, the liquid flashes and generates a number of cavities, which then collapse when the pressure is recovered downstream of the mechanical constriction (Moholkar et al., 1999; Jyoti and Pandit, 2001; Gogate and Pandit, 2005). This can be represented pictorially in Figure 2-13.

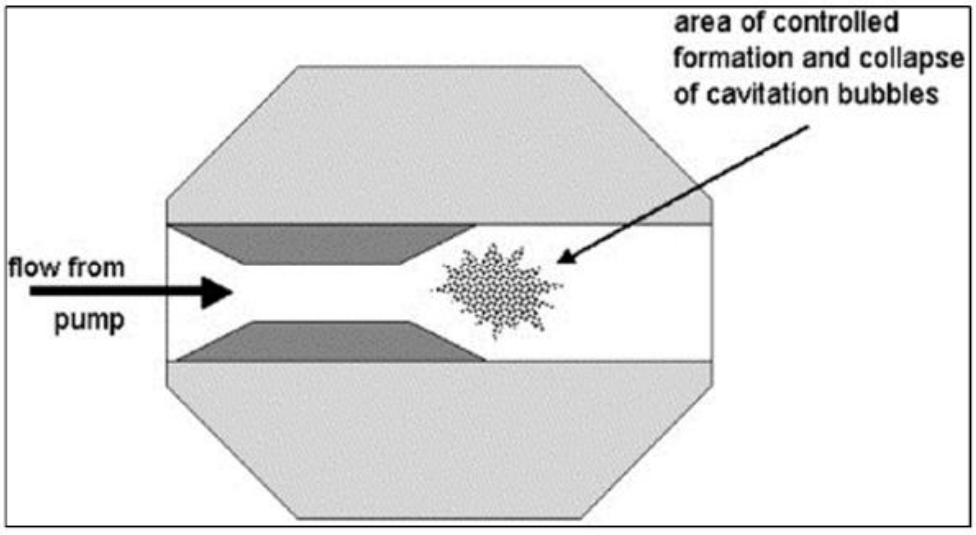

Figure 2-13: Pictorial representation of hydrodynamic cavitation (Madzivire, 2012)

Hydrodynamic cavitation has been applied to disinfect water (Jyoti and Pandit, 2001) but more recently was used in a study to treat AMD by using CFA, lime and aluminium hydroxide (Madzivire et al., 2013). It was found that the impingement and cavitation mixing techniques employed in the jet loop system played an important role in enhancing sulphate removal. What has not been published is using the jet loop system and hydrodynamic cavitation as a method of mixing the CFA with sodium hydroxide and water as a pre-synthesis to replace the high energy requirement of the fusion process to produce zeolites, as will be explored in this study. A study was performed by Nyale (2014) where the jet loop system was used to synthesise geopolymers. The best conditions for preparing the fly ash based geopolymer was a mass ratio of 1:1:5 of fly ash:NaOH:H_2O and 180 minutes of jet loop mixing followed by hydrothermal treatment at 80^0C for 5 days.

A jet loop system was proposed as an alternate and more economical route for the pre-treatment of fly ash with sodium hydroxide and water to replace the high temperature fusion method most predominantly used before aging and hydrothermal synthesis. The jet loop employs the use of cavitation of which there are two kinds, acoustic cavitation and hydrodynamic cavitation with the jet loop employing the latter as well as impingement. Cavitation is the generation, growth and collapse of cavities creating energy densities of 1-1018 kW/m^3 as explained previously. The set-up and running of the jet loop system is described in detail in chapter 3.

2.4. Material balances

Examples of mass or material balances rely on the principle or law of the conservation of mass, which states that matter can neither be created nor destroyed (Himmelblau and Riggs, 2004; Felder and Rousseau, 2005). These examples include statements such as “total input = total output”. This is fundamental to the design of new processes which is not complete without the inputs and outputs of the entire process and each individual unit satisfying these balanced equations (Felder and Rousseau, 2005). Processes can be clarified as batch, continuous or semi batch and can be either in steady state or transient. Zeolite synthesis resembles a batch process where feed is fed into a vessel and the contents are removed at a time later with no mass or material crossing the system boundary within this time (Felder and Rousseau, 2005). The system is an arbitrary portion of, or a whole process, to be analysed. Batch operations are by their nature transient or un-steady state processes due to there usually being changes in temperature, pressure and volume over time. These balances can be performed around single process units, or multiple units or the entire process and is written in the following way:

INPUT + GENERATION - OUTPUT - CONSUMPTION = ACCUMULATION …Equation 2-5

Where the input is what enters through the system boundary, generation is what is produced within the system, output is what leaves through system boundary, consumption is what is consumed within the system and accumulation is the build-up within the system (Felder and Rousseau, 2005).

Batch processes concern what is known as integral balances where the balances describe what happens between two instances of time, where each term is the amount of the balanced quantity

(Felder and Rousseau, 2005). Equation 2-4 can be simplified if the quantity measured is mass, in that the terms of generation and consumption can be set to 0 because mass can neither be created nor destroyed except in nuclear reactions. Flowcharts or block flow diagrams (BFDs) are set up to represent the material balances as can be seen in Figure 2-14 showing the synthesis of zeolites from the fusion method. The system boundary is represented as dashed lines, the red dashes for the overall balance around the whole process and the green dashes for a balance around a specific unit.

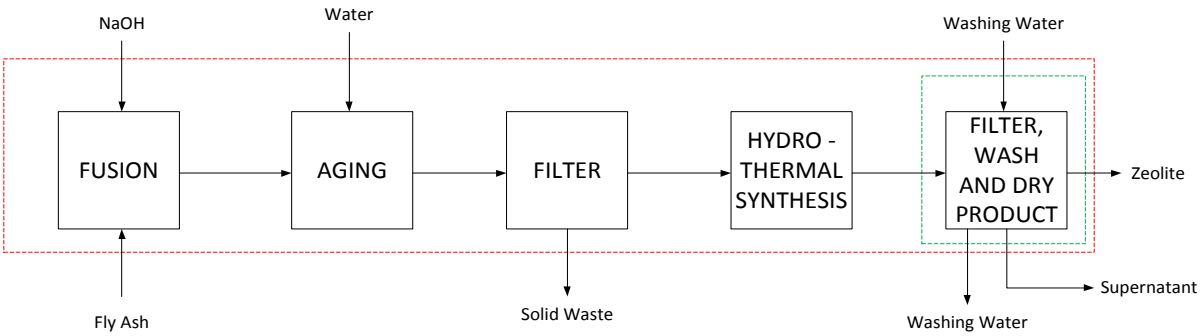

Figure 2-14: BFD of fusion method of zeolite synthesis from fly ash showing the overall system boundary (red) and a unit's boundary (green)

The first step in the balancing of a process is to choose a basis of calculation of which is an amount in mass or moles or a flow rate in mass or moles of one stream or stream component in a process with all the unknown variables being determined in relation to the basis (Felder and Rousseau, 2005). Regarding a previous material balance study concerning producing zeolites from fly ash, it was noted that a sufficient stream to choose for a basis is that of the feed of the fly ash into the process, given that it can be easily controlled (Du Plessis, 2014).

Material balances can be performed using mass, moles, mass fraction, mole fraction and flow rates and these can be applied to an overall balance around the system, or a component balance of the species, or an elemental balance of the actual elements (Himmelblau and Riggs, 2004). An overall balance deals with the total flow rate or mass of the stream concerned, while if the streams has more than one component a component balance can be conducted for just that species, for example, sodium hydroxide. An elemental balance can be conducted for each specific element within all the streams, such as sodium, hydrogen or oxygen (Himmelblau and Riggs, 2004).

The choice of material balance regarding zeolite synthesis from fly ash is an elemental one. This is because it is of importance to identify where certain elements report to in the synthesis. It is essential to know the amount of silicon and aluminium within the feed stream to ascertain the Si/Al ratio which is an important factor to zeolite synthesis as mentioned previously in section 2.2.7.1. Also for environmental concerns, it is important to know the composition of the waste streams in order to clarify if the waste can be recycled or whether it poses a threat to the environment, or contains valuable elements which can be extracted. To obtain comprehensive material balances analytical techniques such as XRF and ICP-AES can be used as XRF can give the elemental compositions of

solid samples while ICP-AES can be used for elemental analysis of liquid samples, as mentioned in sections 2.2.8.1 and 2.2.8.5 respectively.

2.5. Gaps in the literature concerning scale-up of zeolite synthesis

The studies that have investigated zeolite scale-up synthesis recently from South African CFA have focused on the zeolites NaP1 and A (Mainganye, 2012; Du Plessis et al., 2013; Mainganye et al., 2013; Du Plessis et al., 2014; Du Plessis, 2014; Brassell et al., 2016). What has not been investigated is the synthesis of the faujasite zeolite (zeolite X), which could prove more beneficial given that this zeolite is important, being widely employed on industrial scale and used extensively as a fluid catalytic cracking catalyst for refining oil and as materials for adsorbing and removing gaseous emissions (Liu et al., 2013). Indeed the novel finding of the zeolite X with novel hierarchical morphology synthesized by Musyoka (2012) in a recent study would be even more favourable. This novel hierarchical pore structure allows the zeolite to have maximum structural functions in a limited space and volume, thus producing a high degree of diffusion efficiency (Liu et al., 2013).

With recent work concerning the use of a jet loop system along with curing in the production of geopolymers it is reasoned that the same method can be used as an alternative method for pre-synthesis in zeolite synthesis (Nyale, 2014). Although previous work has highlighted the efficiency of using ultrasonication for the pre-synthesis method of zeolite synthesis, it can be argued that the feasibility to scale-up these ultrasonic techniques might prove challenging (Brassell et al., 2016). This is all in regard to replacing the high temperature fusion pre-synthesis technique, which would not be feasible to scale-up to an industrial scale. If a pre-synthesis technique can be explored which incorporates a jet loop pilot plant system followed by low temperature curing of the slurry produced this may prove to be a more feasible process to scale-up.

2.6. Chapter summary

This chapter highlighted the necessary literature pertaining to the basis of this study. This included literature on CFA regarding all its aspects concerning its physical and chemical nature as well as the environmental concerns relating to its disposal in ash dumps. Applications of the CFA were touched upon leading to the application concerned in this study regarding zeolites. This led to a detailed literature study on zeolites and their synthesis from CFA, as well as their applications in industry. Reference work was included regarding the history of zeolite synthesis and zeolite synthesis from CFA. Some of the methods were highlighted of zeolite synthesis from CFA and the formation mechanism was discussed. The chapter also gave literature on the analytical techniques used in this study relating to zeolite and CFA characterisation. There was also a section on the jet loop system to be used in this study regarding its effect of hydrodynamic cavitation. Literature on material balances was discussed as they will be used in this study to determine the fate of the elements in the zeolite synthesis relating to this study. And lastly the gaps which were seen in all the literature reviewed were highlighted in the attempt to justify the need for this study going forward. The following chapter will highlight the experimental and analytical techniques used in this study.

CHAPTER 3

3. Experimental

3.1. Experimental approach overview

The experiments were planned on a successive route where each set of experiments built upon the results of the previous. The two main steps were the pre-synthesis followed by the hydrothermal synthesis step. The pre-synthesis step involved comparing the fusion and aging techniques and the hydrothermal synthesis involved finding the best conditions for hydrothermal treatment. The first of these experiments was the base case study of reproducing Musyoka's (2012) work. This involved a pre-synthesis procedure including fusion and aging and a hydrothermal treatment based on Musyoka's (2012) conditions for the preparation of zeolite X from South African coal fly ash. The synthesis time was optimised given the differing nature of the starting fly ash.

The second stage of experiments involved changing the pre-synthesis conditions but keeping Musyoka's (2012) hydrothermal synthesis conditions that were optimised. The pre-synthesis conditions in this stage used jet loop treatment at varying mixing times and curing times based on Nyale's (2014) study. During jet looping samples were collected after 30, 60 and 90 minutes and each cured at 80 ^{0}C for 0, 3 and 5 days. The cured samples produced were then stirred briefly by hand before being filtered. The optimal jet loop mixing time and curing duration was obtained through analysis of the solid residue and filtrates produced. The filtrates were collected after no curing, curing after 1 day at 80^{0}C and 4 days at room temperature, curing for 3 days at 80^{0}C and curing for 5 days at 80^{0}C. This was done to see if the extra energy required by curing at 80^{0}C could be reduced. Once the optimum dissolution of silicon and aluminium was achieved the conditions were repeated in an attempt to synthesis zeolite X using the same hydrothermal synthesis conditions optimised in the previous stage of experiments. This included an adjustment of the Si/Al ratio and an attempt to optimise the synthesis time for zeolite X. The experimental outline is shown in Figure 3-1.

Material balances were conducted around the fusion process and the jet loop process for synthesis of zeolite X. This was to determine the fate of the elements for these two synthesis routes to serve as a comparison. A material balance was first conducted for the fusion assisted process concerning the fusion, aging, filtering and finally hydrothermal process followed by filtering and washing of the zeolite product produced. A material balance was then conducted around the jet loop pilot plant. An overall balance around the whole jet loop and hydrothermal processes could not be achieved as the filtrate produced from the jet loop system was too large a volume to be processed all at once in the containers used for hydrothermal treatment. Thus a balance was first conducted around the jet loop system and then a separate balance was conducted around the curing and filtering of the slurry

produced. Ratios were then used to quantify the percentage of elements from the original fly ash that reported to the residue; and to the filtrate used for hydrothermal synthesis, while also taking into account the amount of material lost within the overall process.

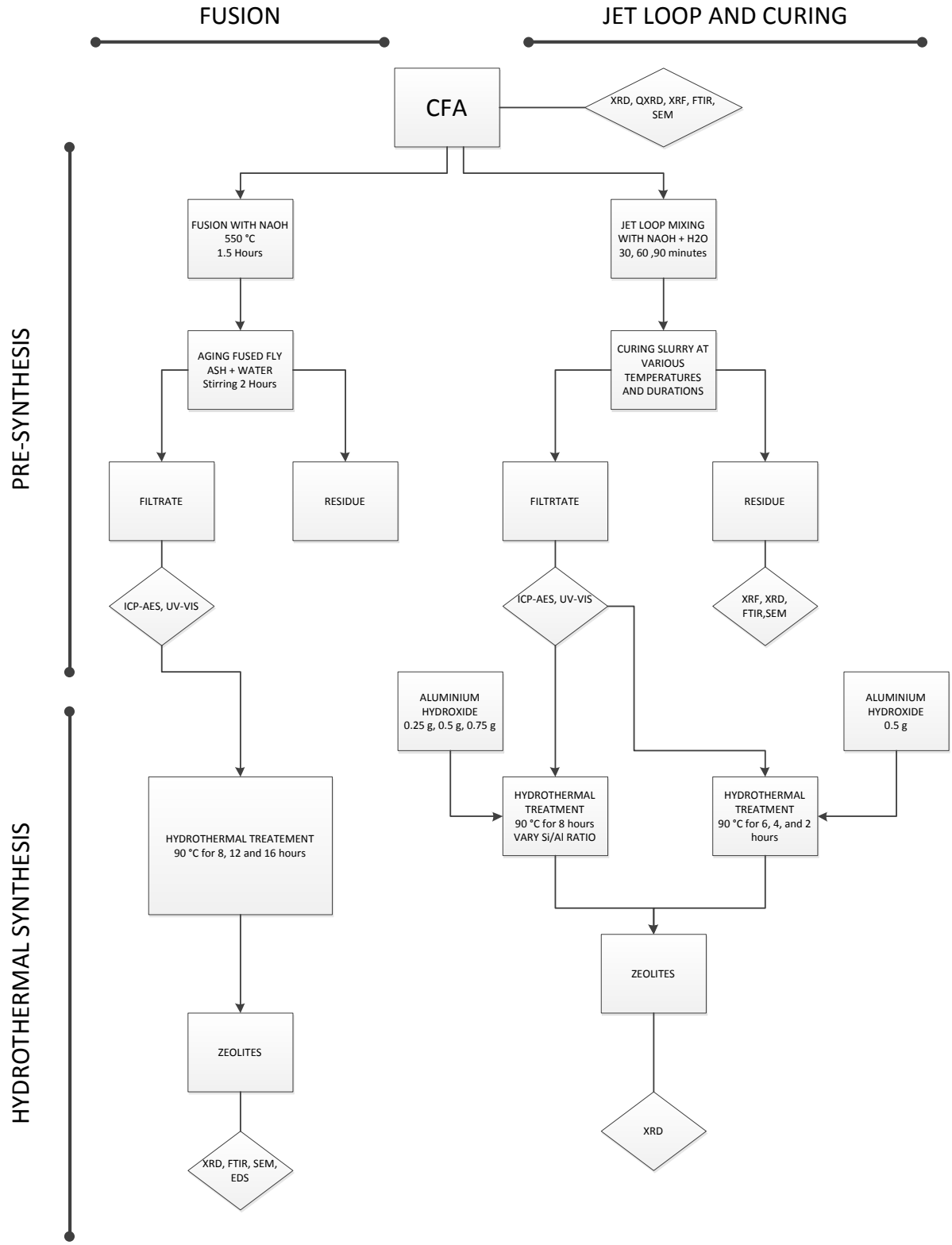

Figure 3-1: Experimental outline

3.2. Materials and chemicals

3.2.1. Fly ash source and handling procedure

The South African coal fly ash used was collected from a power station known as Arnot in the Mpumalanga province. It was stored in sealed containers throughout its use and special care was taken to wear the appropriate face masks and goggles when handling the fly ash. This is due to the particulates in the fly ash which could be inhaled and cause illness (Borm, 1997). The containers were sealed and stored away from sources of moisture and out of direct sunlight to maintain the CFA's initial composition (Musyoka et al., 2011a; Mainganye, 2012).

3.2.2. Chemicals used

All the chemical reagents used in this study are listed in Table 3-1.

Table 3-1: Chemicals used in this study and their supplier

Chemicals	Supplier	Purity
Sodium Hydroxide pellets	Merck Chemicals	Min. 98.00%
Nitric Acid	B & M Scientific cc.	55.00%
Sulphuric Acid	Sigma - Aldrich	95.0-97.0%
Aluminium Hydroxide	Kimix	96.00%
Ammonium Heptamolybdate Tetrahydrate	Fluka	99.00%
Oxalic Acid	Kimix	99.80%
Ascorbic Acid	Kimix	99.00%
Sodium Metasilicate	Rochelle Chemicals	C.P.*

*C.P. = Chemically pure

3.3. Experimental approach for base case zeolite X synthesis

The experimental work was started with a base case study of zeolite X synthesis based on Musyoka's (2012) work which was used to compare the optimization studies. This involved an alkali fusion of the coal fly ash with NaOH followed by an aging step and finally the hydrothermal synthesis.

3.3.1. Preparation of alkali fused fly ash

The fusion step was performed in a furnace at 550^0C for 1.5 hours, with a fly ash to NaOH ratio of 1:1.2, the furnace can be seen in Figure 3-2. The resulting product from the fusion was allowed to cool and ground to a fine powder with a mortar and pestle.

Figure 3-2: Furnace used for alkali fusion of fly ash

3.3.2. Synthesis of zeolite X from fly ash

The aging step was performed by adding 80 g of the fused fly ash to 200 mL of ultrapure water in a 1:2.5 solid to liquid ratio and stirring with a magnetic stirrer at 300 rpm in a 250 mL Erlenmeyer flask as seen in Figure 3-3. The slurry after aging was filtered and only the separated filtrate was used during hydrothermal synthesis while the residue was discarded.

Figure 3-3: Aging step of base case study

Figure 3-4: Hydrothermal synthesis of base case study

The filtrate was placed inside a plastic container (250 mL), sealed tightly, and placed in an oil bath controlled by a temperature probe at 90^0C for 8 hours, 12 hours and 16 hours, as seen in Figure 3-4, so as to determine the optimal hydrothermal synthesis time. A magnetic stirrer was placed inside the oil bath and inside the plastic container to allow for uniform distribution of temperature through the oil and stirred hydrothermal synthesis vessel respectively. After the hydrothermal treatment the product was filtered and washed with ultrapure water and the resulting solid product was allowed to dry overnight and then ground into a fine powder for analysis.

3.3.3. Material balance for zeolite X synthesis from fusion process

A material balance was conducted for zeolite X synthesis, which included the fusion process and zeolite synthesis detailed in sections 3.3.1 and 3.3.2 from the optimum hydrothermal conditions of 8 hours at 90^0C. All the streams in and out of the process were weighed so as to perform an overall material balance. An attempt was then made at an elemental balance by analysing the elemental compositions of all the streams. All solid samples were characterised with XRF while the liquid samples were characterised with ICP – AES.

3.4. Experimental procedure for jet loop pre-synthesis

A jet loop system was used to replace the high temperature fusion process used in the previous base case study. This section highlights its set-up and the materials used. It included an experiment to determine the optimal jet loop mixing time and curing time. A mass balance was also performed around the jet loop as a comparison to the one performed from the fusion method. An attempt was then made to synthesis zeolite X from the jet loop filtrate produced after curing and further mixing the jet loop slurry. The jet loop pilot plant was used previously in a study by Madzivire et al. (2013) except in that case it was used for the treatment of mine water with fly ash and aluminium hydroxide which highlighted the superior mixing in the jet loop system. The jet loop was also used in a study by Nyale (2014) for the synthesis of geopolymers from South African fly ash. The jet loop experiments

followed the procedure used in Nyale's study, which will be explained further in section 3.4.1 and 3.4.2.

3.4.1. Experimental set-up and materials

An 80 litre jet loop pilot plant was used in this study, as can be seen in Figure 3-5. It consisted of an 80 litre tank, a centrifugal pump, piping system and the jet loop mixing "reactor" seen in more detail in Figure 3-6. For the purpose of this study 3.2 kg of CFA was mixed with 3.2 kg of NaOH and 16 litres of tap water in a 1:1:5 mass ratio of CFA:NaOH:H_2O for 30, 60 and 90 minutes and cured for up to 5 days at 80^0C as proposed in Nyale's (2014) study. The process flow diagram (PFD) is shown in Figure 3-7.

Figure 3-5: Set-up of jet loop pilot plant (Madzivire, 2012)

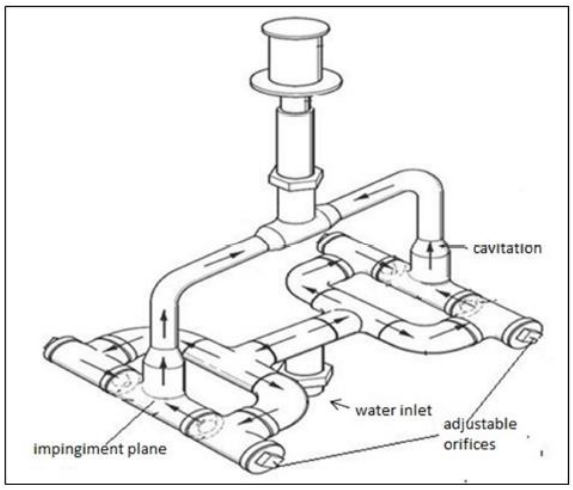

Figure 3-6: Schematic representation of the flow of slurry within the jet loop mixing "reactor" (Madzivire, 2012)

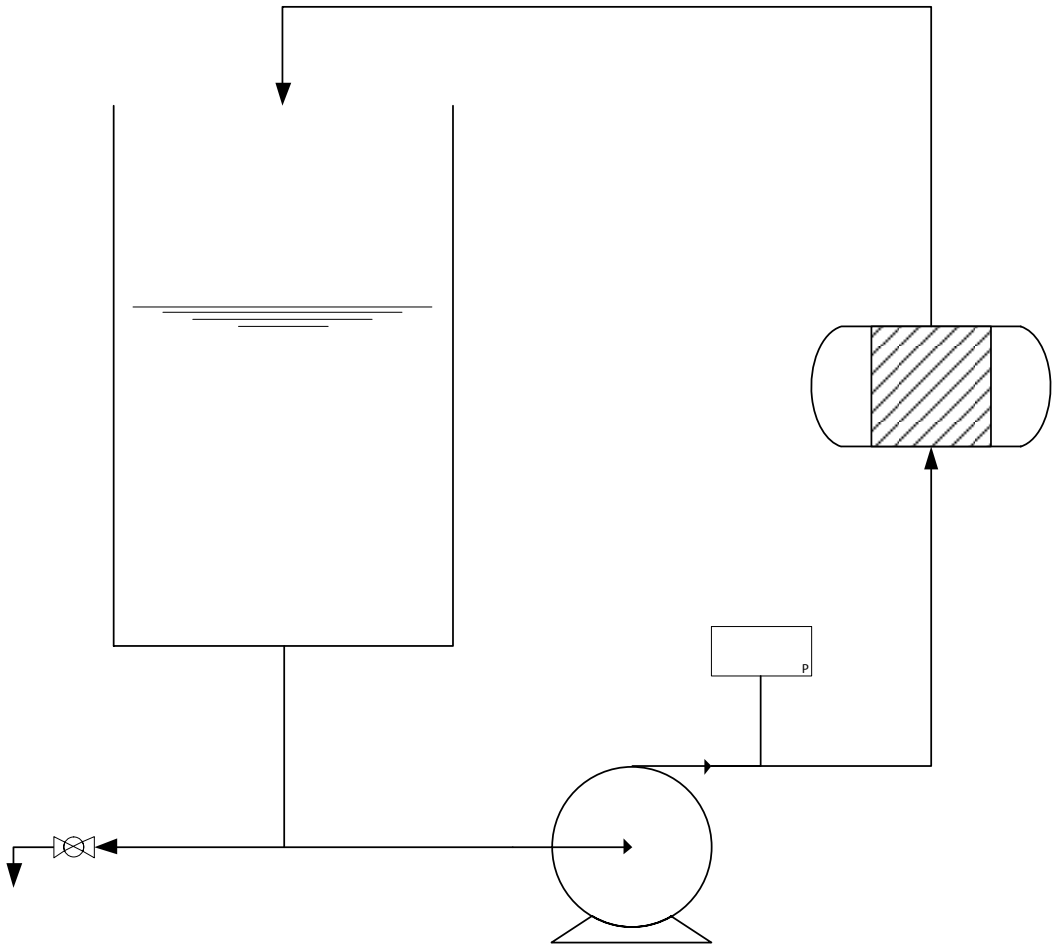

Figure 3-7: PFD of jet loop pilot plant

The hydrodynamic cavitation effect outlined in section 2.3.1 allowed for the dissolution of the amorphous and mineral phases in the fly ash allowing for the release of the silicon and aluminium needed for zeolite synthesis from the fly ash. This was achieved through passing the slurry through the orifices as shown in Figure 3-6 where the mixture's kinetic energy decreased as it is forced through the orifice. When it comes out of the orifice the kinetic energy increases while the pressure decreases causing bubbles to form, grow and collapse as seen in Figure 2-11 (Madzivire, 2012). Also seen in Figure 3-6 are the mixing techniques of impingement. Impingement concerns the collision of two streams of high kinetic energy (Madzivire, 2012).

The freeze drying used in this study was carried out using the machine represented in Figure 3-8, showing a condenser, a heating chamber and a vacuum pump. The process is also known as lyophilisation and is used when the chemical and physical state of a substance is to be preserved. First the substance is frozen and then the surrounding pressure is reduced under vacuum which causes the frozen water to sublimate when heated to room temperature. The freeze drying reduces the quantity of water or solvent first by sublimation, the primary drying, and then by desorption, the

secondary drying, such that biological growth and chemical reactions are no longer supported (Nyale et al., 2014).

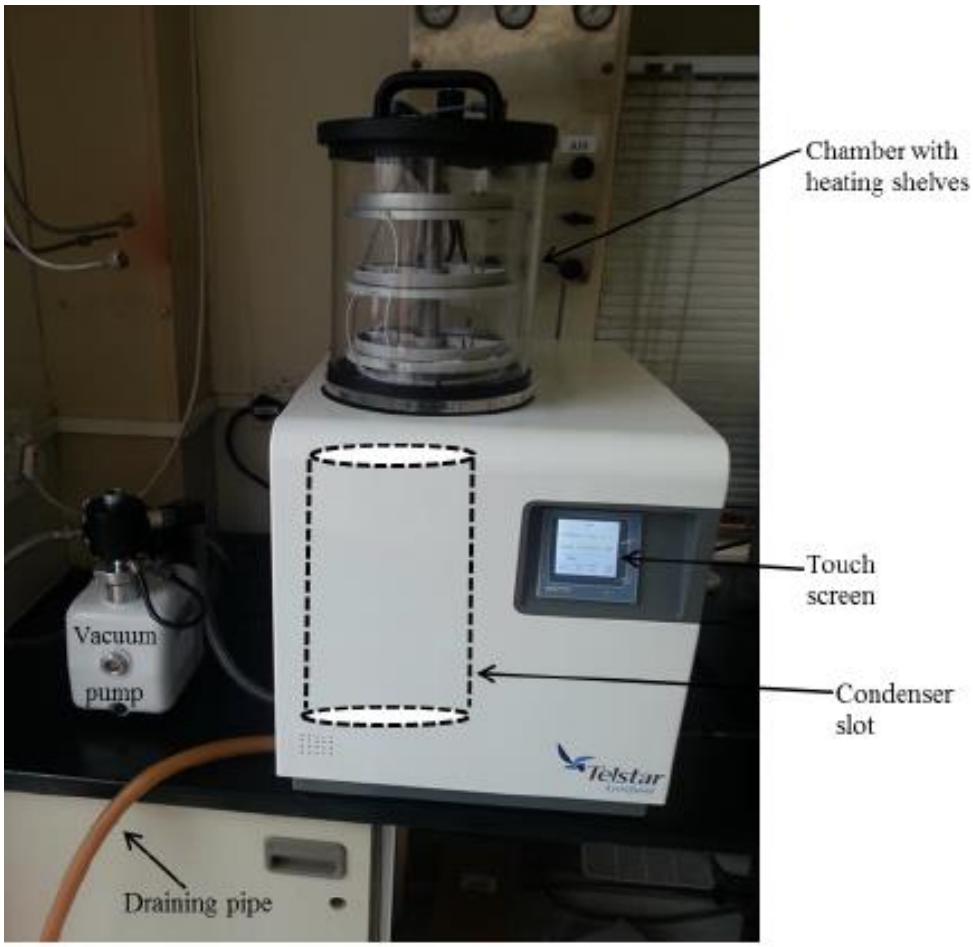

Figure 3-8: The set-up of the freeze drying machine (Nyale, 2014)

3.4.2. Effect of jet loop mixing time and curing of samples

The experiment was carried out according to the methods of Nyale (2014). Therefore, samples were taken after 30, 60 and 90 minutes of jet-looping. The starting materials were as previously mentioned (3.2 kg CFA; 3.2 kg NaOH; 16 L H_2O) in mass ratio of 1:1:5 of CFA:NaOH:H_2O as was used in Nyale's study. The samples were then cured for 5 days with analysis being performed on the solid residues without curing, curing after 3 days and curing after 5 days. The filtrate samples were collected after no curing, or curing for 1 day at 80^0C followed by 4 days curing at room temperature, or curing at 80^0C for 3 days or curing at 80^0C for 5 days. The slurries produced after curing were stirred briefly by hand before the filtration step. The analysis included ICP – AES and UV - Vis analysis on the filtrates produced and FTIR, XRD, SEM and XRF analysis on the solid residues produced. The filtrates after curing could then be compared with the original jet loop filtrate produced prior to curing to see the effect that curing had on pre-synthesis dissolution of the fly ash matrix. The amount of silicon and aluminium produced could then also be compared to the amount produced via the fusion step pre-synthesis. The solid residue samples were examined to determine the effect of curing using

FTIR and XRD analysis. For the jet loop experiments tap water was used in the jet loop instead of ultra-pure water as it would have proven to be costly to use ultra-pure water on this scale. The experiments are represented in Table 3-2.

Table 3-2: Experiments for jet loop study

Pre-synthesis		
Jet loop mixing	Curing	
	Residue analysis	Filtrate analysis
FA:NaOH:H_2O = 1:1:5 for 30 mins	80^0C for 0,3 and 5 days	No curing; 80^0C for 1 day and room temp. for 4 days; 3 and 5 days at 80^0C
FA:NaOH:H_2O = 1:1:5 for 60 mins	80^0C for 0,3 and 5 days	No curing; 80^0C for 1 day and room temp. for 4 days; 3 and 5 days at 80^0C
FA:NaOH:H_2O = 1:1:5 for 90 mins	80^0C for 0,3 and 5 days	No curing; 80^0C for 1 day and room temp. for 4 days; 3 and 5 days at 80^0C

Once the optimum jet loop mixing time and curing duration was determined the hydrothermal synthesis of the filtrate produced was carried out at the same conditions optimised during fusion (90^0C for 8 hrs). By comparison of the filtrate produced during fusion versus that prepared by jet looping, the Si/Al ratio of the jetloop filtrate could be adjusted to try and synthesize the hierarchical zeolite X as had been produced from fusion. The result was then compared to that of the fusion process, regarding the yield and purity of zeolite produced and whether or not zeolite X could be successfully synthesized from the jet loop and cured filtrate.

The samples produced in the jet loop and curing stage of experiments are listed in Table 3-3 along with the codes used for the samples in the experiments.

Table 3-3: Sample codes and experimental conditions for the jet loop and curing experiments

Sample code	Description	Experimental conditions	Replicated
FFAF	Fused fly ash filtrate	80 g FFA + 200 mL H_2O Stirred for 2 hours	X3
JL30	Jet looping for 30 minutes with no curing	3.2 kg CFA + 3.2 kg NaOH + 16 L H_2O	X3
JL60	Jet looping for 60 minutes with no curing	3.2 kg CFA + 3.2 kg NaOH + 16 L H_2O	X3
JL90	Jet looping for 90 minutes with no curing	3.2 kg CFA + 3.2 kg NaOH + 16 L H_2O	X3
JL30C1	Jet looping for 30 minutes + curing for 1 day at 80^0C and 4 days at room temperature	3.2 kg CFA + 3.2 kg NaOH + 16 L H_2O	X3
JL60C1	Jet looping for 60 minutes + curing for 1 day at 80^0C and 4 days at room temperature	3.2 kg CFA + 3.2 kg NaOH + 16 L H_2O	X3
JL90C1	Jet looping for 90 minutes + curing for 1 day at 80^0C and 4 days at room temperature	3.2 kg CFA + 3.2 kg NaOH + 16 L H_2O	X3
JL30C3	Jet looping for 30 minutes + curing for 3 days at 80^0C	3.2 kg CFA + 3.2 kg NaOH + 16 L H_2O	X3
JL60C3	Jet looping for 60 minutes + curing for 3 days at 80^0C	3.2 kg CFA + 3.2 kg NaOH + 16 L H_2O	X2
JL90C3	Jet looping for 90 minutes + curing for 3 days at 80^0C	3.2 kg CFA + 3.2 kg NaOH + 16 L H_2O	X2
JL30C5	Jet looping for 30 minutes + curing for 5 days at 80^0C	3.2 kg CFA + 3.2 kg NaOH + 16 L H_2O	X3

JL60C5	Jet looping for 60 minutes + curing for 5 days at 80^0C	3.2 kg CFA + 3.2 kg NaOH + 16 L H_2O	X3
JL90C5	Jet looping for 90 minutes + curing for 5 days at 80^0C	3.2 kg CFA + 3.2 kg NaOH + 16 L H_2O	X3
JLZ25	Zeolite sample – 8 hours of hydrothermal synthesis at 90^0C	Optimum jet loop and curing filtrate + 0.25 g $Al(OH)_3$	X1
JLZ50	Zeolite sample – 8 hours of hydrothermal synthesis at 90^0C	Optimum jet loop and curing filtrate + 0.50 g $Al(OH)_3$	X1
JLZ75	Zeolite sample – 8 hours of hydrothermal synthesis at 90^0C	Optimum jet loop and curing filtrate + 0.75 g $Al(OH)_3$	X1

3.4.3. Material balance around jet loop system

The material balance around the whole jet loop and curing and hydrothermal treatment process was conducted on a basis of separate unit balances around each stage of the process. This included first a material balance around the jet loop pilot plant. This concerned the 3.2 kg of starting fly ash, the 3.2 kg of NaOH and the 16 L of tap water used. The slurry produced was then weighed to determine an overall material balance around the jet loop process and to quantify the losses that occurred within the process.

A balance was then conducted around the amount of slurry produced from the jet loop that could be cured with the curing process. The curing process was carried out in plastic containers and the total volume of slurry produced from the jet loop pilot plant could not all be cured. Therefore, an overall material balance was conducted around the portion used during the curing process. This included weighing the total residue and filtrate produced after curing a certain amount of jet loop pilot plant slurry.

3.5. Characterisation techniques

The various characterisation techniques that were used in this study are presented in this section.

3.5.1. Elemental analysis

3.5.1.1. XRF

XRF analysis was performed by grinding 5 g of the samples in a ceramic mortar and pestle. After drying at 105 ^{0}C a portion of the finely milled sample was fired at 900 ^{0}C for 4 hours to determine the LOI (Loss on ignition). 0.65 g of material was then weighed out with 5.6 g of lithium borate flux and the mixture was fused in platinum crucibles using a Claisse M4 fusion instrument at 950^0C. The molten material was then cast into a platinum mould to form a disk for presentation to the XRF. The

fusion disk was measured on a Panalytical PW2400 WDXRF instrument calibrated with 17 CRM's (Certified reference material) and a major elemental analysis was performed with full matrix and inter-element corrections.

3.5.1.2. ICP – AES

ICP – AES was conducted to analyse the major and minor elements in the digested samples. Samples were prepared through digestion with 2% nitric acid at 10 times dilution and 100 times dilution. Analysis was always performed in triplicate. The instrument used was a Varian 710 ES. A spectra scan multi element range was used for the standards. The machine has a high solids torch and an axial torch. Calibrations of the instrument were performed daily prior to its operation.

3.5.1.3. EDS

The EDS analysis was performed according to the detailed description in section 3.5.3.1.

3.5.1.4. UV – Vis

The UV-Vis method used to measure Si was developed by Grasshoff in 1964 and modified by Koroleff in 1971, where ascorbic acid was used as the reducing agent (Grasshoff et al., 1999). Only plastic ware was used for all calibration standards and sample dilutions.

The reagents were prepared as follows:

4.5 M Sulphuric acid:	250 mL concentrated H_2SO_4 was added to 750 mL of de-ionised water in a beaker. It was allowed to cool and made up to 1 litre in a 1000 mL volumetric flask.
Acid molybdate reagent: (0.0512 M)	38 g $(NH_4)_6Mo_7O_{24}.4H_2O$ (ammonium heptamolybdate tetrahydrate) was dissolved in 300 mL de-ionised water. This acid molybdate solution was added to 300 mL of the made up 4.5 M H_2SO_4 solution. The total volume was therefore 600 mL and it was stored away from direct sunlight.
Oxalic acid solution: (0.7937 M)	10 g oxalic acid dihydrate, $(COOH)_2.2H_2O$ was added to an approximate 50 mL volume of de-ionised water in a 100 mL volumetric flask. It was dissolved and made up to the 100 mL mark with de-ionised water. This saturated solution was stored in a plastic container at room temperature.
Ascorbic acid: (0.1637 M)	2.8 g ascorbic acid, $C_6H_3O_6$, was added to an approximate 50 mL volume de-ionised water in a 100 mL volumetric flask. It was dissolved and thereafter made up to the 100 ml mark with de-ionised water. The solution was kept in a dark container at a temperature under 8 °C.

Standard stock solution: (0.0361 M)

1000 ppm Si solution was prepared by adding 4.3459 g Na_2SiO_3, (sodium metasilicate), to an approximate 500 mL volume of de-ionised water in a 1000 mL plastic volumetric flask. It was dissolved and thereafter made up to the 1000 mL mark with de-ionised water. The stock solution is stable for at least a year.

Working standards:

Freshly prepared calibration standards were made for each analysis run from the standard stock solution. Serial dilutions were done with deionized water till the desired working standards were obtained.

The calibration standards and samples were prepared for measurement as follows:

The 1000 ppm Si stock solution was sequentially diluted to 10 ppm. Firstly, a 100 ppm Si standard was made by adding 5 mL of the 1000 ppm stock solution to a 50 mL volumetric flask and made up to volume with de-ionised water. 5 mL of the 100 ppm Si standard was then added to another 50 mL plastic volumetric flask and made up to volume with de-ionised water. Working standards of 0.1, 0.3, 0.5, 0.7 and 1 ppm Si were then made by adding 0.5, 1.5, 2.5, 3.5 and 5 mL respectively of the 10 ppm Si standard to 50 mL plastic volumetric flasks. The working standards were then made up to volume of 50 mL with de-ionised water.

1 mL of the X1000 times diluted analyte samples were added to plastic 50 mL volumetric flasks to bring the dilution factor up to X 50000 times. 50 mL of blank sample solution (de-ionised water used to prepare working standards), analyte sample solution and working standards were then each transferred to its own plastic container. 2 mL of the prepared 0.0512 M molybdate acid solution was added to each solution container. The solutions were swirled and allowed to stand for 30 min. 2 mL of the prepared 0.7937 M oxalic acid followed directly by 1 mL of the prepared 0.1637 M ascorbic acid was then added to each solution container. The solution was swirled again and left to stand for 40 minutes. This was to allow the blue colour of the silicomolybdate complex to fully develop. If the blue colour of the analyte samples were darker than the calibration standards, then it could be suitably diluted with acidified zero water (ZW). ZW is made by adding 1 mL of the 4.5 M H_2SO_4 to each 100 mL of de-ionised water used. The blank solution, standards and samples were measured at 810 nm wavelength or 660 nm for higher concentrations. In this study 810 nm wavelength was used. A calibration line was plotted to determine the concentration of the measured samples. The measured concentration was corrected for dilution by multiplying the measured concentration by the factor (50 000 X 50)/55.

3.5.2. Mineralogical characterisation by XRD

3.5.2.1. Qualitative XRD analysis

Qualitative XRD analysis was performed by placing the sample (powder) on a glass slide as seen in Figure 3-9 in the sample holder. The sample was then pressed in a flat disk shape to create a flat

sample surface seen in 3 in Figure 3-9. The sample holder was then inserted in the sample chamber as seen in 4 in Figure 3-9. The specifications of the instrument are as follows:

INSTRUMENT:

Manufacturer: BRUKER AXS (Germany)

Diffractometer: D8 Advance

Measurements: θ - θ scan in locked coupled mode

Tube: Cu-Kα radiation ($\lambda K\alpha_1$=1.5406Å)

Detectors: PSD Vantec-1

MEASUREMENTS:

Tube voltage: 40 kV

Tube current: 40 mA

Variable slits: V20 variable slit

2θ Range: 4 – 60

Step: 0.034

Measurement time: long enough for good statistics (usually 1 sec/step).

SOFTWARE:

ICDD: PDF database 1998

Data evaluation: EVA software from BRUKER

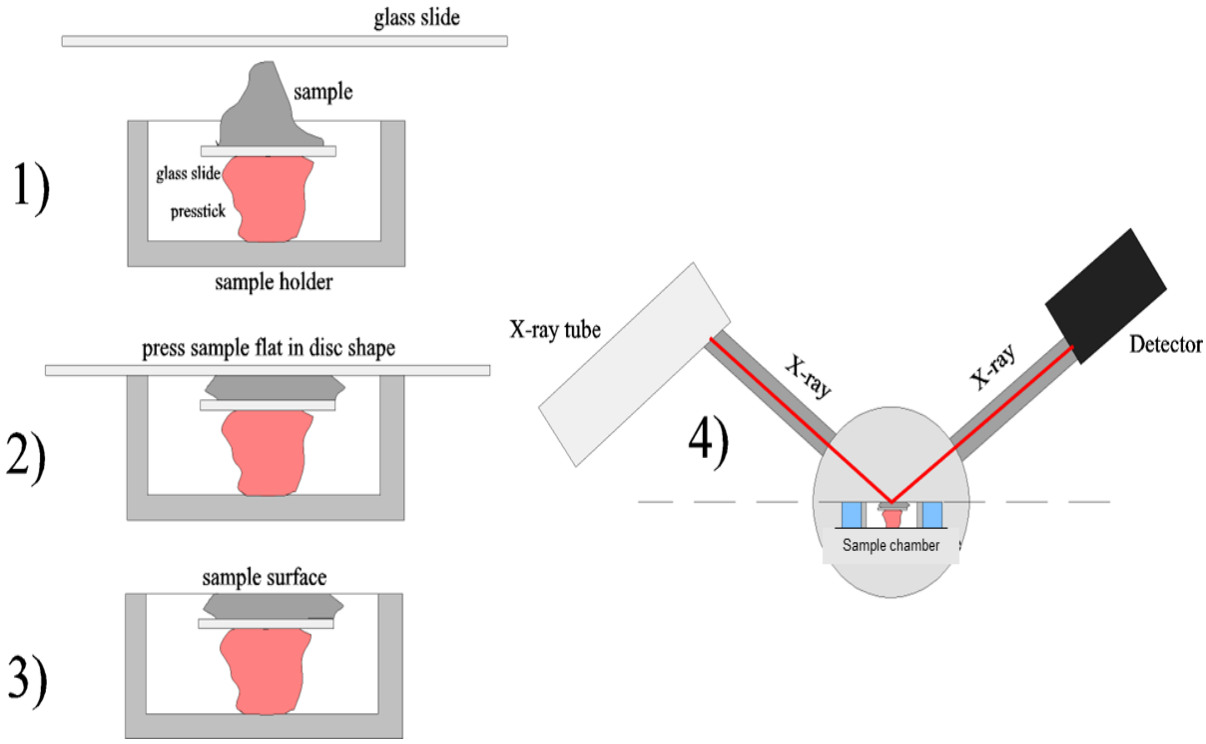

Figure 3-9: Sample preparation for qualitative XRD analysis

3.5.2.2. Quantitative XRD analysis

Quantitative XRD analysis was performed after addition of 20% Si (Aldrich 99% pure) for determination of amorphous content and milling in a McCrone micronizing mill, the sample was prepared for XRD analysis using a back loading preparation method. Analysis was performed using a PANalytical X'Pert Pro powder diffractometer in θ–θ configuration with an X'Celerator detector and variable divergence- and fixed receiving slits with Fe filtered Co-Kα radiation (λ=1.789Å). The data was collected in the angular range 5°≤2θ≤90° with a step size 0.008° 2θ and a 13 s scan step time. The phases were identified using X'Pert Highscore plus software. The relative phase amounts (weight %) were estimated using the Rietveld method (Autoquan Program).

3.5.3. Physical characterisation by morphological analysis

3.5.3.1. SEM

The SEM and EDS analysis was prepared by mounting the samples on aluminium stubs using carbon tabs so the samples would stick to the stubs. The samples were then coated with Au and Pd to make them conductive for the SEM to work. The machine used for this coating process was a Quorom Q150T ES Sputter coater. The samples were coated for 60 seconds. The samples were then placed inside the SEM machine. The model of the SEM machine was an AURIGA Field Emission High Resolution Scanning Electron Microscope from the company Zeiss (Germany). The imaging software used was SmartSEM and the EDS software used was AZTEC. The images were scanned in the range from 2000 X magnification to 10 000 X magnification depending on the sample. The

accelerating voltage used for obtaining images was 5 KV and the KV used for EDS was 20 KV. The working distance for EDS was 9 mm. The gun vacuum was $7.7x10^{-10}$ mbar and the system vacuum was $7.3x10^{-7}$ mbar. The filament current was 2.359 amps.

3.5.4. Structural analysis

3.5.4.1. FTIR

FTIR analysis was performed using a Spectrum Two PerkinElmer FT-IR Spectrometer and PerkinElmer Spectrum software. The samples were prepared using the KBr pelletizing technique. First a background was produced using KBr by placing a small amount of KBr in the pelletizer, subjecting it to pressure and creating a clear solid sample in the sample holder. Then placing this sample holder inside the spectrometer and using the software to scan a background. Once this was completed the samples to be scanned for FTIR were mixed with KBr in small proportions and ground together with a mortar and pestle. The sample was then again pelletized under pressure and placed in the spectrometer. The software on a computer was used to scan the sample and also to perform background correction and the plots produced were smoothed. The scanning mode was set to % transmittance.

3.6. Chapter summary

This chapter outlined the overall experimental approach for the following chapters. It also gave the procedures and equipment used in all the analytical techniques used within this study. The following chapter 4 will deal with the characterisation of the starting CFA and the base case experiment of zeolite X synthesis via the fusion method including a material balance around the fusion process.

CHAPTER 4

4. Characterisation of starting material and base case study

4.1. Introduction

This chapter deals with the characterisation of the starting CFA material and also presents the results of a base case study which attempted to reproduce existing work reported by Musyoka (2012). It is necessary to characterise the CFA used in order to assess its suitability for zeolite synthesis. The characterisation involves XRF analysis for the major oxides content and trace elemental composition; SEM analysis for the morphology of the fly ash; FTIR analysis for the structural make-up of the fly ash and finally XRD analysis for the mineralogical composition of the fly ash (both qualitatively and quantitatively).

The zeolite targeted from previous study (Musyoka, 2012) is that of zeolite X belonging to the faujasite group of zeolites. More specifically the novel finding of hierarchical zeolite X was targeted given its unique morphology. The zeolite is synthesised from the clear extract after filtering, as this is necessary for the synthesis of zeolite X with hierarchical morphology (Musyoka, 2012; Cornelius, 2015). The zeolites obtained after hydrothermal synthesis were characterised with XRD, FTIR, SEM and EDS. Once the optimum synthesis conditions were obtained an overall material balance was produced to determine the yield of the zeolite from the staring CFA material.

4.2. Characterisation of starting material

The characterisation of the starting CFA from the Arnot power station in the Mpumalanga province can be found in the following section. Table 4-1 shows the XRF analysis of the major oxides found within the CFA used for the experiments. The procedure for XRF is detailed in section 3.6.1.1.

Table 4-1: XRF analysis of starting fly ash

Major Oxides (%)	Sample A	Sample B	Average	Std. Dev.
SiO_2	53.86	53.34	53.60	0.37
Al_2O_3	25.44	25.44	25.44	0.00
Fe_2O_3	5.56	5.57	5.56	0.01
CaO	5.25	5.21	5.23	0.02
TiO_2	1.58	1.57	1.58	0.00
MgO	1.53	1.56	1.54	0.02
K_2O	0.56	0.55	0.55	0.01
P_2O_5	0.35	0.35	0.35	0.00
MnO	0.05	0.05	0.05	0.00
V_2O_5	0.03	0.02	0.02	0.01
Cr_2O_3	0.02	0.02	0.02	0.00
Na_2O	0.00	0.00	0.00	0.00
LOI	6.64	6.89	6.76	0.18
Total	100.86	100.56	100.71	0.21
SiO_2/Al_2O_3	2.12	2.10	2.11	0.01
Si/Al	1.80	1.78	1.79	0.01

The major oxides that were prevalent in the two CFA samples produced from the bulk CFA were SiO_2, Al_2O_3, Fe_2O_3, CaO, TiO_2 and MgO with percent compositions of 53.60 ± 0.37, 25.44 ± 0.00, 5.56 ± 0.01, 5.23 ± 0.02, 1.58 ± 0.00 and 1.54 ± 0.02 respectively, errors were expressed standard deviation from average values. The other remaining oxides that were also found were K_2O, P_2O_5, Na_2O, MnO, V_2O_5 and Cr_2O_3, Table 4-1. The predominant species was the SiO_2 and Al_2O_3 which totalled 79.04% within the CFA followed by the 5.56% of iron oxide and the 5.23% of calcium oxide. It can be seen that the SiO_2 and Al_2O_3 would provide sufficient amounts of silicon and aluminium needed in the zeolite production. The CFA used in this study was classified as class F according to Ahmaruzzaman (2010). This is due to class F fly ash, as stated by the American Society for Testing Materials (ASTM C618), which exceeds 70% content of SiO_2+Al_2O_3+Fe_2O_3 and having a low lime content of approximately 5% (Ahmaruzzaman, 2010; Blissett and Rowson, 2012). The SiO_2+Al_2O_3+Fe_2O_3 content of this fly ash being 84.60% and the lime content being 5.23%. The SiO_2/Al_2O_3 mass ratio of the starting fly ash was 2.11 giving a Si/Al atomic ratio of 1.79. These ratios are an important factor in zeolite synthesis as mentioned in section 2.2.7.1.

Table 4-2 shows the trace elemental analysis of the starting fly ash determined through XRF analysis.

Table 4-2: XRF trace elemental analysis of the starting fly ash

Trace element (ppm)	Sample A	Sample B	Sample C	Average	Std. Dev.
S	1 779	1 755	1 793	1 776	19
Ba	932	957	942	944	13
Sr	850	824	818	831	17
Zr	434	418	448	433	15
Ce	233	230	217	227	9
La	109	111	123	114	8
Nd	88	83	82	84	3
Y	80	76	75	77	3
Ni	78	74	60	71	9
Zn	63	61	58	61	3
Pb	59	55	52	55	4
Th	45	42	47	45	3
Ga	42	43	42	42	1
Cu	37	35	34	35	2
Nb	34	33	33	33	1
Rb	32	32	32	32	0
Co	32	20	29	27	6
U	12	12	16	13	2
Cl	11	7	25	14	9

In Table 4-2, the most prominent trace elements in the fly ash are S, Ba and Sr with concentrations of 1776 ± 19, 944 ± 13 and 831 ± 17 ppm respectively. There are also significant concentrations of Zr, Ce and La of 433 ± 15, 227 ± 9 and 114 ± 8 ppm respectively. This trace elemental analysis revealed that toxic elements are concentrated in the fly ash during the combustion process (Mainganye, 2012; Du Plessis et al., 2014). In order to understand the major phases found within the CFA in this study, both quantitative and qualitative XRD spectra are depicted in Figures 4-1 and 4-2 respectively.

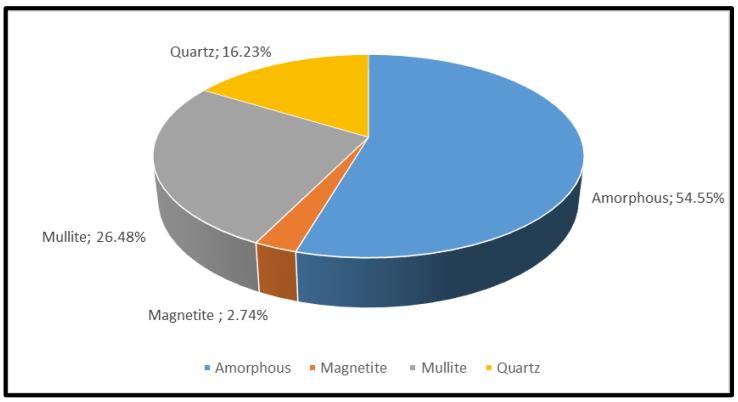

Figure 4-1: Quantitative XRD analysis of starting fly ash

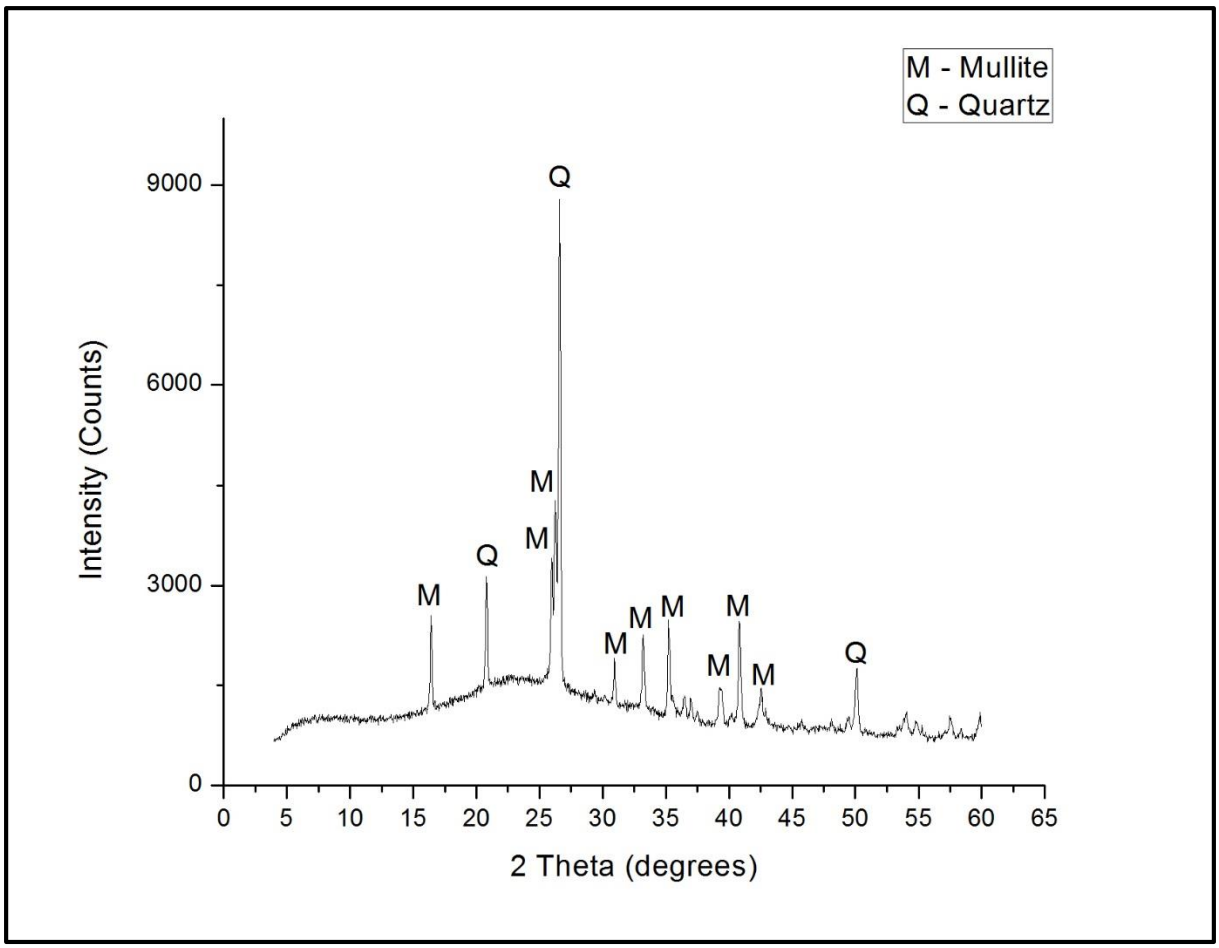

Figure 4-2: Qualitative XRD of starting fly ash

The quantitative XRD represented in Figure 4-1 shows the major phases found in the CFA on a relative weight percent. The order of the phases based on relative weight percent are: Amorphous (54.55%) > Mullite (26.48%) > Quartz (16.23%) > Magnetite (2.74%). It can be seen the CFA is mainly composed of the amorphous glassy phase which is the most reactive phase and predominantly determines the type and composition of the zeolite formed. A higher amorphous content can lead to a higher yield of zeolite (Querol et al., 2001; Musyoka, 2012). The mullite phase is generally the least reactive phase with lower quantities favouring zeolite crystallisation (Rayalu et al., 2001; Querol et al., 2002; Musyoka, 2012) The Figure 4-2 showing the qualitative XRD of the CFA shows the quartz and mullite present in the fly ash. The amorphous phase is represented in Figure 4-2 by the broad hump in the region of $20^0 – 40^0$ 2θ as reported by others (Inada et al., 2005b; Criado et al., 2007; Ríos et al., 2009; Musyoka, 2012). The FTIR spectra of the CFA is shown in Figure 4-3.

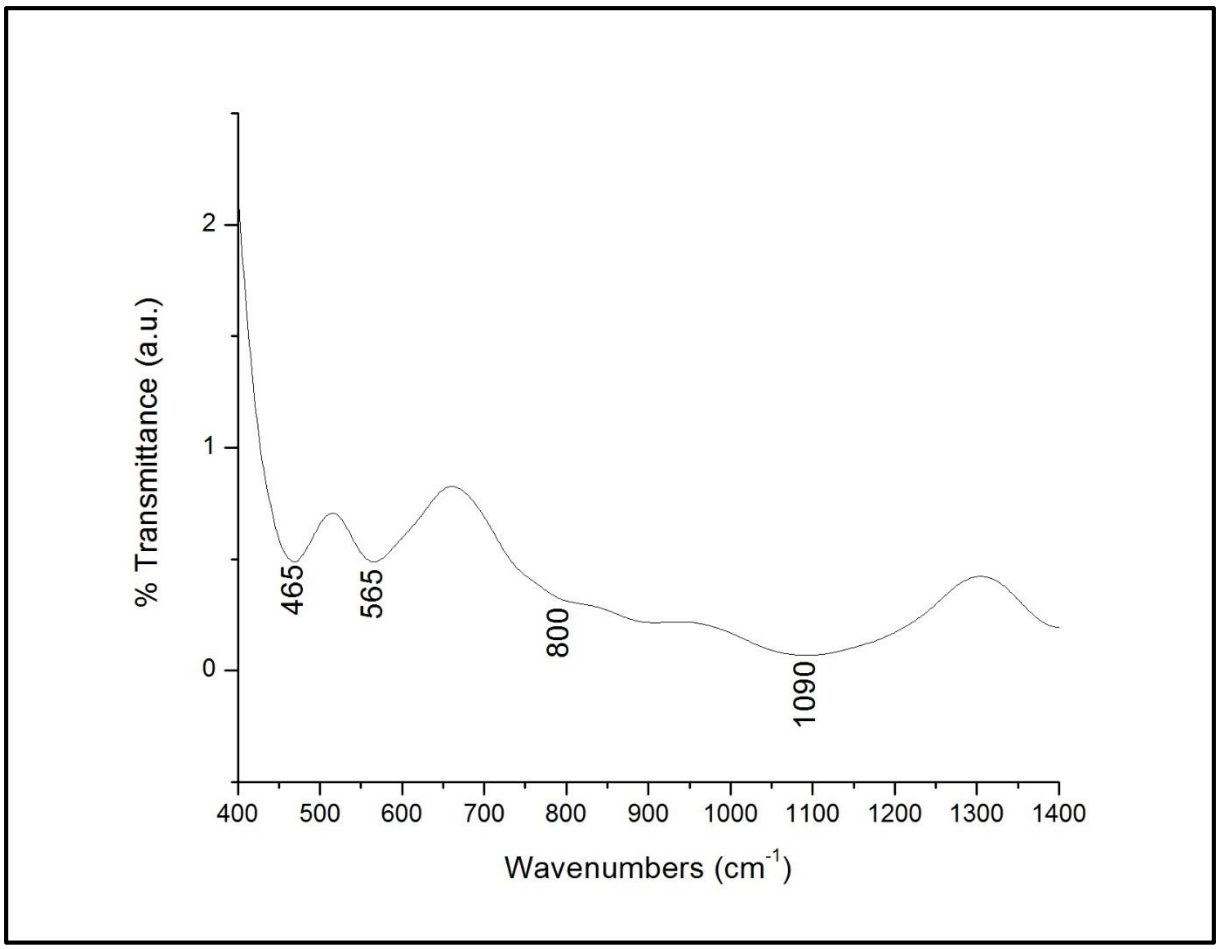

Figure 4-3: FTIR spectra of starting fly ash

The FTIR spectra presented in Figure 4-3 shows 4 main peaks which coincide with the vibration bands associated with aluminosilicates. The small band around 465 cm^{-1} is associated with T-O bending vibrations (Fernández-Jiménez and Palomo, 2005; Musyoka, 2012). The small distinct band around 565 cm^{-1} is associated with octahedrally coordinated aluminium in the mullite and corresponds to a region assigned for Si-O-Al vibrations (Fernández-Jiménez and Palomo, 2005; Nyale, 2014). The broad band appearing at 800 cm^{-1} represents the quartz found within the fly ash which generates Si-O and Al-O symmetric stretching vibrations (Fernández-Jiménez and Palomo, 2005; Musyoka, 2012; Nyale, 2014). Finally the broad band situated around 1090 cm^{-1} corresponds to a region assigned to Si-O-Si or Al-O-Si asymmetric stretching vibrations generated by the crystalline matrix of the fly ash and the glassy surface layer (Fernández-Jiménez and Palomo, 2005; Nyale, 2014). The following Figure 4-4 shows the morphology of the CFA particles obtained through SEM analysis.

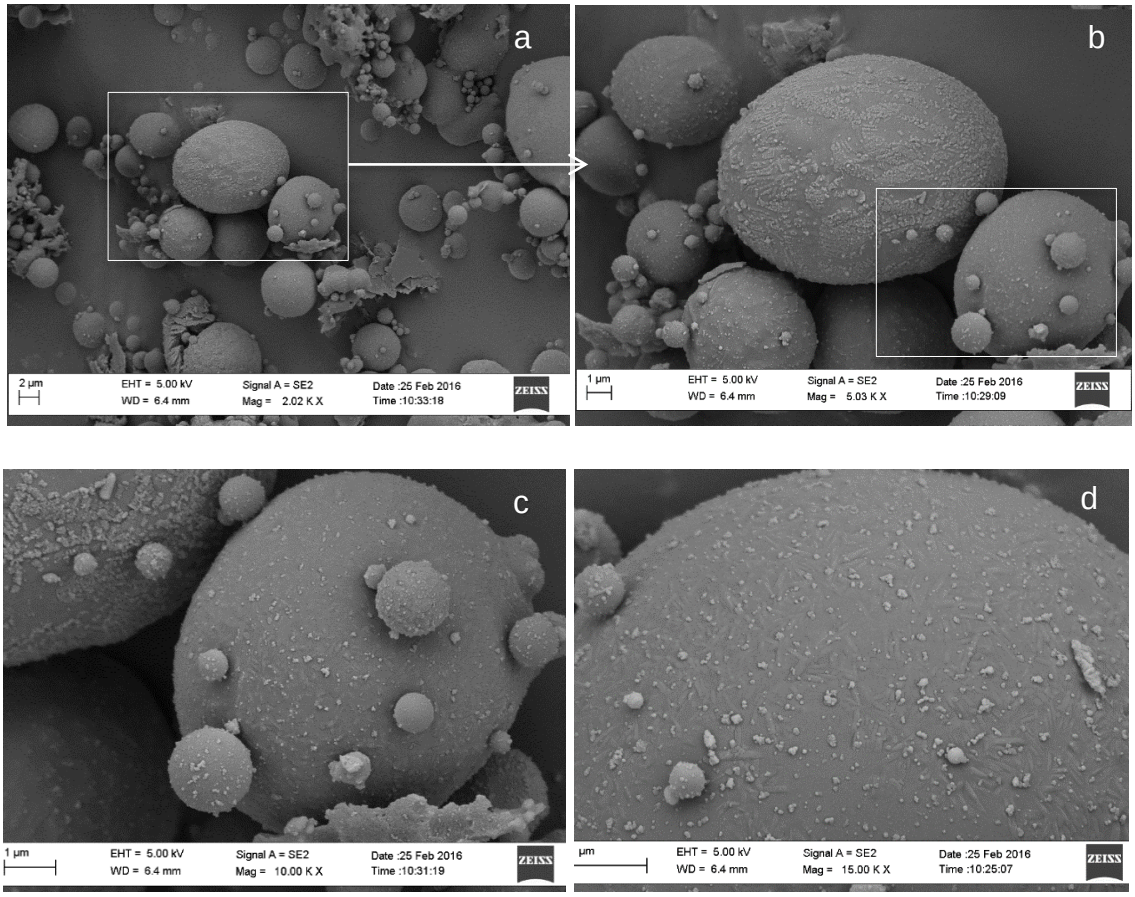

Figure 4-4: SEM micrographs of starting fly ash with magnification at: (a) 2000 X (b) 5000 X (c) 10 000 X (d) 15 000 X

From the SEM micrographs shown in Figure 4-4 it can be seen that CFA particles are mostly spherical in shape, which is in agreement with most literatures on this subject (Kutchko and Kim, 2006). This shape is due to the fly ash particles solidifying when suspended in the flue gas, which produces the spherical shape from the cooling effect (Kutchko and Kim, 2006; Musyoka, 2012). The smoothness of the particles, which can be seen close up in Figure 4-4(d), is due to the mineral particles being covered with the amorphous glassy phase (Inada et al., 2005b; Musyoka, 2012). The following section will deal with the base case study results of producing zeolite X with hierarchical morphology via the existing fusion method from CFA.

4.3. Base case study of zeolite X synthesis from fusion method

The results represented here for the base case study of the fusion method to synthesize the novel hierarchical morphology of zeolite X from CFA using the fusion pre-synthesis. The experimental method for this synthesis is highlighted in Chapter 3. There was a need to optimise the synthesis of the zeolite X due to the differing nature of the starting fly ash. This is due to the fact that even though fly ash was used from the same power station as in Musyoka's (2012) study, namely the Arnot power station, it was found to differ in nature from batch to batch (Mainganye, 2012). The zeolites produced were characterised with XRD, FTIR and SEM/EDS. The following Figure 4-5 represents the XRD

spectra of the zeolites produce at 90^{0}C and varying hydrothermal synthesis times of 8 hours, 12 hours and 16 hours.

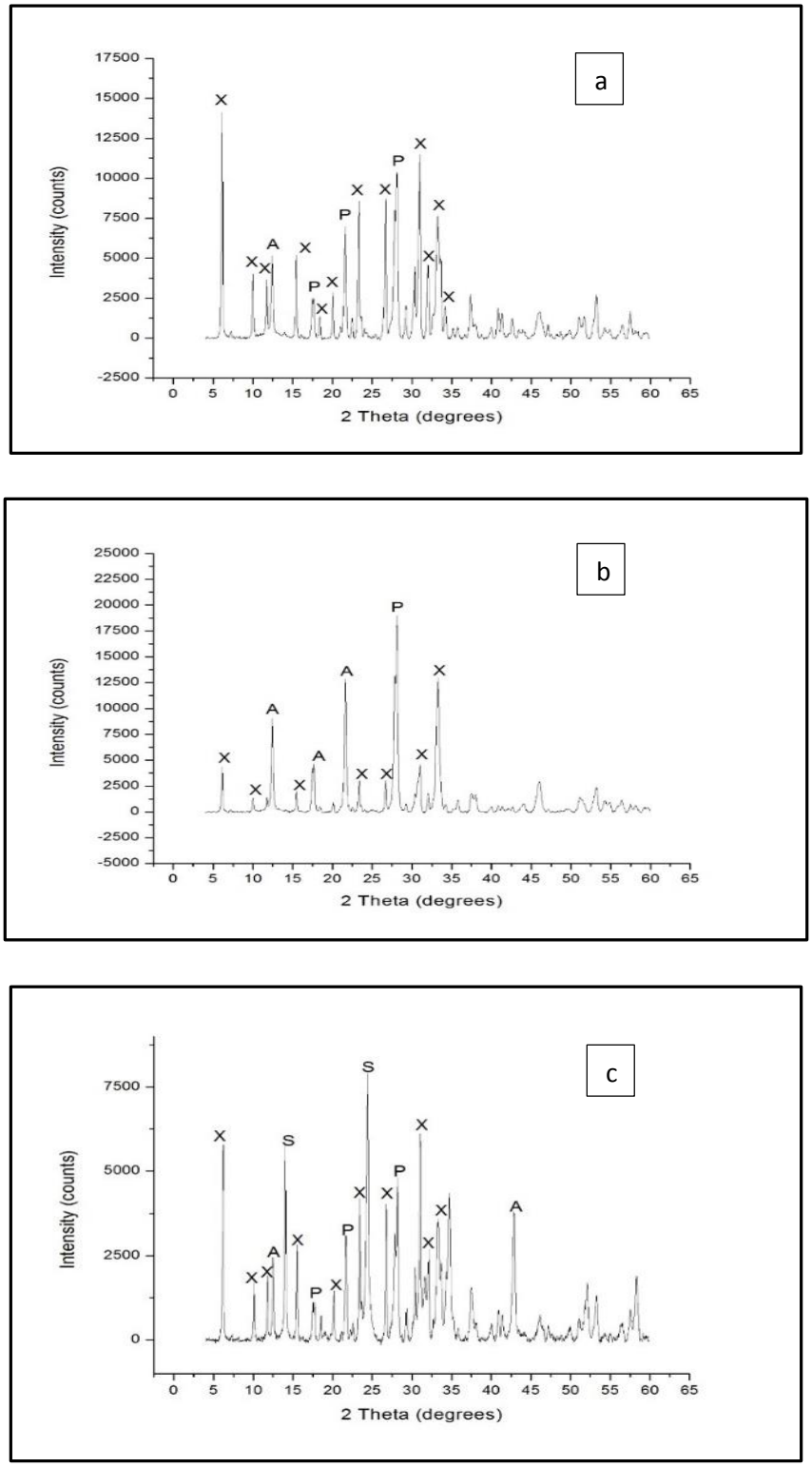

Figure 4-5: XRD spectra for the base case study of fusion process with varying of hydrothermal synthesis time at 90^{0}C: (a) 8 hours (b) 12 hours (c) 16 hours (X – Zeolite X; A – Zeolite A; P – Zeolite NaP1; S – Sodalite)

From the XRD spectra displayed in Figure 4-5, it can be seen that the best result regarding zeolite X crystallisation was found after 8 hours of hydrothermal treatment at 90^0C. This is due to the high phase purity and the intensity of the XRD peak found at 6.1 degrees 2θ, along with the majority of peaks being assigned to zeolite X. This is shown quantitatively in Table 4-3 regarding the phase crystallinity of the mixed phase zeolites with zeolite X having a 66.85% phase crystallinity. There were however trace amounts of zeolite A and zeolite P having phase crystallinities of 4.90% and 28.25% respectively. The XRD spectra after 12 hours showed very little crystallisation of zeolite X with the highest intensity peak being zeolite P accounting for a 31.06% phase crystallinity of zeolite P. However, after 16 hours of hydrothermal treatment there were a significant amount of zeolite X peaks but not as intense as what was found after only 8 hours of hydrothermal treatment. Also there were impurities after 16 hours of treatment of not only zeolite A and P but also sodalite seen by a 22.87% phase crystallinity of sodalite. The result of producing zeolite X after 8 hours of treatment at 90^0C improves dramatically timewise on the optimised conditions proposed in Musyoka's (2012) study of 24 hours at 80^0C, even though the result here had minor impurities of zeolite A and P. Figure 4-6 displays the FTIR spectra of the zeolites obtained.

Table 4-3: Phase crystallinity of synthesised zeolites in base case study at various synthesis times at 90^0C

Synthesis time (Hours)	% Phase of zeolite			
	Zeolite X	Zeolite A	Zeolite P	Sodalite
8	66.85	4.90	28.25	0.00
12	39.09	29.85	31.06	0.00
16	48.25	12.20	16.68	22.87

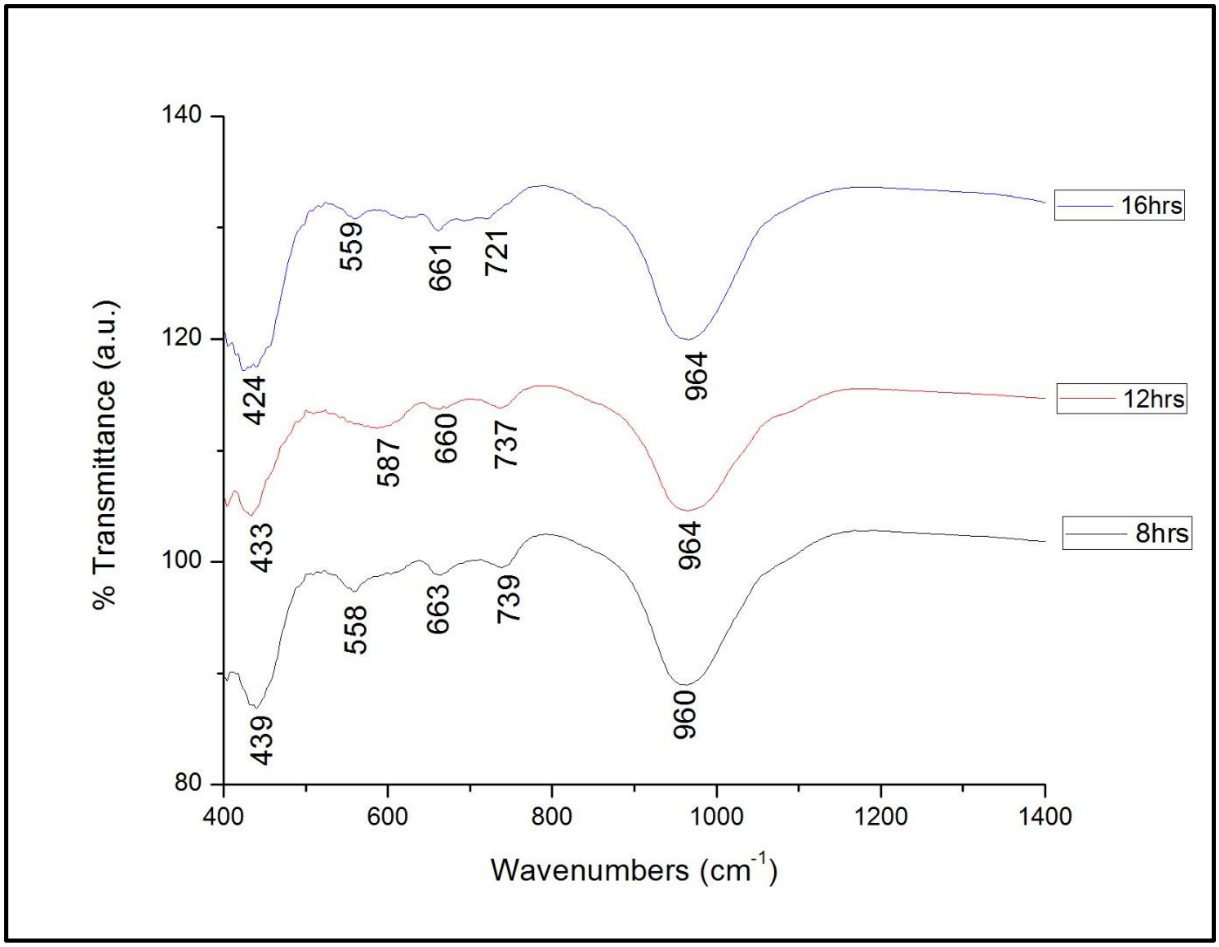

Figure 4-6: FTIR spectra for the base case study of fusion process with varying hydrothermal synthesis time at 90^0C

The Figure 4-6 shows the FTIR spectra for the synthesised zeolites at varying hydrothermal synthesis time at 90^0C. The main bands and what they correspond to regarding the literature that was presented in Table 2-4 in section 2.2.8.3 is summarised in Table 4-4.

Table 4-4: Summary of FTIR vibrations for base case synthesis of zeolite X from fusion method

Wavenumbers (cm^{-1})					
8 hrs	12 hrs	16 hrs	Literature values	Assignment	Reference
439	433	424	420 - 500	(Si-O-Al) T-O Bend (Internal tetrahedra)	Table 2-4
558	587	559	500 - 650	Double Ring (External linkage)	Table 2-4
663	660	661	650 - 720	Symmetrical stretch (O-T-O group) (Internal tetrahedra)	Table 2-4
739	737	721	720 - 730	D4R units	Table 2-4
960	964	964	950 - 1250	Assymetric stretch (Si-O-Si)(T-O) stretch (Internal tetrahedra)	Table 2-4

Looking at Table 4-3, it can be seen that the wave numbers for the zeolites X synthesized correlate well with the accepted literature values from Table 2-4. What is of importance regarding zeolites co-crystallising with one another is the double ring region of vibrations. This double ring region can be used to check the existence of "contaminant" phases that co-crystallise with the expected zeolite X (Musyoka, 2012). The two main zeolites that co-crystallise with zeolite X are zeolites A and P (Inayat et al., 2012; Musyoka, 2012). Regarding the double ring region in Table 4-3, it can be seen that there is a significant shift in the sample after 12 hours compared to the 8 hours and 16 hours. This, according to Balkus and Ly (1991), would imply that the sample after 12 hours is more siliceous. This is because a shift to higher frequencies indicates a higher Si/Al ratio. The band at 600 cm^{-1} is characteristic of zeolite P as seen after 12 hours, the double ring region being at 587 cm^{-1}. This therefore correlates with the XRD spectra as the more intense peak after 12 hours was of zeolite P. Zeolite P is indicated as forming at higher Si/Al ratios as indicted in the literature in Table 2-2. Also from Table 2-4, it shows the double ring region for zeolite X being at 560 cm^{-1} which again favours the lower values of the double ring region, which samples (8 hours and 16 hours) tend towards, being 558 cm^{-1} and 559 cm^{-1} respectively. It can also be seen that the D4R units found in zeolite A were seen to correspond to the frequency at about 730 cm^{-1} in all the samples which correlates with the zeolite A peaks in Figure 4-5, showing zeolite A co-crystallizing with all the samples. However, the band at 739 cm^{-1} in the sample after 8 hours could be linked to the asymmetric stretch found in the spectra for zeolite X as shown in Table 2-4 at 746 cm^{-1}. The following Figure 4-7 shows the SEM micrographs of the zeolites obtained at the varying hydrothermal synthesis times and at 90^0C.

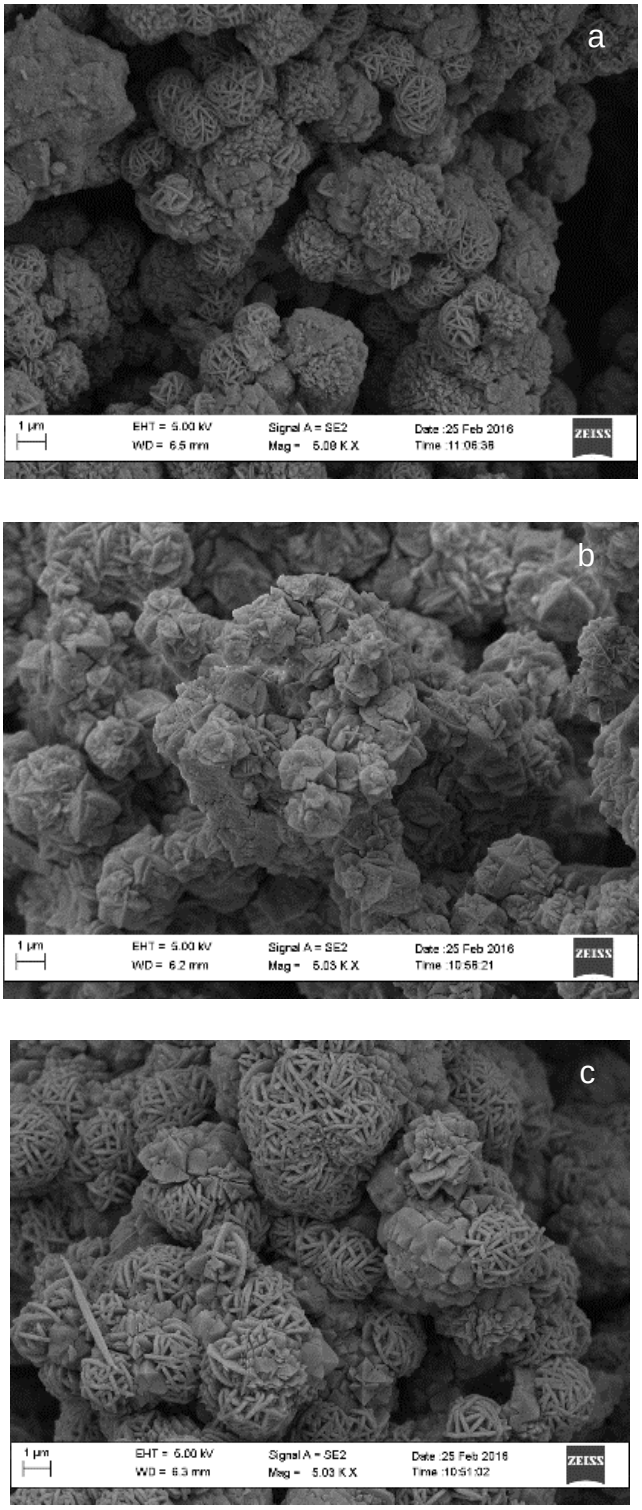

Figure 4-7: SEM micrographs for the base case study of the fusion process for varying hydrothermal synthesis time at 90^0C and 5000X magnification: (a) 8 hrs (b) 12 hrs (c) 16 hrs

The SEM micrographs depicted in Figure 4-7 correlate well with the XRD spectra in Figure 4-5. The synthesis for 8 hours at 90^0C shows the hierarchical structure of zeolite X reported by Musyoka (2012), along with some contaminant phases as shown in the XRD spectra. The synthesis after 12 hours though does not show any hierarchical structure and mainly shows the agglomerated crystals

with a spikey outer surface which represent the morphology of zeolite P (Musyoka, 2012). This correlates with the XRD spectra as the most intense peak after 12 hours was zeolite P. It also corresponds with the FTIR results mentioned previously with the shift in the double ring region representing the zeolite P formation. For the synthesis after 16 hours the hierarchical structure of zeolite X is apparent again with some contaminant phases as confirmed by the XRD spectra after 16 hours of synthesis time.

The following Table 4-5 shows the results of the EDS analysis performed alongside the SEM analysis of the base case fusion results. It was used as a semi-quantitative method to obtain the elemental weight percentage of silicon and aluminium with the samples as to determine the Si/Al ratio. It can be seen all the Si/Al ratios reported are in the region associated with zeolite X. Thus it can be concluded that the faujasite zeolites produced in this base case study are that of zeolite X and not of zeolite Y in conjunction with the values in Table 2-2. It also indicates the highest Si/Al ratio was found in the sample after 12 hours (1.20) and this corresponds with the XRD, FTIR and SEM. Although it is only a slight increase in the Si/Al it is noted that the EDS is only a semi-quantitative tool and cannot give precise quantitative measurements.

Table 4-5: EDS results of base case fusion method at 90^0C for 8 hours, 12 hours and 16 hours

16 hrs	Atomic %						
Element	Sample 1	Sample 2	Sample 3	Sample 4	Sample 5	Average	Std. Dev.
O	59.45	60.11	60.25	58.97	59.60	59.68	0.518
Na	14.53	15.30	13.87	14.13	13.71	14.31	0.635
Al	12.20	11.35	12.42	12.72	12.52	12.24	0.533
Si	13.81	13.24	13.45	14.18	14.17	13.77	0.422
Si/Al	1.13	1.17	1.08	1.11	1.13	1.13	0.030
12 hrs **Element**							
O	58.74	58.92	58.23	58.09	58.34	58.46	0.351
Na	12.35	12.83	12.83	12.00	12.47	12.50	0.350
Al	13.10	12.94	13.29	13.46	13.17	13.19	0.196
Si	15.82	15.31	15.65	16.45	16.02	15.85	0.425
Si/Al	1.21	1.18	1.18	1.22	1.22	1.20	0.020
8 hrs **Element**							
O	58.26	57.90	57.22	58.54	56.95	57.77	0.675
Na	12.21	12.96	13.47	12.76	12.58	12.80	0.467
Al	13.40	13.61	13.57	13.17	13.58	13.47	0.185
Si	16.14	15.53	15.75	15.52	16.90	15.97	0.578
Si/Al	1.20	1.14	1.16	1.18	1.24	1.19	0.040

The following section deals with the material balance performed around the best result from the base case synthesis (8 hours at 90^0C) so as to determine the fate of the elements within this synthesis. This will also be able to serve as a comparison to the material balance that will be performed in the following chapter 5.

4.3.1. Material balance for base case study of zeolite X synthesis from fusion method

This section concerns the material balance performed around the synthesis of zeolite X with hierarchical morphology obtained through the fusion process with the hydrothermal conditions of 90^0C for 8 hours. The overall material balance is shown in Figure 4-8 as a block flow diagram (BFD).

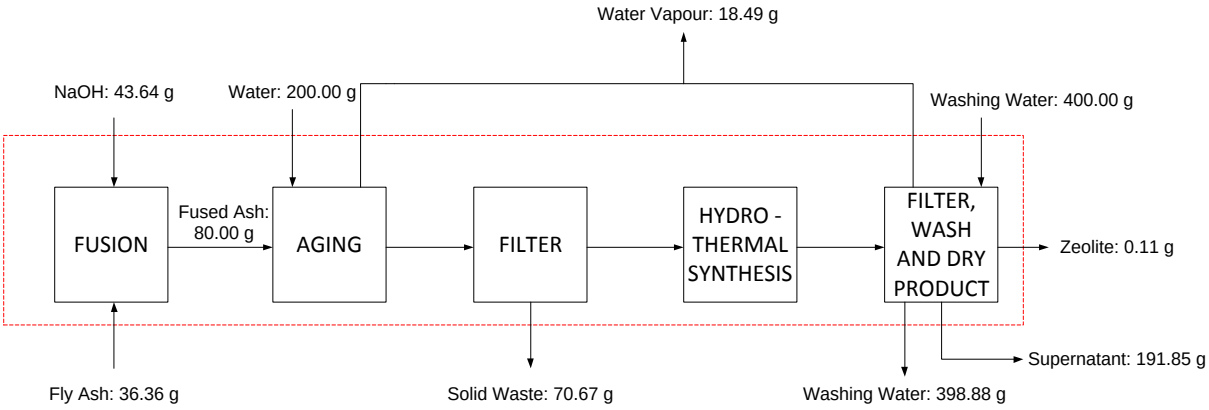

Figure 4-8: Overall material balance of base case fusion process for synthesis of zeolite X at 90^{0}C for 8 hours

It can be seen from Figure 4-8 that the efficiency of the synthesis process regarding the yield of zeolite produced from the amount of starting CFA used is remarkably poor only producing 0.11 g of zeolite. There were also significant amounts of solid and liquid waste produced. The solid waste produced after filtering was 70.67 g, which when compared to the amount of solid fed into the process (80 g of fused fly ash which served as the basis for the material balance) was a very significant amount going to the solid waste. The basis for the material balance was as mentioned 80 g of the fused fly ash which was produced by fusing CFA with NaOH in a 1:1.2 mass ratio of CFA:NaOH. Also of the 200 g of ultra-pure water used for the synthesis a liquid supernatant waste of 191.85 g is being produced. This too is a remarkable amount of waste. The zeolite produced from using 36.36 g of starting CFA is only 0.11 g of zeolite. Due to this remarkably low yield of zeolite, it precluded the ability to perform an accurate elemental balance of all the streams entering and exiting the process. This low yield was also found by Musyoka (2012) when dealing with shorter synthesis times. With this optimised time being only 8 hours of hydrothermal treatment a low yield could be expected.

4.4. Chapter summary

In this study CFA used for zeolite synthesis was characterised with respect to elemental composition, its crystalline nature, its structural configuration as well as its morphology. It showed the CFA used in this study from the Arnot power station is an adequate starting material for zeolite synthesis. This chapter also presented the base case study of synthesising zeolite X with hierarchical morphology using the CFA from the Arnot power station characterised previously thus confirming its suitability for zeolite synthesis. The synthesis conditions for the base case fusion method were optimised and found to be 8 hours at 90^{0}C. The zeolite X produced was then characterised with XRD, SEM and FTIR. The phase crystallinity of the zeolite X produced from the optimum conditions was 66.85%, while when the synthesis time was extended to 12 and 16 hours at 90^{0}C it was 39.09% and 48.25% respectively. An overall material balance was produced for the base case fusion synthesis of the optimum conditions. However, it showed a remarkably poor yield concerning the synthesis of this zeolite with the hierarchical morphology. This then precluded the ability to perform an accurate

elemental balance for all the streams within the process. The following chapter will deal with the replacement of the fusion process with a jet loop system, also incorporating the curing of the slurry produced. This will serve as a comparison to the base case fusion process in an attempt to increase the yield of zeolite obtained by increasing the dissolution of the silicon and aluminium from the starting CFA.

CHAPTER 5

5. Jet loop assisted pre-synthesis

5.1. Introduction

As previously mentioned the process to synthesize zeolites from CFA involves a pre-synthesis stage followed by a hydrothermal synthesis stage. This chapter will first deal with the pre-synthesis stage in an attempt to replace the high temperature fusion pre-synthesis that was used as a base case in the previous chapter 4. It will then focus on the hydrothermal synthesis stage to synthesize zeolite X. Studies have focused on the replacement of the fusion process with processes such as microwave and ultrasound irradiation (Querol et al., 1997a; Inada et al., 2005b; Belviso et al., 2011; Musyoka et al., 2011b; Musyoka, 2012). A recent study was performed in which the 90 minute fusion process could be replaced by a short 10 minute ultrasonication process in the production of zeolite A (Ojumu et al., 2016). It was revealed however that the ultrasonication process might not easily be scaled to industrial scale (Moholkar et al., 1999). The ultrasound process implements the effect of acoustic cavitation to supply intense mixing of the fly ash with the sodium hydroxide. It was envisaged that this intense mixing could also be supplied by the hydrodynamic cavitation and impingement processes that take place within a jet loop reactor system.

Indeed, it was found in two recent studies that the jet loop pilot plant could provide intense mixing using the cavitation and impingement techniques (Madzivire et al., 2013; Nyale, 2014). The jet loop equipment would be significantly easier to scale-up than the high intensity ultrasound process. Therefore, a study is needed to ascertain the ability of the jet loop to release the necessary silicon and aluminium into solution prior to hydrothermal synthesis of the zeolites. Nayle (2014) reported that the superior mixing in the jet loop increased the amorphous content of the fly ash during the production of a geopolymer from the fly ash. It is believed that the same process could be used to replace the fusion step using the jet loop. This pre-synthesis stage first needs to be compared with fusion and ultrasonication in determining its feasibility as a suitable pre-synthesis stage, as this work seeks to achieve. In addition, it is also necessary to investigate the effect of curing of the jet loop slurry on the amount of silicon and aluminium which can be released into solution for zeolite synthesis; which this study aims to determine. The following section deals with the experimental results to establish the effect of the jet loop mixing time used and the effect of the curing time used during the pre-synthesis stage.

5.2. Effect of jet loop mixing time and curing time on Si and Al dissolution

The effect of the jet loop mixing time and the curing time after jet looping was investigated as described in section 3.4.2. The filtrates produced from each condition were analysed for Si and Al

concentrations using ICP – AES (see section 3.5.1.2) these are represented in Figures 5-1, 5-2, 5-3 and 5-4.

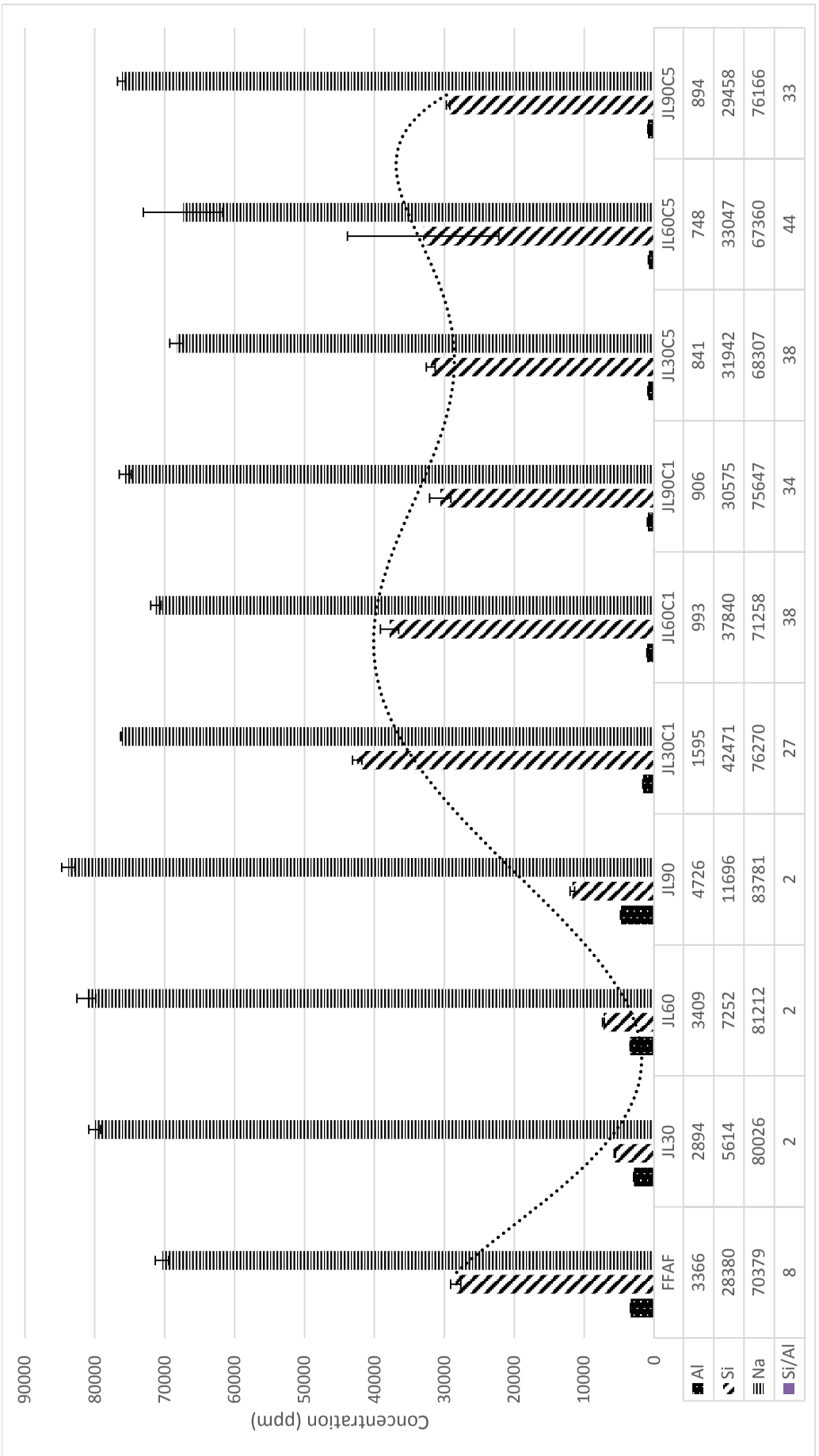

Figure 5-1: ICP – AES results of the aluminium, silicon and sodium within the fusion filtrate and the jet loop filtrates, mass ratio in jet loop mixing was 1:1:5 of CFA:NaOH:H_2O, mixing time varied from 30, 60 and 90 minutes and curing time varied from no curing; 1 day at 80^{0}C then 4 days at room temperature; 5 days at 80^{0}C, analysis done in triplicate

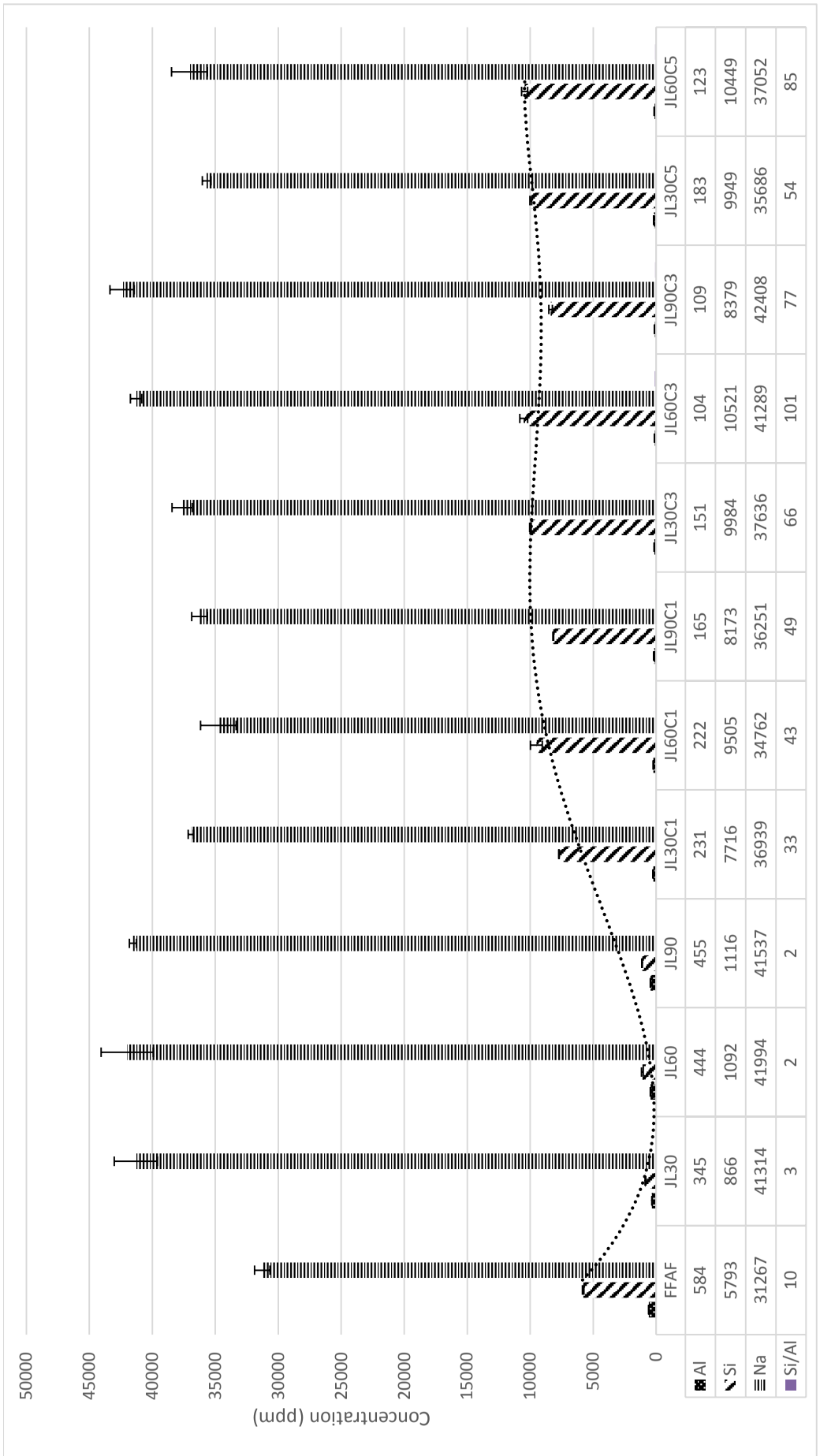

	FFAF	JL30	JL60	JL90	JL30C1	JL60C1	JL90C1	JL30C3	JL60C3	JL90C3	JL30C5	JL60C5
Al	584	345	444	455	231	222	165	151	104	109	183	123
Si	5793	866	1092	1116	7716	9505	8173	9984	10521	8379	9949	10449
Na	31267	41314	41994	41537	36939	34762	36251	37636	41289	42408	35686	37052
Si/Al	10	3	2	2	33	43	49	66	101	77	54	85

Figure 5-2: ICP – AES results of the aluminium, silicon and sodium within the fusion filtrate and the jet loop filtrates, mass ratio in jet loop mixing was 1:1:5 of CFA:NaOH:H_2O, mixing time varied from 30, 60 and 90 minutes and curing time varied from no curing; 1 day at 80^{0}C then 4 days at room temperature; 3 days at 80^{0}C; 5 days at 80^{0}C, analysis done in triplicate

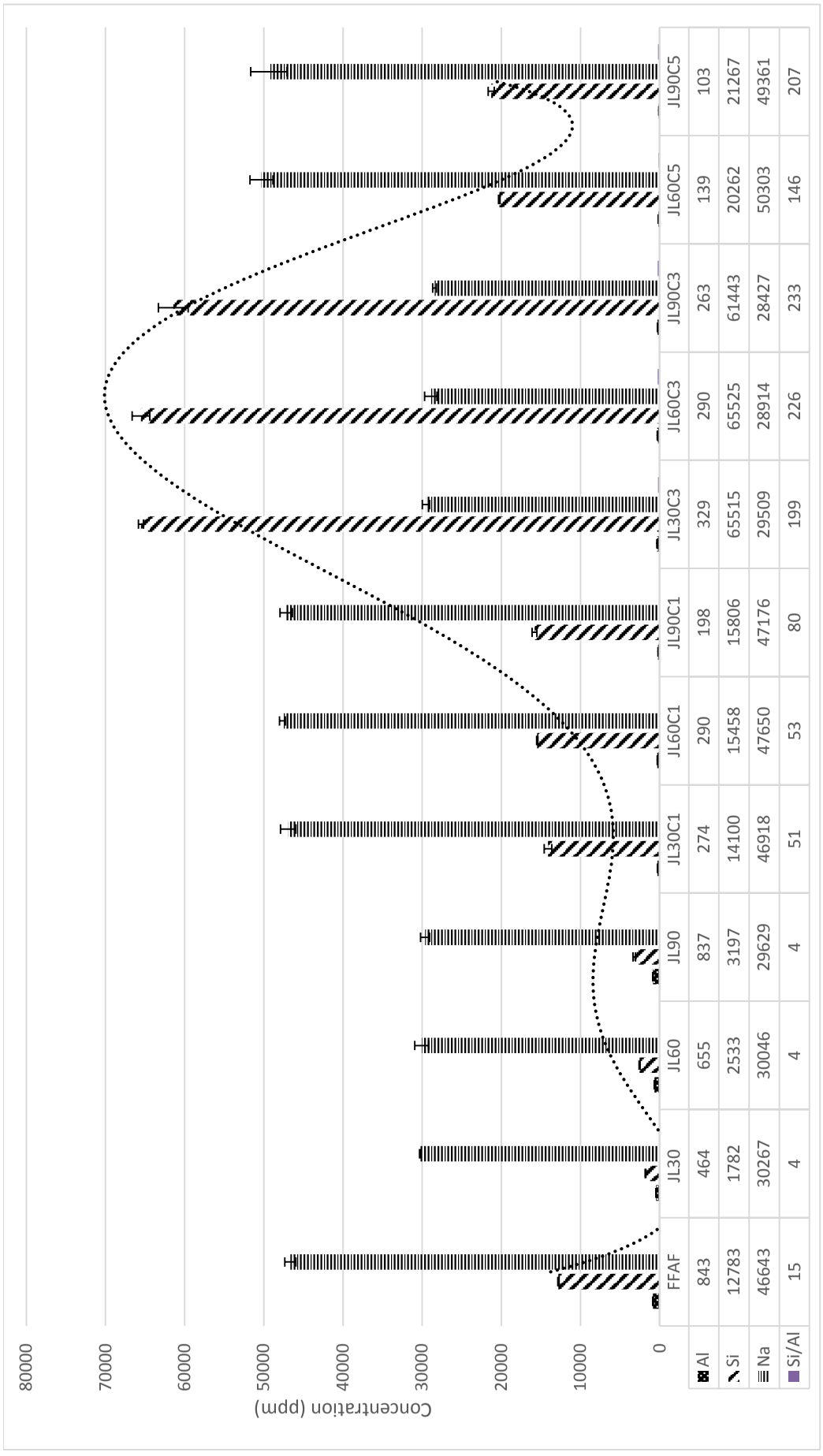

	FFAF	JL30	JL60	JL90	JL30C1	JL60C1	JL90C1	JL30C3	JL60C3	JL90C3	JL60C5	JL90C5
Al	843	464	655	837	274	290	198	329	290	263	139	103
Si	12783	1782	2533	3197	14100	15458	15806	65515	65525	61443	20262	21267
Na	46643	30267	30046	29629	46918	47650	47176	29509	28914	28427	50303	49361
Si/Al	15	4	4	4	51	53	80	199	226	233	146	207

Figure 5-3: ICP – AES results of the aluminium, silicon and sodium within the fusion filtrate and the jet loop filtrates, mass ratio in jet loop mixing was 1:1:5 of CFA:NaOH:H_2O, mixing time varied from 30, 60 and 90 minutes and curing time varied from no curing; 1 day at 80^{0}C then 4 days at room temperature; 3 days at 80^{0}C; 5 days at 80^{0}C, analysis done in triplicate

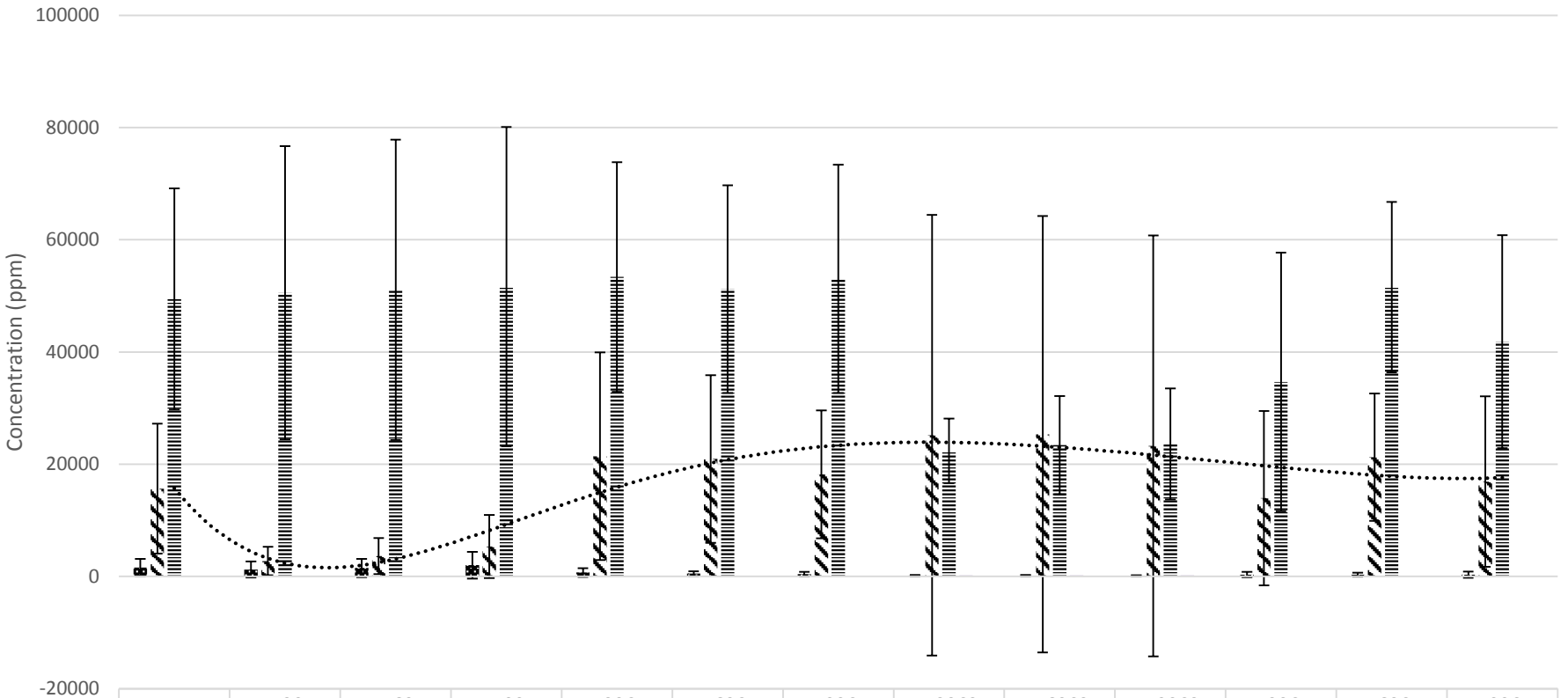

	FFAF	JL30	JL60	JL90	JL30C1	JL60C1	JL90C1	JL30C3	JL60C3	JL90C3	JL30C5	JL60C5	JL90C5
Al	1598	1234	1502	2006	700	502	423	160	131	124	341	337	332
Si	15652	2754	3626	5337	21429	20934	18185	25166	25349	23274	13963	21253	16908
Na	49429	50536	51084	51649	53376	51224	53025	22382	23401	23612	34664	51572	41842
Si/Al	10	2	2	3	31	42	43	157	193	188	41	63	51
n	3	3	3	3	3	3	3	2	2	2	2	3	2

Figure 5-4: ICP – AES results of the aluminium, silicon and sodium within the fusion filtrate and the jet loop filtrates, mass ratio in jet loop mixing was 1:1:5 of CFA:NaOH:H_2O, mixing time varied from 30, 60 and 90 minutes and curing time varied from no curing; 1 day at 80^0C then 4 days at room temperature; 3 days at 80^0C; 5 days at 80^0C, analysis done in triplicate, average for all runs showing reproducibility, n = number of runs

Regarding Figure 5-1, 5-2, 5-3 and 5-4 the samples were coded based on the fused fly ash filtrate (FFAF), the jet loop mixing times of 30, 60 and 90 minutes with no additional curing (JL30, JL60, JL90) the curing of these jet loop samples for 1 day at 80^0C followed by 4 days at room temperature (JL30C1, JL60C1, JL90C1) the curing of the jet loop samples for 3 days at 80^0C (JL30C3, JL60C3, JL90C3) and the curing of the samples for 5 days at 80^0C (JL30C5, JL60C5, JL90C5). What can be seen initially between the comparison of the jet loop mixing times without factoring the curing of the samples is that there is no remarkable difference between jet looping for 30, 60 and 90 minutes overall. It can be concluded from this based on an energy perspective that jet looping for 30 minutes is sufficient for the extraction of the necessary silicon and aluminium for zeolite synthesis. Considering the difficulty of producing accurate ICP – AES results from repeated runs, the experiment was repeated 3 times to determine the reproducibility of the process. It is noted however that not all varying conditions were replicated 3 times. This is due to the first experiment (Figure 5-1) not including the sampling after 3 days curing. Also in the second experiment (Figure 5-2) there is no result for the JL90C5 sample, as this sample was more of a paste and could not be filtered. This is the same for the sample JL30C5 in the third experiment (Figure 5-3). Figure 5-4 thus shows the average for all 3 experiments and indicates where the runs were repeated 2 or 3 times. All the trend lines on the figures represent that of the silicon within the filtrates, as it was more prominently dissolved than the aluminium. The aluminium dissolution was not as prominent as the silicon dissolution which had a dramatic effect on the Si/Al ratios within the filtrates. This would mean that in order to synthesize zeolite X, additional aluminium may need to be added to decease the Si/Al ratio enough to be comparable to the fusion filtrate Si/Al ratio of 9.8. An anomaly in analysis appeared in Figure 5-3 with the samples that were cured for 3 days. ICP results showed a spike in the silicon concentration to roughly 65 000 ppm. This anomaly produced the dramatic error bars seen in Figure 5-4. Due to the difficulty experienced of producing accurate data using the ICP – AES, a UV – Vis method was then used to compare the concentrations that were averaged over the three experiments for silicon. The third set of samples were thus subjected to UV – Vis analysis and the results are presented in Figure 5-5 alongside the average ICP – AES results for all three runs.

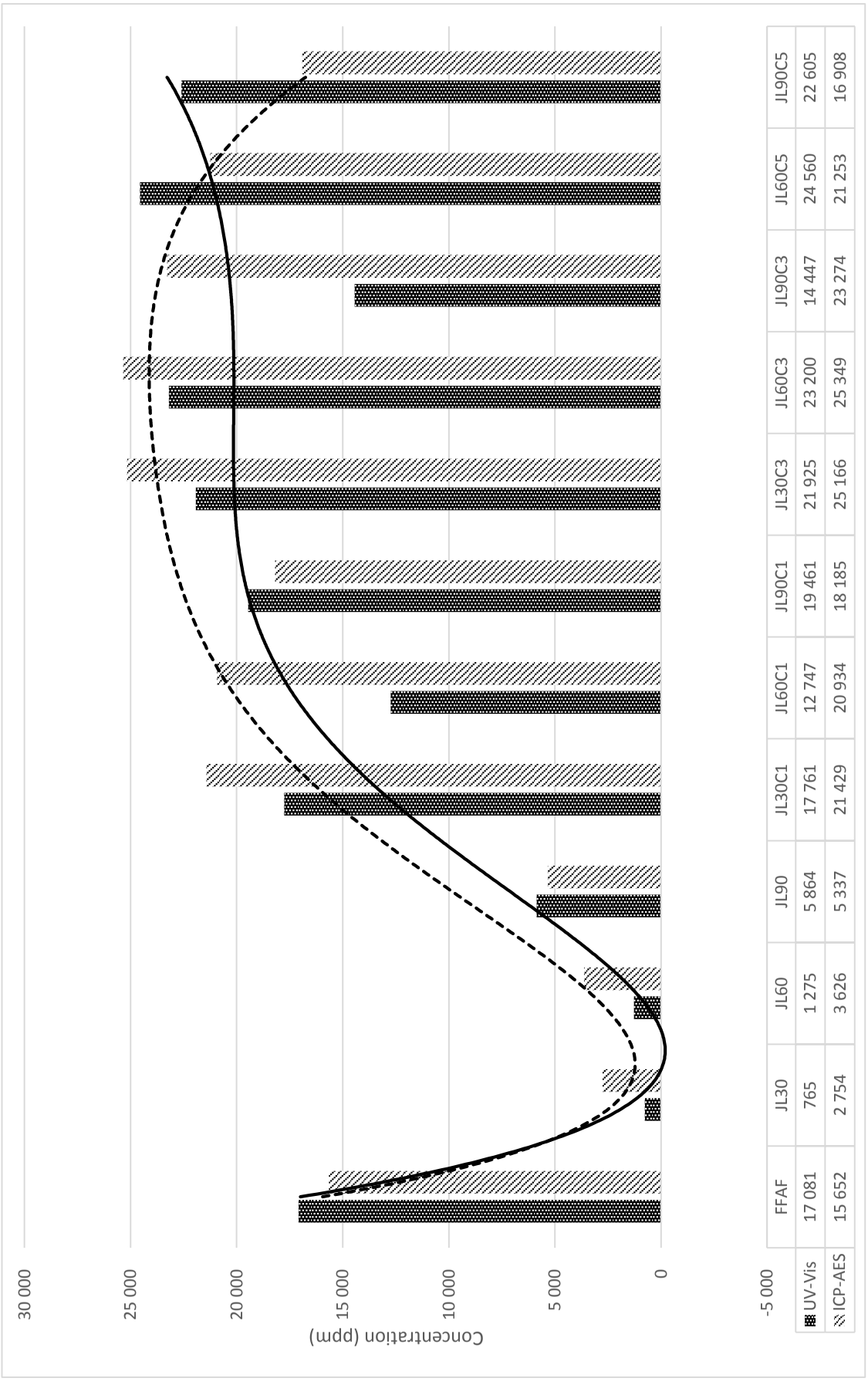

	FFAF	JL30	JL60	JL90	JL30C1	JL60C1	JL90C1	JL30C3	JL60C3	JL90C3	JL60C5	JL90C5
UV-Vis	17 081	765	1 275	5 864	17 761	12 747	19 461	21 925	23 200	14 447	24 560	22 605
ICP-AES	15 652	2 754	3 626	5 337	21 429	20 934	18 185	25 166	25 349	23 274	21 253	16 908

Figure 5-5: UV – Vis results of silicon concentration in comparison to ICP – AES results of average silicon concentrations for all runs

It can be seen in Figure 5-5 that there is a general correlation between the UV – Vis results and the average ICP – AES results. Thus given the nature of the ICP – AES technique that suffers from matrix effects which can skew the data, the UV – Vis method is shown to be a good complimentary technique. Another problem with the analysis of soluble silica in solution with ICP – AES is that the solution can become more viscous with the higher concentration of soluble silica. This would therefore interfere with the ICP – AES instrument and produce the anomalies seen in the ICP – AES results. Therefore, the experiment was conducted again at the optimal jet looping time of 30 minutes and cured specifically for 3 days at 80^0C and analysed with ICP – AES again to see whether the higher concentration was indeed an anomaly in analysis. The result is represented in Figure 5-6.

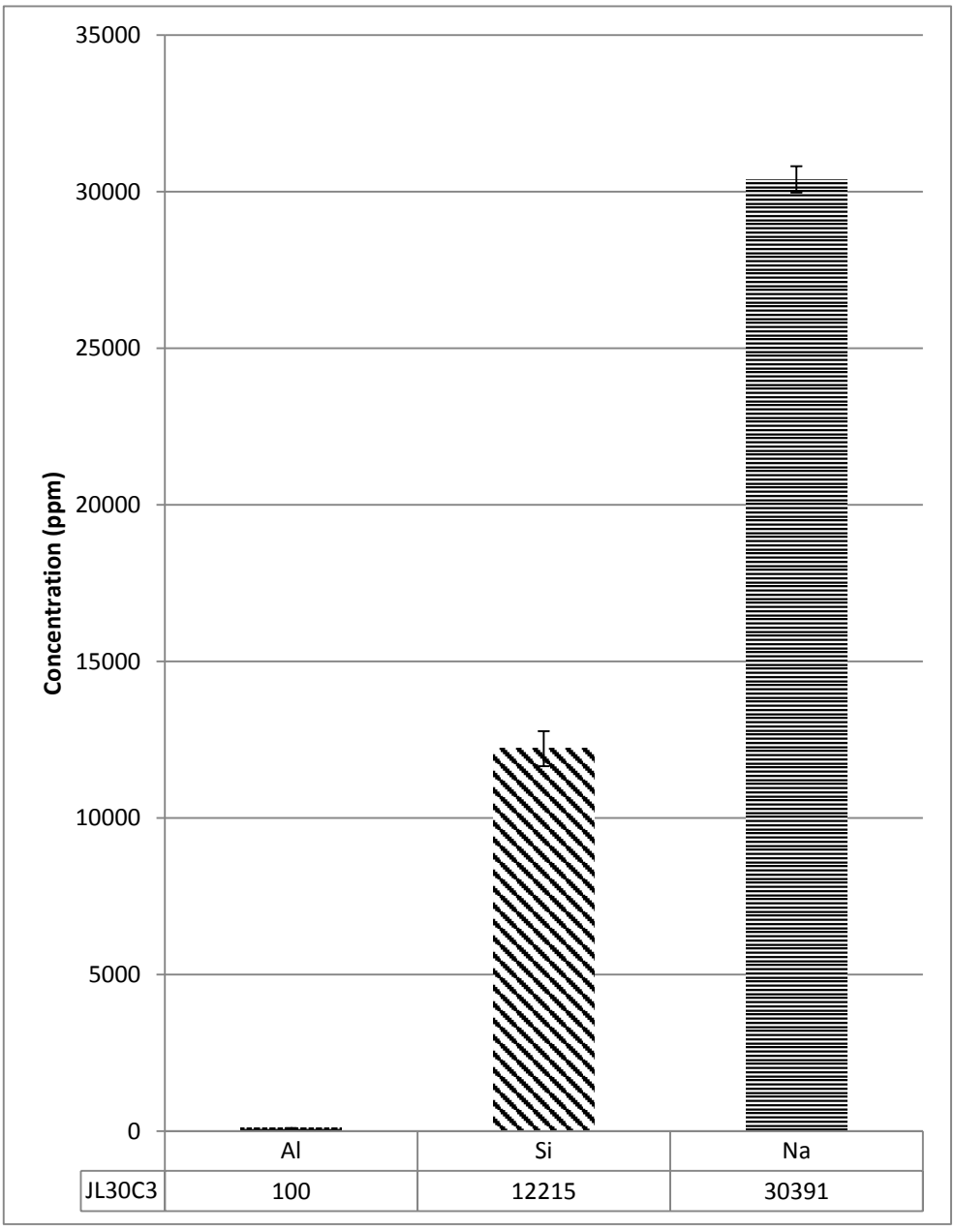

Figure 5-6: ICP – AES result for jet looping mixing for 30 minutes and curing for 3 days at 80^0C, analysis done in triplicate

Figure 5-6 shows that the anomaly seen in ICP data shown in Figure 5-3 when curing the jet loop samples for 3 days at 80^0C was an error of ICP analysis. From all the data it can be concluded that the optimal jet loop mixing and curing time is 30 minutes of jet loop mixing followed by curing for 1 day at 80^0C followed by 4 days at room temperature (JL30C1), which may be the most economical, energy wise, at least within the jet loop and cured samples. In further characterisation of the jet loop and curing pre-synthesis method the solid residues separated from the filtrates were analysed. First the XRF of the residues of only the optimal jet loop mixing time were analysed to see the relation of the distribution of elements to that within the filtrates produced, shown in Table 5-1. The XRF is reported on a dry basis after normalizing the loss on ignition (LOI).

Table 5-1: XRF of solid residues after 30 minutes' jet loop mixing compared with starting CFA

Major Oxides (%)*	CFA	JL30	JL30C1	JL30C3	JL30C5
SiO_2	57.46	50.36	34.81	30.16	33.88
Na_2O	0.00	8.55	30.18	39.53	38.45
Al_2O_3	27.27	29.36	25.49	21.64	19.96
CaO	5.61	4.70	4.35	3.58	3.23
Fe_2O_3	5.96	3.58	3.27	2.93	2.79
TiO_2	1.69	1.58	1.46	1.23	0.98
MgO	1.65	1.32	1.21	1.04	0.78
K_2O	0.59	0.57	0.40	0.46	0.72
P_2O_5	0.38	0.22	0.13	0.10	0.16
MnO	0.05	0.04	0.03	0.03	0.02
Cr_2O_3	0.02	0.04	0.03	0.01	0.02
V_2O_5	0.02	0.02	0.00	0.00	0.00
Total	100.71	100.33	101.36	100.70	100.99
SiO_2/Al_2O_3	2.11	1.72	1.37	1.39	1.70
Si/Al	1.79	1.46	1.16	1.18	1.44

*LOI corrected

Table 5-1 shows the decrease in the silica content from 50.36% with no curing (JL30) to 34.81% after curing of the residues for 1 day at 80^0C followed by 4 days at room temperature (JL30C1) in correlation with the increase of the silicon content found in filtrates after curing. Thus these results show that the curing of the jet loop slurry allowed greater silicon dissolution into the filtrate. However, the aluminium content within the filtrates was shown previously to decrease in concentration after curing, which does not correlate well with the XRF results in Table 5-1. The alumina content of the residues also decreases from 29.36% to 19.96% after curing the samples from 0 days curing to 5 days curing. Even though there is not an increase in the alumina content within the residues with curing, the decrease in content of alumina is not as substantial as the decrease of silica content within

the residues. Therefore, the silica dissolution is greater than the alumina dissolution when curing the samples.

For further investigation into the effect of curing the jet loop samples the solid residues produced after filtering the jet loop samples were analysed after 0, 3 and 5 days curing at 80^{0}C as set out in section 3.4.2, including XRD and FTIR analysis. The XRD results are presented in Figure 5-7.

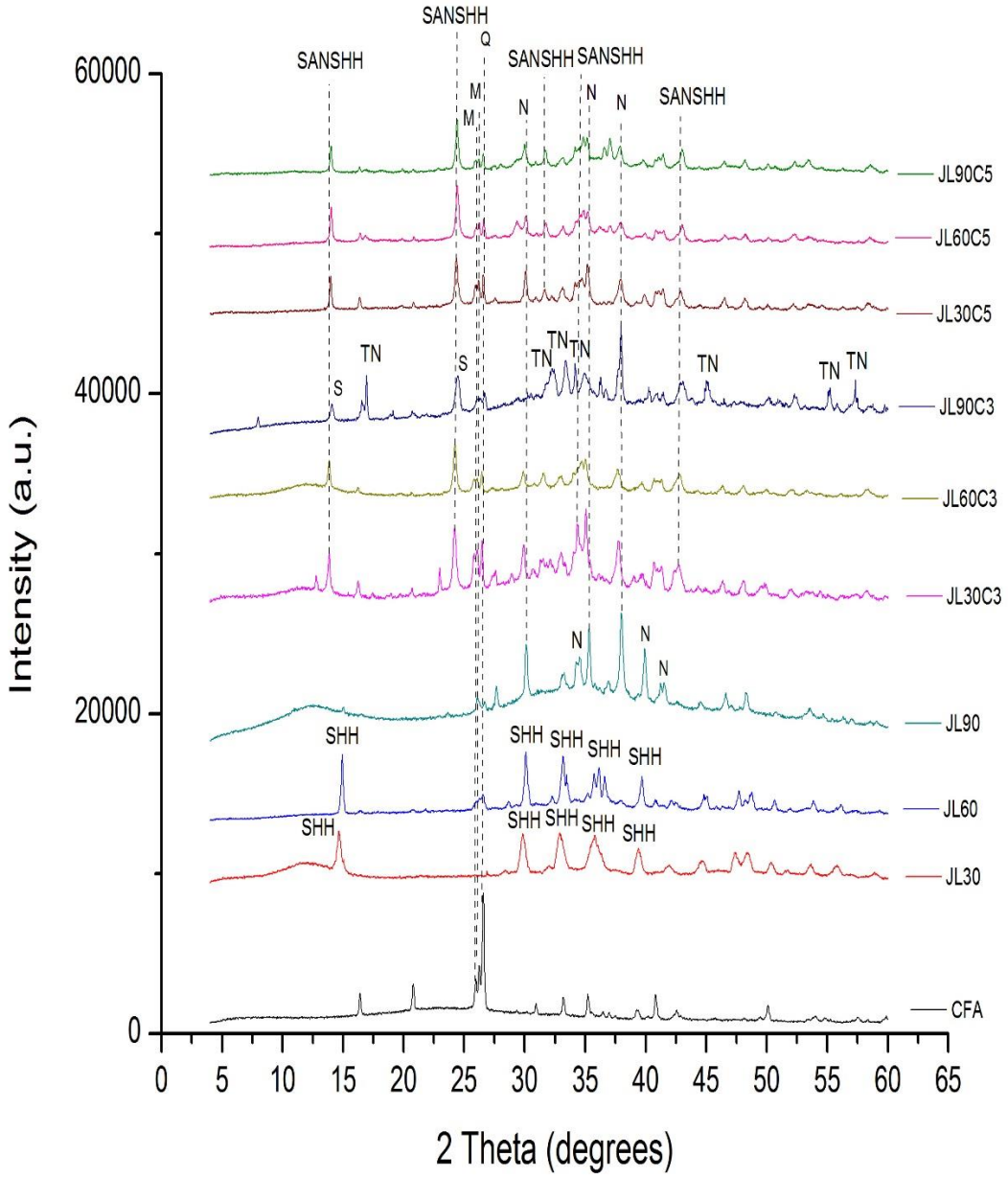

Figure 5-7: XRD spectra of jet loop residues after 30, 60 and 90 minutes' jet looping and 0, 3 and 5 days of curing at 80^{0}C (SHH – Sodium hydroxide hydrate; N – Natrite; TN – Thermonatrite; S – Sodalite; M – Mullite; Q – Quartz; SANSHH – Sodium aluminium nitrite silicate hydroxide hydrate)

Figure 5-7 shows the XRD spectra of the jet loop solid residues in comparison with the XRD spectra for the raw CFA. The codes corresponding to the samples are jet loop mixing times of 30, 60 and 90 minutes with no additional curing (JL30, JL60, JL90), the curing of the jet loop samples for 3 days at 80^0C (JL30C3, JL60C3, JL90C3) and the curing of the samples for 5 days at 80^0C (JL30C5, JL60C5, JL90C5). It can be seen that the quartz and mullite intensities decreased with increasing curing duration, however these minerals were not all that present in the jet loop samples prior to curing (JL30, JL60, JL90), the samples that were freeze dried. In these freeze dried samples the main crystalline phase was that of sodium hydroxide hydrate, which shows the sodium hydroxide was prevalent within the freeze dried samples. After mixing for 90 minutes in the non-cured samples (JL90) there was a formation of natrite, that was also seen in the samples further cured for 5 days (JL30C5, JL60C5, JL90C5). The presence of natrite and thermonatrite with chemical formulas of Na_2CO_3 and $Na_2CO_3.H_2O$ respectively, given that they are carbonate mineral phases, is that there is a possibility for CO_2 capture as previously reported by Nyale (2014). The curing of the samples for 3 or 5 days led to the formation of sodium aluminium nitrite silicate hydroxide hydrate, of which was not present within the non-cured or CFA spectra. This could show the formation of the geopolymer structure forming within the cured residues. The XRD spectra also shows the amorphous content within the jet loop residues, which tended to decrease given the longer curing times and is displayed by the hump between $18^0 – 30^0$ 2θ within the spectra. This could imply that the greater curing time allowed for more dissolution of the amorphous phase of the CFA along with the formation of the geopolymers in the residues. To further investigate the residues, FTIR analysis was performed and is presented in Figure 5-8.

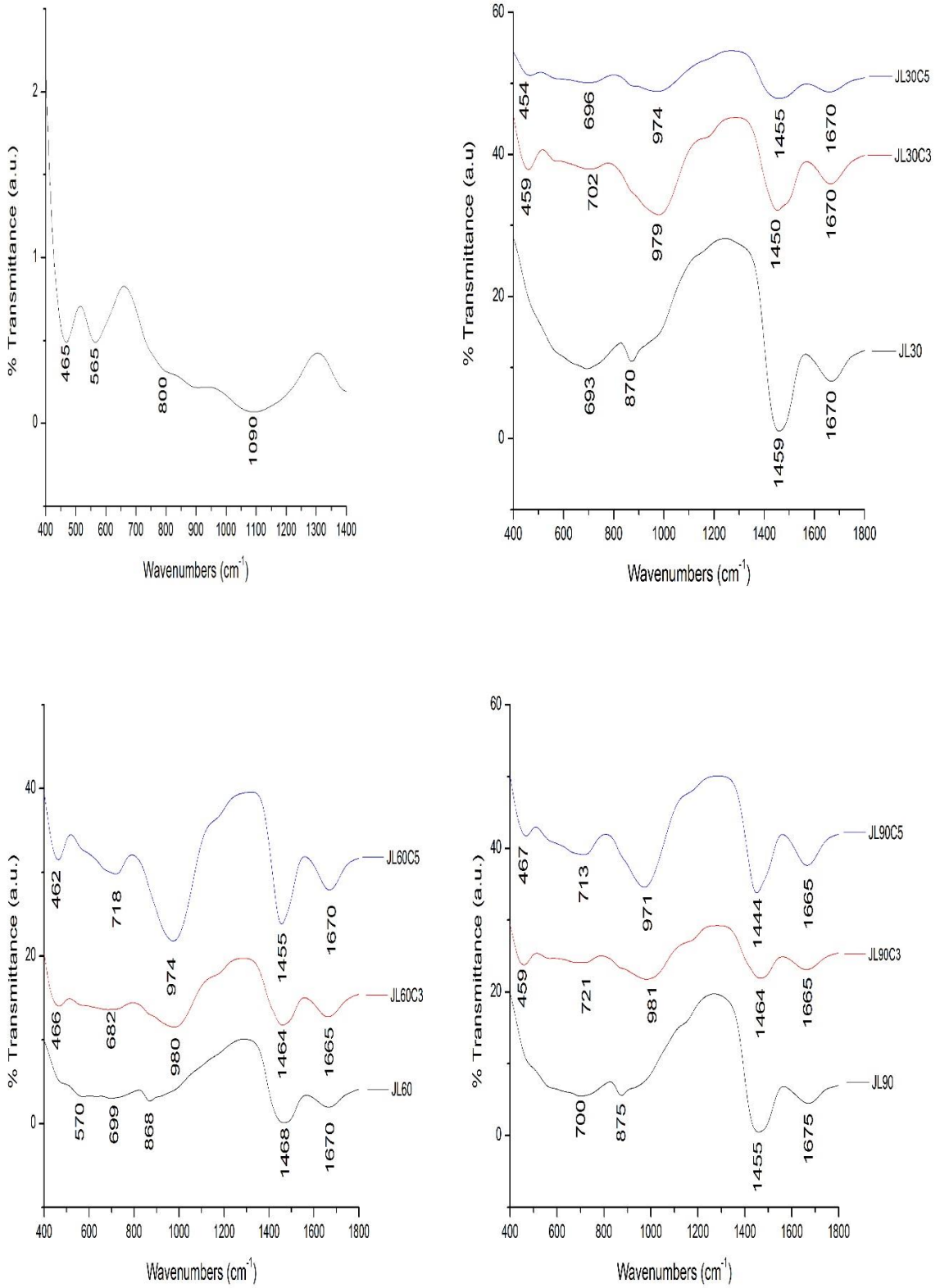

Figure 5-8: FTIR spectra of jet loop residue samples after jet looping for 30, 60 and 90 minutes and then 0, 3 and 5 days curing, including the CFA spectra

The FTIR spectra of the residues collected from the jet loop experiments are represented in Figure 5-8. The main bands appearing are tabulated in Table 5-2 with their relative assignments.

Table 5-2: Summary of FTIR vibrations for jet loop pre-synthesis

Wavenumbers (cm^{-1})					
JL30	JL60	JL90	Literature values	Assignment	Reference
693	699	700	650 - 720	Symmetrical stretch (O-T-O group) (Internal tetrahedra)	Table 2-4
870	868	875	882	Si-O Stretching and OH bending (Si-OH)	(Lee and Van Deventer, 2003)
1459	1468	1455	1440	Sodium Carbonate (Na_2CO_3)	(Miller and Wilkins, 1952)
1670	1670	1675	1600 - 1700	OH^- deform (bending)	Table 2-4
JL30C3	JL60C3	JL90C3	Literature values	Assignment	Reference
459	466	459	420 - 500	(Si-O-Al) T-O Bend (Internal tetrahedra)	Table 2-4
702	682	721	650 - 720	Symmetrical stretch (O-T-O group) (Internal tetrahedra)	Table 2-4
979	980	981	950 - 980	Si-O Stretching ($Si\text{-}O^-Na^+$)	(Lee and Van Deventer, 2003)
1450	1464	1464	1440	Sodium Carbonate (Na_2CO_3)	(Miller and Wilkins, 1952)
1670	1665	1665	1600 - 1700	OH^- deform (bending)	Table 2-4
JL30C5	JL60C5	JL90C5	Literature values	Assignment	Reference
454	462	467	420 - 500	(Si-O-Al) T-O Bend (Internal tetrahedra)	Table 2-4
696	718	713	650 - 720	Symmetrical stretch (O-T-O group) (Internal tetrahedra)	Table 2-4
974	974	971	950 - 980	Si-O Stretching ($Si\text{-}O^-Na^+$)	(Lee and Van Deventer, 2003)
1455	1455	1444	1440	Sodium Carbonate (Na_2CO_3)	(Miller and Wilkins, 1952)
1670	1670	1665	1600 - 1700	OH^- deform (bending)	Table 2-4

Table 5-2 shows the jet loop slurries before curing had similar vibrations regardless of jet loop mixing time. What is notable being the group corresponding in literature to the Si-O stretching and OH bending (Si-OH) in the uncured freeze dried jet loop samples (JL30, JL60, JL90) and the Si-O stretching ($Si\text{-}O^{-}Na^{+}$) in the cured samples, in relation to the broad peak seen in the raw fly ash FTIR spectra. The broad peak of the CFA spectra appearing at 1090 cm^{-1} and as previously mentioned corresponding to the Si-O-Si or Al-O-Si asymmetric stretching of the crystalline matrix can be seen to shift to lower frequencies after jet loop mixing (+/- 870 cm^{-1}) and then to higher frequencies after curing the jet loop slurry for 3 days at 80^0C (+/- 980 cm^{-1}) and 5 days at 80^0C (+/- 974 cm^{-1}) while also becoming narrower in the residues. This shift in a pendular manner from low and then back up to high frequencies can be explained as follows. Initially the vitreous component dissolves due to the contact between the CFA and alkaline solution, giving a gel rich in Al content to immediately precipitate. There would therefore be a higher content of Al^{3+} than Si^{4+} ions in the early stage of the process i.e. after 30 to 90 minutes of jet loop mixing. This is also due to Al-O bonds being weaker than Si-O bonds and more easily broken. Therefore, regarding the filtrate analysis previously there is more aluminium found in the filtrate after jet loop mixing prior to curing as there is more aluminium released in the slurry from the jet loop mixing. Therefore, when this slurry was freeze dried the FTIR showed the shift to lower wavenumbers. Also the narrow band appearing at +/- 870 cm^{-1} also corresponds (Table 2-5) to the silicon monomers with a high degree of depolymerisation $Si(OH)_4$ which would have been released into the slurry and found in the freeze dried samples. The jet loop mixing with NaOH therefore sufficiently breaks down the quartz in the fly ash to the monomers resulting in the release the silicon found in the CFA. As the reaction progresses though the curing for 3 days at 80^0C more Si-O groups in the original CFA are released, which raises the Si concentration and boosts the formation of the zeolite precursors or geopolymer formation in the residue, hence the band shifts to higher more siliceous wavenumbers in the residues (Fernández-Jiménez and Palomo, 2005). This also corresponds to the filtrate analysis showing the highest dissolution of silicon after curing of the slurry. Therefore, the curing is releasing more silicon into the slurry which is producing a more siliceous filtrate when filtered. Although the shift after curing for 5 days compared to 3 days decreased slightly to lower frequencies and shows the incorporation of the Al into the Si-O-Si structure and an increases in the number of non-bridging oxygens in the silicon tetrahedra (Böke et al., 2015). Thus the longer curing time is allowing the geopolymers to form in the residues, incorporating the silicon and aluminium into the geopolymer structure as can be seen by the main bands around 975 cm^{-1} becoming narrower with curing (Böke et al., 2015). This correlates with the XRD spectra in Figure 5-7 with the sodium aluminium nitrate silicate hydroxide hydrate species that formed in the residues with only the samples produced after curing the jet loop slurry. Another correlation is with the sodium carbonate found in the residues as mentioned previously in the XRD spectra showing natrite and thermonatrite in the residues. The FTIR spectra all show the very strong band found around 1440 cm^{-1} which corresponds in literature to a band of sodium carbonate, thus complementing the XRD spectra. This confirms the possibility for CO_2 capture in the residues. The lower temperature curing at 80^0C favours more dissolution of the silicon into the filtrates as seen in the ICP – AES results of the filtrates. The curing at 80^0C for 3 days favours the release of the silicon

into the filtrates while further curing results in geopolymer formation in the residues incorporating Si, instead of releasing the silicon into the filtrates. This confirms that the optimum time for jet loop curing is 80^{0}C for 1 day followed by 4 days at room temperature. The residue -produced from this pre-synthesis condition could then be further cured to produce a geopolymer once the filtrate has been filtered off for the zeolite synthesis from the filtrate. Figure 5-9 shows the comparison in morphology of the cured residues after 80^{0}C for 5 days with that of the fused fly ash used in the fusion process.

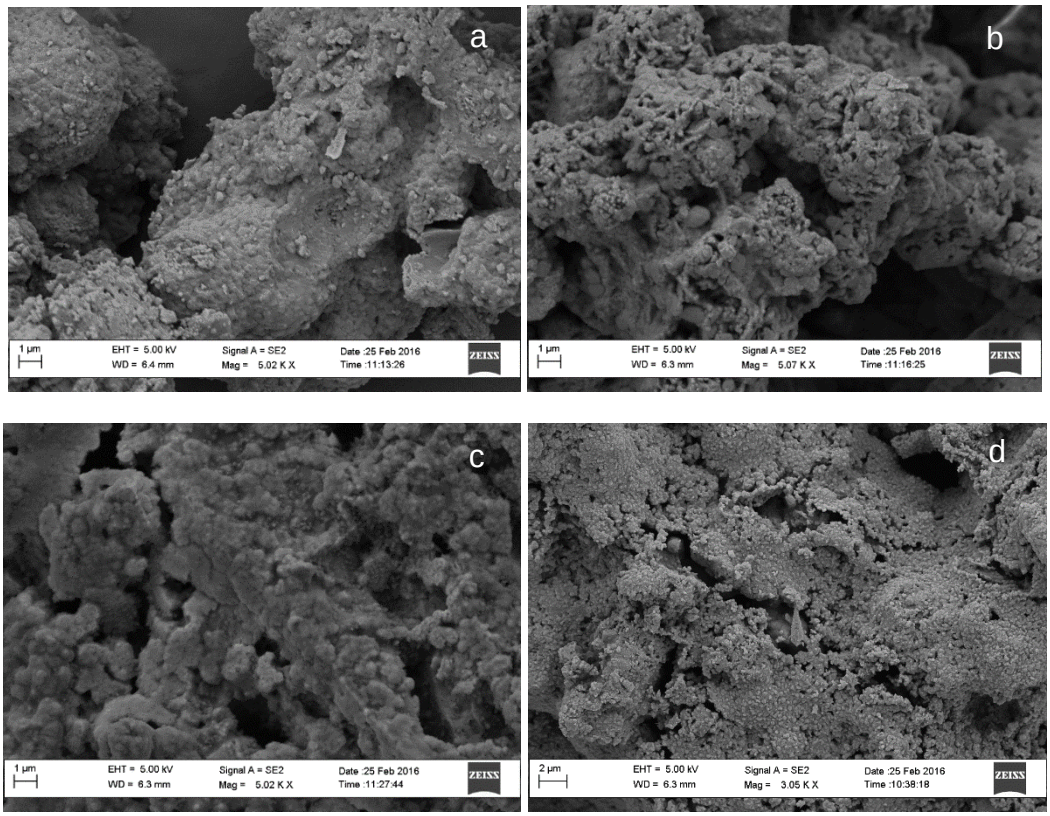

Figure 5-9: SEM micrographs of jet loop residues after 5 days of curing at 80^{0}C at varying jet looping times: (a) 30 mins (b) 60 mins (c) 90 mins (d) Fused fly ash

As can be seen in Figure 5-9, the jet loop mixing and curing can be seen as comparable to the fusion of the fly ash with NaOH at 550 ^{0}C regarding the breaking down of the fly ash as seen in the similar morphologies of the residues. It can be seen that the morphology of the fused fly ash revealed the coarseness of the particle, the gelly nature of the slurry obtained due to curing increased progressively with jet looping time. The following section will deal with the material balance around the pre-synthesis process of jet loop mixing and curing and will be followed by an attempt to synthesis zeolite X from the optimal conditions found within this section, namely jet looping for 30 minutes followed by curing for 1 day at 80^{0}C and 4 days at room temperature.

5.3. Material balance around jet loop and curing process

A material balance was performed around the pre-synthesis of jet loop and curing, as will be presented in this section. The material balance was performed in sections around each of the processes within the total process of the jet loop mixing, curing and hydrothermal treatment. This is

shown in Figure 5-10, where the red border shows the overall process and the green borders show the individual balances performed. Ratios were then used to relate the scale of the mass of elements back to the original basis for the material balance, being the 3200 g of starting CFA within the process.

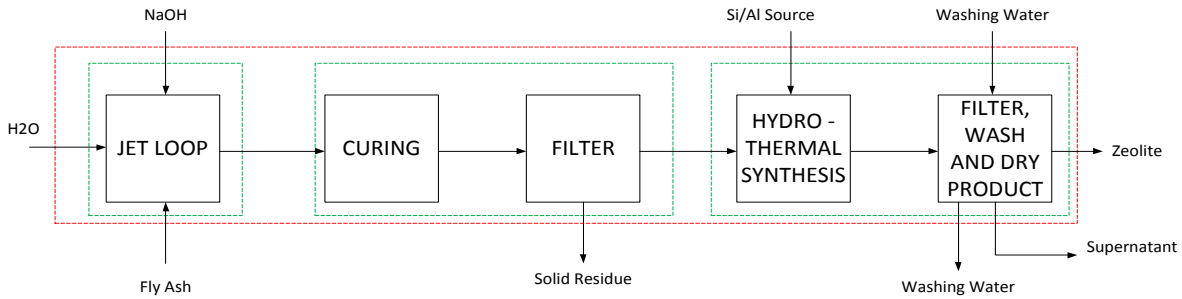

Figure 5-10: BFD of overall jet loop and curing pre-synthesis with hydrothermal synthesis

Figure 5-11 shows the overall material balance around the jet loop mixing process, it is followed by Figure 5-12, which shows the overall material balance conducted around the curing and filtering of the cured slurry. Analysis was performed previously on the CFA starting material and was performed in this section on the solid residue and filtrate produced after jet loop mixing for 30 minutes and curing the slurry at the optimised conditions (1 day at 80^0C and 4 days at room temperature). An elemental balance could then be performed showing the distribution of the major elements and whether they report to the solid residue or the filtrate used for hydrothermal synthesis. This is presented in Table 5-3. There was water vapour lost within the processes but there were also losses concerning the spillages during the transferring the slurry as well as vestiges found in the jet loop and after curing the samples, which constitute about 25% of the total mass fed into the process.

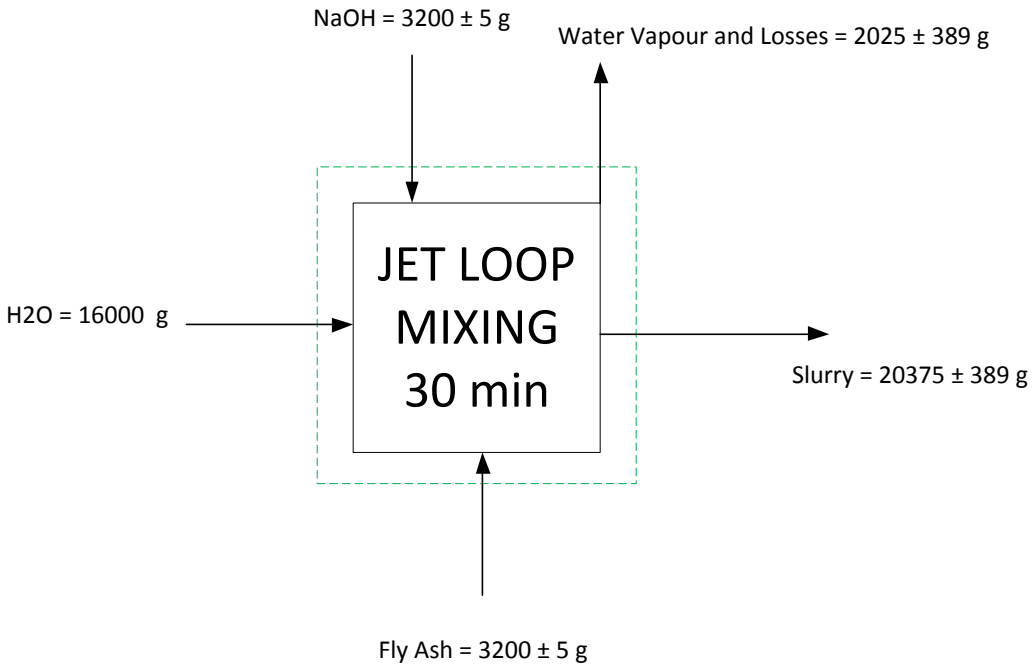

Figure 5-11: BFD of overall material balance around jet loop mixing

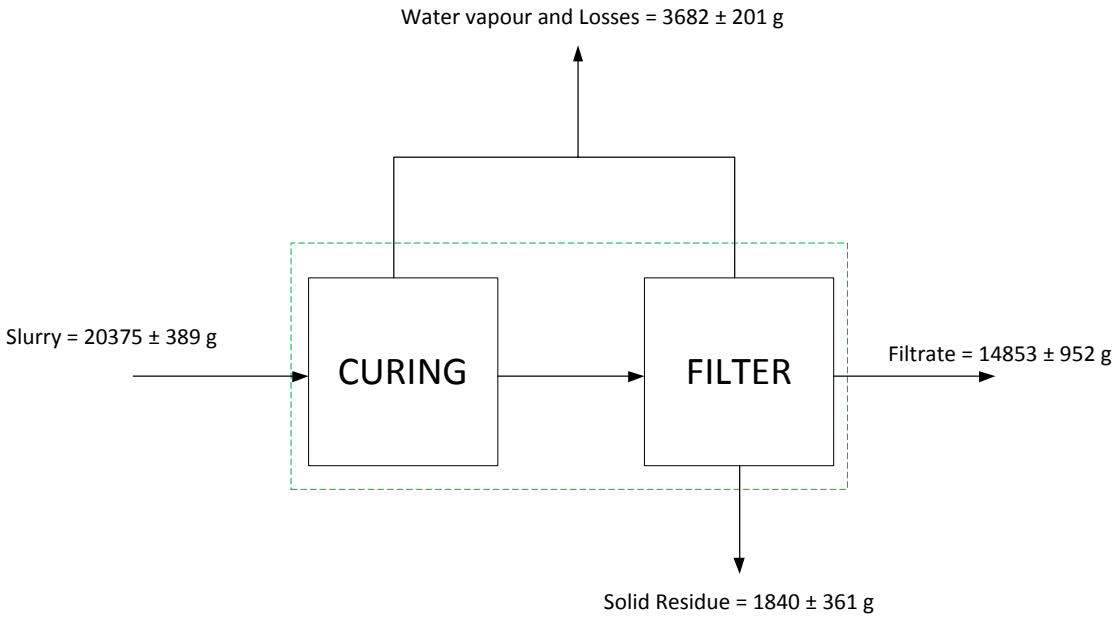

Figure 5-12: BFD of overall material balance around curing process (curing at 80^0C for 1 day and 4 days at room temperature)

When scaling up the solid residue produced from the curing process (on a dry basis) the total dry solids amounts to 1840 g of solid residue. Considering the total solids fed into the process totals to approximately the 3.2 kg of CFA fed into the process (as majority of the NaOH is dissolved into the water) this is only a 50% recovery of the solids within the process. This can only be explained through the spillages and vestiges mentioned previously. Table 5-3 shows the elemental distribution of the major elements and whether they report to the solid residue or the filtrate used for hydrothermal synthesis. The ICP results of the filtrate were used as a basis to calculate the percentage of elements reporting to the solid residue. Table 5-4 shows a comparison of this calculated solid residue percentage in contrast to the percentage obtained through the XRF analysis of the solid residue. This is in order to show how far the two values deviate from one another, highlighting the matrix effects that can be experienced through analytical techniques.

Table 5-3: Percentage weight distribution of major elements within the output streams of the jet loop mixing and curing process

Weight % of Element	Residue	std. dev.	Filtrate	std. dev.	Recovery
Si	68.52	2.02	31.48	2.02	100.00
Al	98.09	0.12	1.91	0.12	100.00
Fe	99.94	0.00	0.06	0.00	100.00
Ca	99.77	0.01	0.23	0.01	100.00
Ti	99.92	0.01	0.08	0.01	100.00
Mg	99.97	0.00	0.03	0.00	100.00
K	39.51	3.88	60.49	3.88	100.00
P	35.78	4.11	64.22	4.11	100.00
Mn	99.82	0.01	0.18	0.01	100.00
V	76.27	1.52	23.73	1.52	100.00
Cr	99.15	0.05	0.85	0.05	100.00
Na	62.30	2.42	37.70	2.42	100.00

From Table 5-3 it can be seen that the jet loop mixing of 30 minutes and curing at 80^0C for 1 day followed by 4 days at room temperature releases 31.48 ± 2.02% of silicon from the starting CFA. This can be compared to the calculated value of 26.19% of silicon released from CFA during the fusion process reported in Chapter 4 and calculated based on the ICP – AES results in Figure 5-4 and the overall material balance in Chapter 4. Therefore, there is an improvement on the silicon that can be extracted from CFA using a process that can be argued to be more easily scalable than the fusion process. In comparison to a recent study by Ojumu et al. (2016) which is summarized in Table 5-5 the silicon released using a short sonochemical treatment of 10 minutes was 24% compared to using the fusion process within that study where 32% of silicon was reported to be extracted. Therefore, it can be argued that it may be more feasible to scale-up the jet loop and curing process to industrial scale. This is due to the fact that the jet loop pilot plant can already treat up to 80 litres of volume, which can be scaled to much greater volumes more readily. However, the aluminium extraction using the jet loop and mixing process is poor, extracting only 1.91 ± 0.12% of the aluminium from the CFA at the optimum conditions. This means there would need to be an aluminium addition to the hydrothermal process when using the filtrate, although low Al extraction was also the case for the study involving sonochemical treatment (Ojumu et al., 2016). Based on the ICP analysis, the majority of the elements seemed to report to the solid residue overall. In comparison to these ICP results the results of the XRF analysis on the residue is shown in Table 5-4.

Table 5-4: Comparison of the elemental weight percent found in the solid residue based on ICP – AES and XRF analysis

Weight % of Element	ICP - AES Residue	XRF Residue	std. dev.
Si	68.52	34.83	23.82
Al	98.09	53.74	31.36
Fe	99.94	31.52	48.38
Ca	99.77	44.65	38.98
Ti	99.92	49.86	35.40
Mg	99.97	41.91	41.05
K	39.51	38.53	0.69
P	35.78	19.61	11.43
Mn	99.82	34.39	46.26
V	76.27	0.00	53.93
Cr	99.15	85.98	9.31
Na	62.30	23.08	27.74

It should be noted regarding Table 5-4 that the ICP – AES residue results were produced as a percentage based on the ICP – AES analysis of the filtrate in Table 5-3. The ICP – AES of the filtrate was analysed and then the assumption of a total recovery of each element was made. Then the remaining balance was assumed to report to the residue, based on ICP analysis of the filtrate. In Table 5-4 it is showing the comparison of the balanced ICP – AES residue with the actual weight percentage calculation based on the XRF analysis of the residues, therefore showing the comparison between what is expected through ICP and what was produced through XRF. The difference found between the two analytical methods can only be explained through inaccuracies in the XRF and ICP – AES analysis techniques. The inaccuracy of the ICP – AES technique was already reported in this chapter which could be made more accurate regarding silicon analysis through comparison with an UV – Vis technique. However, this lack of accuracy was not the case for all the other major elements analysed. There is also a body of literature supporting this finding on the matrix effects that can be experienced through various analytical techniques when determining major elements such as Si and Al, which could play a part when trying to produce accurate elemental balances (Kola and Perämäki, 2004; Windom and Hahn, 2009; Patel, 2011; Eze, 2014).

Table 5-5: Comparison of silicon extraction

Process	% Silicon extracted	Reference
Fusion	26	This study
Jet loop and curing	31	This study
Fusion	32	Ojumu et al., (2016)
Ultrasonictaion	24	Ojumu et al., (2016)

The next section will deal with the attempt to synthesize zeolite X from the filtrate obtained after the jet loop and curing process using the optimum conditions found within this section. There would need to be adjustments to the Si/Al ratio of the designated filtrate in order to achieve a similar ratio of Si and Al as was found in the filtrate produced with the fusion process prepared in Chapter 4.

5.4. Synthesis of zeolite X from the jet loop and cured filtrate

Based on the results of the analysis of the filtrates in the previous section it was calculated that approximately 0.5 g of $Al(OH)_3$ would need to be added to the filtrate extracted after applying the optimized conditions of the jet loop and curing process to resemble the Si/Al ratio found within the fusion pre-synthesis filtrate. Thus 3 experiments were run where the Al addition was varied to ratios both higher and lower to that of the calculated value while keeping the optimised hydrothermal conditions applied in Chapter 4. The Si/Al ratio is the fusion filtrate in Chapter 4 was 10 while the Si/Al ratio from the jet loop and curing process was 28. Thus Al needed to be added and it was calculated that 0.5 g of $Al(OH)_3$ would bring the Si/Al ratio in the jet loop and cured filtrate down to 10. The addition of $Al(OH)_3$ was then varied to give Si/Al ratios of 15 and 8 when 0.25 g and 0.75 g of $Al(OH)_3$ was added respectively. It is noted however, that adjustment of only the Al content and the Si/Al ratio may not be enough to target zeolite X. A more precise adjustment of the whole molar formulation may be needed, where the Si, Na, Al, and water content is taken in to account. The XRD results are displayed in Figure 5-13.

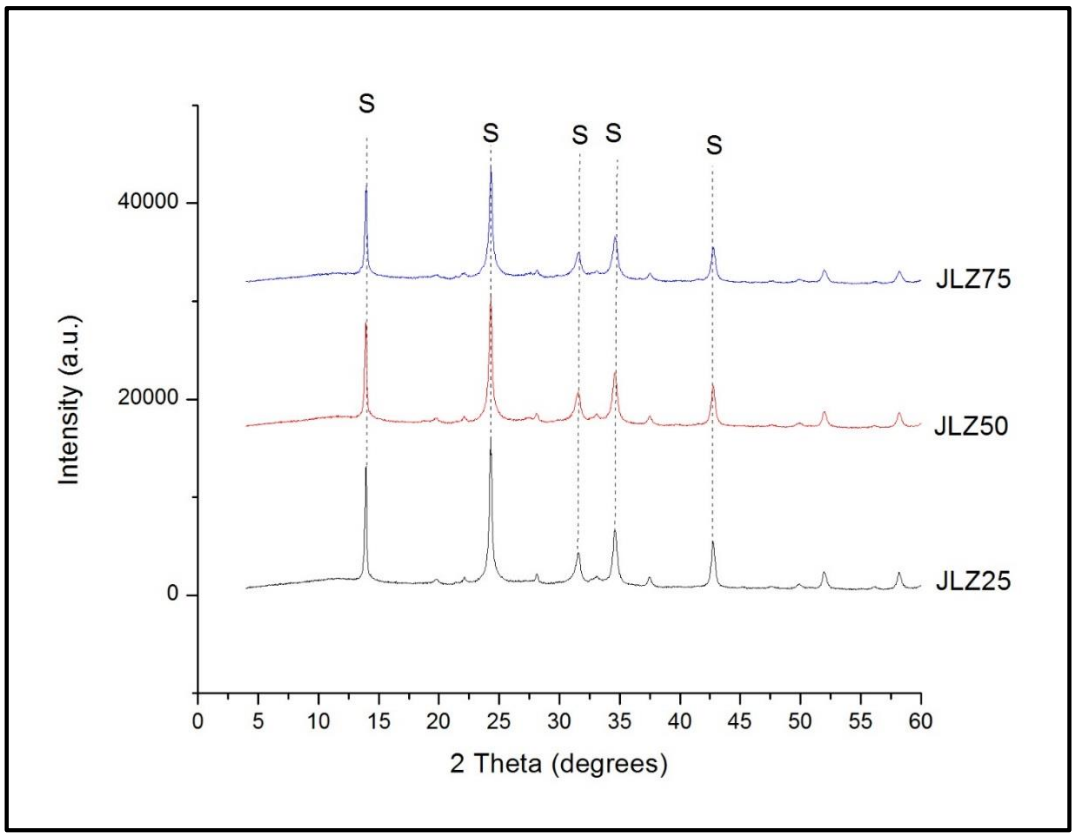

Figure 5-13: XRD spectra of hydrothermal synthesis of jet loop and cured filtrate for 8 hours at 90^0C at varying $Al(OH)_3$ addition: JLZ25 = 0.25 g; JLZ50 = 0.5 g; JLZ75 = 0.75 g (S = sodalite)

As can be seen from the XRD spectra in Figure 5-13, regardless of the calculated Al addition mentioned previously the only phase achieved was that of the sodalite zeolite. As sodalite is a denser phase than zeolite X it may be due to Ostwald's rule of ripening; thus the reaction time needs to be reduced in order to target zeolite X, if it is at all possible to target it through changing of the physical parameters. Thus the calculated value of 0.5 g of $Al(OH)_3$ addition was held constant while the synthesis time was reduced from 8 hours to 6, 4 and 2 hours, keeping the synthesis temperature at 90^0C, and XRD results are presented in Figure 5-14.

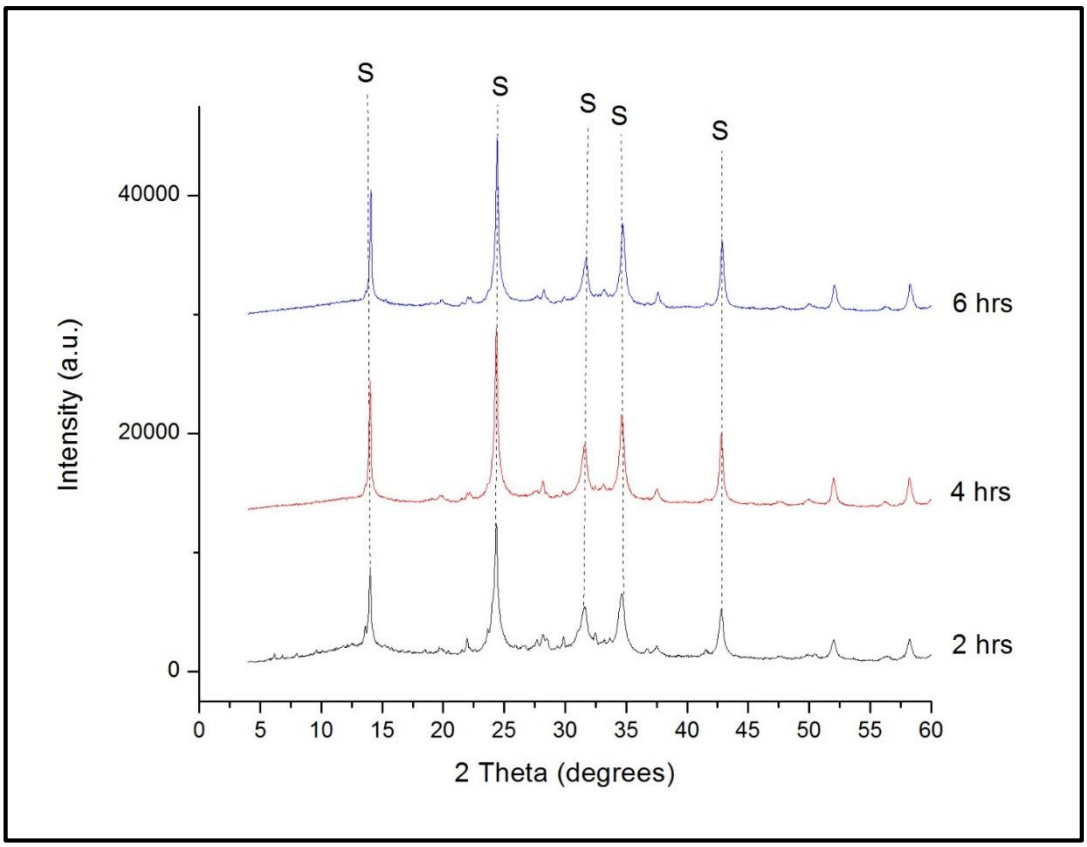

Figure 5-14: XRD spectra of varying the hydrothermal synthesis time of jet loop and cured filtrate at 90^0C with 0.5 g of $Al(OH)_3$ addition

Figure 5-14 shows that reducing the hydrothermal synthesis time down to as low as 2 hours did not favour the formation of zeolite X, again sodalite was the only phase that was achieved. This would demonstrate that varying only the physical parameters does not have an effect when trying to obtain the zeolite X. Thus in order to gain a better insight into the molar composition of the filtrate compared to that of the fusion filtrate as well as two filtrates from other studies that synthesized hierarchical zeolite X, the molar regimes were calculated for all the differing studies. To have an understanding of how these molar regimes differ, a ternary diagram was constructed to represent the molar regimes of these studies pictorially and is presented in Figure 5-15.

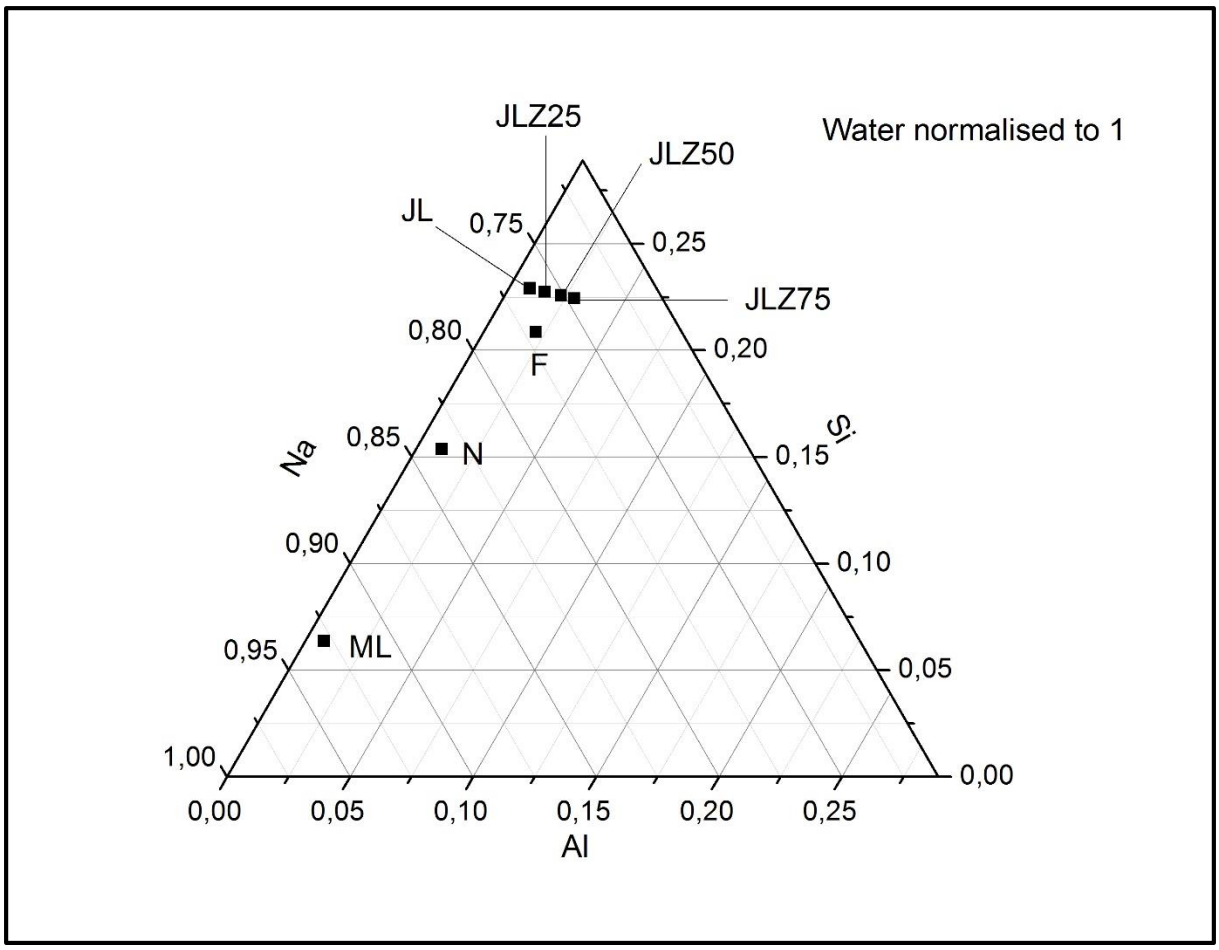

Figure 5-15: Ternary plot of the molar regimes in differing studies: JL = Jet loop and curing in this study; F = Fusion method in this study; N = Musyoka, (2012); ML = Cornelius, (2015); JLZ25, JLZ50, JLZ75 = Sodalite zeolites formed through $Al(OH)_3$ addition to jet loop and cured filtrate

Looking at the ternary diagram in Figure 5-15, it can be seen that the molar concentration of silicon within the filtrate obtained from the jet loop and curing process was higher than the other molar compositions used to synthesize zeolite X. However, what is also noted is that the other routes where zeolite X was successfully synthesised had higher concentrations of sodium than found in the filtrates obtained from the jet loop and curing process. Also seen on the ternary plot are the molar formulations of the sodalite zeolites achieved through hydrothermal synthesis of the jet loop filtrate with $Al(OH)_3$ addition as explained previously. This shows that adjustment of the Si/Al ratio could not target the hierarchical zeolite X. Therefore, additional NaOH may need to be added to the jet loop and curing process. Thus, it may be advisable to change the mass ratio of 1:1:5 of CFA:NaOH:H_2O that is initially fed into the jet loop mixing process to allow for the excess sodium that is required to synthesis zeolite X. This is due to the fact that in all the other studies using the fusion pre-synthesis process the mass ratio used to fuse the fly ash with NaOH is that of 1:1.2 of CFA:NaOH compared to the 1:1 of CFA:NaOH used in the jet loop and curing process. This optimisation however, did not form a part of this study. It would be advisable to optimise this mass ratio in the jet loop as it can also be seen by looking at the molar regimes of the various studies in Table 5-6 that there was also a

higher water content in the synthesis mixtures. Therefore, there may be a need to adjust the water content as well. It is also highlighted that in the all the studies where hierarchical zeolite X was synthesised, ultra-pure water was used while when using the jet loop only tap water was used as a solvent, which could contain contaminants inhibiting the formation of zeolite X.

A material balance was not performed around the hydrothermal section of the process because as before the yields of the zeolite were less than a gram in all instances and would again have precluded an accurate balance around the process. What is needed is to optimize the process for greater yields of product which would allow for elemental analysis and an accurate material balance.

Table 5-6: Comparison of molar formulations

Study*	Al	Na	Si	H_2O
Musyoka (2012)	0.07	5.43	1.00	123
Cornelius (2015)	0.12	14.6	1.00	163
Fusion in this study	0.10	3.69	1.00	95.33
Jet loop and cured in this study	0.04	3.34	1.00	79.63

*Normalized to Si

5.5. Chapter summary

Within this chapter the jet loop and curing pre-synthesis process was investigated as a replacement to the energy intensive fusion process. It was found that the optimum conditions for jet loop mixing was 30 minutes of mixing time, given that the length of jet loop mixing time did not have a substantial effect on the amount of silicon and aluminium dissolution from the CFA. What did have a substantial impact on the silicon dissolution was the curing of the slurry produced from jet loop mixing. The optimum conditions were therefore jet looping for 30 minutes and then curing the slurry produced for 1 day at 80^0C followed by 4 days at room temperature. This was the most energy efficient route while also yielding 31% of silicon from the starting CFA. This was an improvement on the fusion process in chapter 4 which yielded only 26% of silicon from the CFA. The jet loop and curing process could be more readily scalable than the fusion process. Not requiring large purpose built furnaces, with fewer safety concerns for the scaled-up process. Using longer times and lower temperatures would be the safer avenue regarding large scale silicon extraction from the CFA for zeolite synthesis. The jet loop and curing process also out-performed the ultrasonication process of a previous study that only extracted 24% of silicon from the process (Ojumu et al., 2016). It has been mentioned previously how it may be more feasible to scale-up the jet loop and curing process compared to the ultrasonication process.

The study also showed that there is a possibility to use the solid residue produced after jet loop and curing to produce geopolymers. With the filtrate being used for zeolite synthesis and the residue being used for geopolymer production this would utilise all of the slurry produced from the pre-synthesis process and lead to overall process of zero waste. There were however discrepancies in

the elemental balance produced around the jet loop and curing process. Majority of the elements seemed to report to the solid residue based on the ICP – AES analysis of the filtrate. The XRF analysis of the residue deviated quite substantially to the expected value based on the ICP – AES results for the filtrate. The only explanation could be due to the inaccuracies concerning the analytical techniques used. Coupled with the overall solid recovery from the jet loop and curing process, with only 50% of the solids being recovered due to spillages and vestiges within the process.

Regarding the attempt to synthesize zeolite X from the jet loop and cured filtrate, this study showed that zeolite sodalite could be synthesised directly by adjusting the Si/Al ratio of the jet loop and cured filtrate. It was further shown that lower concentrations of Na and H_2O, and higher concentration of Si precluded the modified filtrate to be suited for zeolite X synthesis. Therefore, a more precise optimisation study should be conducted through molar regime manipulation of not only the aluminium content but also the NaOH content and the water content. It was reasoned that optimising the mass ratio values fed into the jet loop pilot plant could improve zeolite X phase production.

CHAPTER 6

6. Conclusions and recommendations

6.1. Introduction

In this chapter the objectives and research questions set out in chapter 1 are reviewed pertaining to the major findings and conclusions of this study. Also recommendations are given concerning future work that was not within the scope of this study. The objectives of this research were as follows: to establish a base case of faujasite zeolite synthesis using the existing fusion pre-synthesis step; to determine the effect that jet loop mixing has on the dissolution of silicon and aluminium from the CFA; to determine the effect that curing the jet loop slurry after jet loop mixing has on the dissolution of silicon and aluminium from the CFA; to determine whether a high purity zeolite can be synthesised from the filtrate produced from the jet loop and curing pre-synthesis; and to compare the fate of elements from the two pre-synthesis methods of fusion and jet loop and curing.

6.2. Conclusions

The aim of this study is to investigate an alternative method to improve dissolution of Si and Al from a South African coal fly ash for the synthesis of faujasite zeolites with the potential for scale-up of the process. The scale-up conditions investigated consisted of comparing the existing pre-synthesis fusion method with jet-looping for the extraction of silicon needed for zeolite synthesis. This involved a jet looping and curing process on a pilot plant scale, which would be more easily scaled-up to industrial scale than high temperature fusion. The study began with a thorough characterisation of the fly ash starting material used for synthesis. This involved XRF, XRD, FTIR and SEM analytical technique. All the analytical characterisation techniques showed the CFA composition was suitable for zeolite synthesis. This was due to the CFA being characterised as class F fly ash given the dominance of aluminosilicate and silicate phases and the low lime content. Also there was a significant amorphous glassy content which too proved favourable for zeolite synthesis.

The CFA's suitability for zeolite synthesis was confirmed by replicating the base case study of zeolite faujasite synthesis from the Arnot CFA. Conditions from a previous study were optimised regarding the hydrothermal synthesis time used and the hierarchical zeolite X was successfully synthesised. The best hydrothermal synthesis conditions were 8 hours' hydrothermal treatment at 90 ^{0}C after varying the hydrothermal synthesis time from 8, 12 and 16 hours. This was an improvement of 16 and 24 hours' hydrothermal synthesis times reported in previous studies (Musyoka, 2012; Cornelius, 2015). The faujasite zeolite produced was characterised by XRD, FTIR and SEM which confirmed the synthesis of hierarchically structured zeolite X with a phase crystallinity of 66.85% of zeolite X and minor impurities of zeolite A and P. Due to the low product yield of the zeolite obtained under the conditions applied it precluded the ability to perform an elemental balance, however an overall balance was performed. It showed that 0.11 g of zeolite was produced from 36.36 g of starting CFA.

An attempt was made to improve this low yield by altering the pre-synthesis protocol and replace the fusion method with a jet loop and curing method.

The next objective was to determine the degree of dissolution of silicon and aluminium that can be achieved by replacing the pre-synthesis fusion step with a jet loop mixing and curing pre-synthesis. A jet loop pilot plant was used, which was able to mix and process 3.2 kg of starting CFA per run. The formulation used in the jet loop mixing process was 3.2 kg of CFA, 3.2 kg of NaOH and 16 litres of tap water, giving a 1:1:5 mass ratio of CFA:NaOH:H_2O. The slurry obtained by mixing the formulation with the jet loop pilot plant for various times was then cured in plastic containers at a smaller scale for a varying number of days, so as to see the effect that curing had on the dissolution of the silicon and aluminium. It was seen that while jet loop mixing alone for up to 90 minutes did not dissolve the same quantity of silicon and aluminium as the fusion process, the incorporation of a curing period after jet-loop mixing the slurry promoted the dissolution of Si to a greater extent to that obtained with fusion. The fusion process released 26% of silicon from the starting CFA while the jet loop and curing process, at the optimum conditions, released 31% of silicon from the CFA. The optimal conditions found was jet loop mixing for 30 minutes followed by curing the slurry obtained for 1 day at 80^0C followed by 4 days at room temperature. These were the most economical conditions energy wise for the jet loop and curing pre-synthesis process. The scalability of the jet loop and curing process is far easier and practical than the large industrial furnaces that would be required for the high temperature pre-synthesis fusion step. Another factor are the safety conditions that would be required when using large furnaces operating at 550^0C compared to having a jet loop mixing plant coupled with large industrial ovens only operating at a temperature of 80^0C max and lower. The jet loop and curing process did not extract a sufficient amount of aluminium however, although this was also the case with previous studies and an addition of aluminium would be required prior to hydrothermal synthesis to achieve the correct Si to Al ratio for a low silica zeolite such as faujasite. It was also shown that the solid residue produced from the jet loop and curing process could also be used for geopolymer production. This means that the overall pre-synthesis process could produce zero waste, as the filtrate would be used for zeolite synthesis and the residue for geopolymer production.

Thereafter the study focused on the hydrothermal conditions in order to synthesize zeolite X from the jet loop and cured filtrate. First an attempt was made to vary a calculated amount of aluminium hydroxide based on the Si/Al ratios of the jet loop and cured filtrate compared to the filtrate produced from pre-synthesis fusion. The zeolite phase formed in all instances was that of sodalite. Therefore, the synthesis time was varied so as to prepare the more metastable phase of zeolite X. In all instances again the zeolite phase of sodalite was formed. It was concluded that the zeolite X could not be achieved by alteration of only the physical parameters but a more precise alteration of the chemical parameters would be needed. A comparison was then drawn up of the molar regimes used within this study compared to previous studies where hierarchical zeolite X was synthesised.

When looking at the range of the molar regimes applied in this study and previous studies it was concluded that not only is the jet loop and curing process producing a more siliceous filtrate, but also

the sodium within the filtrate from the jet looping and curing step was not as high as in previous studies or in this study using the pre-synthesis fusion method. The molar regimes normalized to silica used by Musyoka (2012) was: 0.07 Al·5.43 Na·1.00 Si·123 H_2O; and that used by Cornelius (2015) was: 0.12 Al·14.6 Na·1.00 Si·163 H_2O. In this study during fusion the molar regime was: 0.10 Al·3.69 Na·1.00 Si·95.33 H_2O; while the molar regime of the jet loop and curing was: 0.04 Al·3.34 Na·1.00 Si·79.63 H_2O. It was also highlighted by these calculations that the water content in the pre-synthesis fusion method was also higher than the water content found in the jet loop and cured filtrate.

Due to the small volumes used in the hydrothermal synthesis stage in this study for both the fusion pre-synthesis or jet loop and curing pre-synthesis step it precluded the ability to analyse the small amount of zeolite product and achieve an accurate and conclusive overall elemental balance around the entire processes. This made it impossible to compare the fate of the elements in the two pre-synthesis routes applied. The material balance that could be performed was of the jet loop mixing and curing pre-synthesis process. This balance showed that regarding the jet loop and curing pre-synthesis majority of the major elements reported to the solid residue. However, there was significant deviation of the elemental weight percent of the elements based on ICP – AES and XRF analysis. This could be due to the vestiges and spillages concerned with using the jet loop pilot plant and the containers used for curing. It could also be reasoned to be due to inaccuracies in the analytical techniques used to analyse the filtrate and solid residue.

This study elucidated that an alternative pre-synthesis method of jet loop mixing and curing could replace the pre-synthesis fusion method. It showed that the jet-loop and curing is an alternative method and can extract more silicon than the fusion method used in this study and other alternative methods such as ultrasonication. It can be argued that the jet loop and curing process is more readily scalable than fusion or ultrasonication. It is also safer to scale-up processes that work at lower temperatures overall than to scale a process that requires large industrial furnaces operated at high temperatures. Therefore, this work has contributed to the end goal of making the scale-up of zeolite synthesis to industrial scale a reality. With some recommendations for future work presented in the next section, further studies can be conducted using the pre-synthesis method in this study to target any number of zeolites in the hydrothermal synthesis process by incorporating suitable molar formulation adjustments.

This study improved on hydrothermal synthesis conditions for the formation of hierarchical zeolite X from fusion pre-synthesis. As well as produce an alternative pre-synthesis method to extract more silicon from the CFA compared to fusion and ultrasonication pre-synthesis while also being more readily scaled to industrial scale compared to fusion and ultrasonication. It also provided a comparison of the molar regimes to target zeolite X from the jet loop and curing filtrate in further studies.

6.3. Recommendations for future work

There were significant restraints in this study given the equipment needed for the scale required to process the amount of starting materials fed in to the jet loop pilot plant mixing process. However, if analysis could be conducted on more of the total jet loop slurry produced and cured in a larger oven and averages taken over a wider range to produce more homogeneity, a more precise material balance could be achieved. Therefore, some recommendations can be found here for future work in continuing the research to scale-up zeolite synthesis from CFA. A more extensive optimisation study needs to be conducted around the adjustment of the molar regime of the jet loop and cured filtrate. This could focus on altering the amount of sodium to be added along with adjusting the amount of aluminium and water. It was noted however that the mass ratio of sodium hydroxide and water in relation to the CFA used in the jet loop mixing process could also be altered to provide these constituents as this was not investigated within this study. The recommendations are as follows:

- optimising the 1:1:5 mass ratio of CFA:NaOH:H_2O fed into the jet loop pilot plant,
- using a larger oven and containers to cure a greater amount of slurry produced from the jet loop pilot plant,
- optimising the jet loop and cured filtrate by variation of the molar regime in comparison to the molar regimes utilized in this study,
- using larger bench scale reactors equipped with stirring for a greater volume of filtrate to be generated for hydrothermal synthesis so that accurate elemental balances can be performed,
- performing energy balances for both processes so as to compare the two pre-synthesis routes within this study.

References

Adamczyk, Z. & Białecka, B. 2005. Hydrothermal synthesis of zeolites from Polish coal fly ash. *Polish Journal of Environmental Studies,* 14**,** 713-719.

Ahmaruzzaman, M. 2010. A review on the utilization of fly ash. *Progress in Energy and Combustion Science,* 36**,** 327-363.

Ahmaruzzaman, M. 2011. Industrial wastes as low-cost potential adsorbents for the treatment of wastewater laden with heavy metals. *Advances in colloid and interface science,* 166**,** 36-59.

Auerbach, S. M., Carrado, K. A. & Dutta, P. K. 2003. *Handbook of zeolite science and technology,* New York, Marcel Dekker.

Babajide, O., Musyoka, N., Petrik, L. & Ameer, F. 2012. Novel zeolite Na-X synthesized from fly ash as a heterogeneous catalyst in biodiesel production. *Catalysis Today,* 190**,** 54-60.

Baerlocher, C., Mccusker, L. & Olson, D. 2007. *Atlas of zeolite framework types,* Amsterdam, Elsevier.

Balkus, K. J. & Ly, K. T. 1991. The preparation and characterization of an X-type zeolite: An experiment in solid-state chemistry. *Journal of Chemical Education,* 68**,** 875.

Belviso, C., Cavalcante, F., Di Gennaro, S., Palma, A., Ragone, P. & Fiore, S. 2015. Mobility of trace elements in fly ash and in zeolitised coal fly ash. *Fuel,* 144**,** 369-379.

Belviso, C., Cavalcante, F. & Fiore, S. 2010. Synthesis of zeolite from Italian coal fly ash: Differences in crystallization temperature using seawater instead of distilled water. *Waste Management,* 30**,** 839-847.

Belviso, C., Cavalcante, F., Javier Huertas, F., Lettino, A., Ragone, P. & Fiore, S. 2012. The crystallisation of zeolite (X- and A-type) from fly ash at 25°C in artificial sea water. *Microporous and Mesoporous Materials,* 162**,** 115-121.

Belviso, C., Cavalcante, F., Lettino, A. & Fiore, S. 2011. Effects of ultrasonic treatment on zeolite synthesized from coal fly ash. *Ultrasonics Sonochemistry,* 18**,** 661-668.

Bhandari, R., Volli, V. & Purkait, M. K. 2015. Preparation and characterization of fly ash based mesoporous catalyst for transesterification of soybean oil. *Journal of Environmental Chemical Engineering,* 3**,** 906-914.

Blissett, R. S. & Rowson, N. A. 2012. A review of the multi-component utilisation of coal fly ash. *Fuel,* 97**,** 1-23.

REFERENCES

Böke, N., Birch, G. D., Nyale, S. M. & Petrik, L. F. 2015. New synthesis method for the production of coal fly ash-based foamed geopolymers. *Construction and Building Materials,* 75**,** 189-199.

Borm, P. J. 1997. Toxicity and occupational health hazards of coal fly ash (CFA). A review of data and comparison to coal mine dust. *The Annals of occupational hygiene,* 41**,** 659-676.

Bose, B. 2012. Geo-engineering properties of expansive soil stabilized with fly ash. *Electronic Journal of Geotechnical Engineering,* 17 J**,** 1339-1353.

Boycheva, S., Zgureva, D. & Shoumkova, A. 2014. Recycling of Lignite Coal Fly Ash by its Conversion into Zeolites. *Coal Combustion and Gasification Products,* 6**,** 1-8.

Brassell, J. P., Ojumu, T. V. & Petrik, L. F. 2016. Upscaling of Zeolite Synthesis from Coal Fly Ash Waste: Current Status and Future Outlook. In *Zeolites: Useful Minerals.* C. Belviso (ed.). Intech. 3-23.

Bukhari, S. S., Behin, J., Kazemian, H. & Rohani, S. 2015. Conversion of coal fly ash to zeolite utilizing microwave and ultrasound energies: A review. *Fuel,* 140**,** 250-266.

Bukhari, S. S., Rohani, S. & Kazemian, H. 2016. Effect of ultrasound energy on the zeolitization of chemical extracts from fused coal fly ash. *Ultrasonics sonochemistry,* 28**,** 47-53.

Butt, W. A. 2015. Collapsible behavior of compacted coal ash. *International Journal of Advanced Research,* 3**,** 272-275.

Cardoso, A. M., Horn, M. B., Ferret, L. S., Azevedo, C. M. N. & Pires, M. 2015. Integrated synthesis of zeolites 4A and Na–P1 using coal fly ash for application in the formulation of detergents and swine wastewater treatment. *Journal of Hazardous Materials,* 287**,** 69-77.

Casci, J. L. 2005. Zeolite molecular sieves: preparation and scale-up. *Microporous and Mesoporous Materials,* 82**,** 217-226.

Chang, H.-L. & Shih, W.-H. 1998. A general method for the conversion of fly ash into zeolites as ion exchangers for cesium. *Industrial & engineering chemistry research,* 37**,** 71-78.

Chang, H.-L. & Shih, W.-H. 2000. Synthesis of Zeolites A and X from Fly Ashes and Their Ion-Exchange Behavior with Cobalt Ions. *Industrial & Engineering Chemistry Research,* 39**,** 4185-4191.

Chareonpanich, M., Jullaphan, O. & Tang, C. 2011. Bench-scale synthesis of zeolite A from subbituminous coal ashes with high crystalline silica content. *Journal of Cleaner Production,* 19**,** 58-63.

REFERENCES

Choi, S. K., Lee, S., Song, Y. K. & Moon, H. S. 2002. Leaching characteristics of selected Korean fly ashes and its implications for the groundwater composition near the ash disposal mound. *Fuel,* 81**,** 1083-1090.

Cornelius, M. U. 2015. *The role of aluminium content in the control of the morphology of fly ash based hierarchical zeolite X.* MSc: Chemistry, Unpublished Thesis, University of the Western Cape.

Criado, M., Fernández-Jiménez, A. & Palomo, A. 2007. Alkali activation of fly ash: Effect of the SiO2/Na2O ratio. Part I: FTIR study. *Microporous and Mesoporous Materials,* 106**,** 180-191.

Cullity, B. 1956. *Elements of X-ray Diffraction,* USA, Adisson-Wesley Publishing.

Cundy, C. S. & Cox, P. A. 2003. The hydrothermal synthesis of zeolites: History and development from the earliest days to the present time. *Chemical Reviews,* 103**,** 663-701.

Cundy, C. S. & Cox, P. A. 2005. The hydrothermal synthesis of zeolites: Precursors, intermediates and reaction mechanism. *Microporous and Mesoporous Materials,* 82**,** 1-78.

Du Plessis, P., Ojumu, T., Fatoba, O., Akinyeye, R. & Petrik, L. 2014. Distributional Fate of Elements during the Synthesis of Zeolites from South African Coal Fly Ash. *Materials,* 7**,** 3305-3318.

Du Plessis, P. W. 2014. *Process design for the up-scale zeolite synthesis from South African coal fly ash* MTech: Chemical Engineering, Unpublished thesis, Cape Peninsula University of Technology.

Du Plessis, P. W., Ojumu, T. V. & Petrik, L. F. 2013. Waste minimization protocols for the process of synthesizing zeolites from South African coal fly ash. *Materials,* 6**,** 1688-1703.

Dutta, B. K., Khanra, S. & Mallick, D. 2009. Leaching of elements from coal fly ash: Assessment of its potential for use in filling abandoned coal mines. *Fuel,* 88**,** 1314-1323.

Dyer, A. 1988. *An introduction to zeolite molecular sieves*, New York, NY; John Wiley and Sons Inc.

El-Naggar, M. R., El-Kamash, A. M., El-Dessouky, M. I. & Ghonaim, A. K. 2008. Two-step method for preparation of NaA-X zeolite blend from fly ash for removal of cesium ions. *Journal of hazardous materials,* 154**,** 963-72.

Epa. 2016. *Air emission factors and quantification* [Online]. https://www3.epa.gov/ttnchie1/ap42/ch01/. [Accessed 2nd February 2017].

Eskom. 2016. *Integrated report 2016* [Online]. http://www.eskom.co.za/IR2016/Documents/Eskom_integrated_report_2016.pdf. [Accessed 22nd November 2016].

Eze, C. P. 2014. *Determination of toxic elements, rare earth elements and radionuclides in coal fly ash, products and waste.* PhD: Chemistry, Unpublished thesis, University of the Western Cape.

Felder, R. M. & Rousseau, R. W. 2005. *Elementary Principles of Chemical Processes, Third Edition,* USA, John Wiley & Sons.

Fernández-Jiménez, A. & Palomo, A. 2005. Mid-infrared spectroscopic studies of alkali-activated fly ash structure. *Microporous and Mesoporous Materials,* 86**,** 207-214.

Fisher, G. L., Prentice, B. A. & Silberman, D. 1978. Physical and morphological studies of size-classified coal fly ash. *Environmental Science and Technology,* 12**,** 447-451.

Fotovat, F., Kazemian, H. & Kazemeini, M. 2009. Synthesis of Na-A and faujasitic zeolites from high silicon fly ash. *Materials Research Bulletin,* 44**,** 913-917.

Franus, W., Wiatros-Motyka, M. M. & Wdowin, M. 2015. Coal fly ash as a resource for rare earth elements. *Environmental Science and Pollution Research,* 22**,** 9464-9474.

Gogate, P. R. & Pandit, A. B. 2005. A review and assessment of hydrodynamic cavitation as a technology for the future. *Ultrasonics sonochemistry,* 12**,** 21-7.

Goldstein, J., Newbury, D. E., Joy, D. C., Lyman, C. E., Echlin, P., Lifshin, E., Sawyer, L. & Michael, J. R. 2012. *Scanning Electron Microscopy and X-ray Microanalysis: Third Edition,* USA, Springer US.

Grasshoff, K., Kremling, K. & Ehrhardt, M. 1999. *Methods of seawater analysis,* Weinheim, Wiley-VCH.

Guan, Q., Hu, X., Wu, D., Shang, X., Ye, C. & Kong, H. 2009. Phosphate removal in marine electrolytes by zeolite synthesized from coal fly ash. *Fuel,* 88**,** 1643-1649.

Hendricks, N. R. 2005. *The application of high capacity ion exchange absorbent material, synthesized from fly ash and acid mine drainage, for the removal of heavy and trace metals from secondary co-disposed process waters.* MSc: Chemistry, Unpublished thesis, University of the Western Cape.

Himmelblau, D. M. & Riggs, J. B. 2004. *Basic Principles and Calculations in Chemical Engineering, 7th Edition,* New Jersey, Prentice Hall PTR.

Holler, H. & Wirsching, U. 1985. Zeolite formation from fly-ash. *Fortschritte der Mineralogie,* 63**,** 21-43.

Hollman, G. G., Steenbruggen, G. & Janssen-Jurkovičová, M. 1999. A two-step process for the synthesis of zeolites from coal fly ash. *Fuel,* 78**,** 1225-1230.

Hui, K. S. & Chao, C. Y. H. 2006. Pure, single phase, high crystalline, chamfered-edge zeolite 4A synthesized from coal fly ash for use as a builder in detergents. *Journal of Hazardous Materials,* 137**,** 401-409.

Inada, M., Eguchi, Y., Enomoto, N. & Hojo, J. 2005a. Synthesis of zeolite from coal fly ashes with different silica-alumina composition. *Fuel,* 84**,** 299-304.

Inada, M., Tsujimoto, H., Eguchi, Y., Enomoto, N. & Hojo, J. 2005b. Microwave-assisted zeolite synthesis from coal fly ash in hydrothermal process. *Fuel,* 84**,** 1482-1486.

Inayat, A., Knoke, I., Spiecker, E. & Schwieger, W. 2012. Assemblies of Mesoporous FAU-Type Zeolite Nanosheets. *Angewandte Chemie International Edition,* 51**,** 1962-1965.

Iyer, R. 2002. The surface chemistry of leaching coal fly ash. *Journal of Hazardous Materials,* 93**,** 321-329.

Iza. 2013. *IZA Synthesis Commission* [Online]. Available: http://www.iza-online.org/synthesis/default.htm [Accessed 3rd August 2015].

Izidoro, J. D. C., Fungaro, D. A., Abbott, J. E. & Wang, S. 2013. Synthesis of zeolites X and A from fly ashes for cadmium and zinc removal from aqueous solutions in single and binary ion systems. *Fuel,* 103**,** 827-834.

Izquierdo, M. & Querol, X. 2012. Leaching behaviour of elements from coal combustion fly ash: An overview. *International Journal of Coal Geology,* 94**,** 54-66.

Jegadeesan, G., Al-Abed, S. R. & Pinto, P. 2008. Influence of trace metal distribution on its leachability from coal fly ash. *Fuel,* 87**,** 1887-1893.

Jenkins, R. 1984. X-ray fluorescence analysis. *Analytical Chemistry,* 56**,** 1099A-1106A.

Jha, B. & Singh, D. N. 2011. A Review on Synthesis , Characterization and Industrial Applications of Flyash Zeolites. *Journal of Materials Education,* 33**,** 65-132.

Jha, V. K. & Budhamagar, G. P. 2013. Synthesis of Geopolymer from Coal Fly Ash. *Journal of Nepal Chemical Society,* 30**,** 24-28.

Jha, V. K., Nagae, M., Matsuda, M. & Miyake, M. 2009. Zeolite formation from coal fly ash and heavy metal ion removal characteristics of thus-obtained Zeolite X in multi-metal systems. *Journal of environmental management,* 90**,** 2507-14.

Ji, X., Zhang, M., Wang, Y., Song, Y., Ke, Y. & Wang, Y. 2015. Immobilization of ammonium and phosphate in aqueous solution by zeolites synthesized from fly ashes with different compositions. *Journal of Industrial and Engineering Chemistry,* 22**,** 1-7.

Jyoti, K. K. & Pandit, A. B. 2001. Water disinfection by acoustic and hydrodynamic cavitation. *Biochemical Engineering Journal,* 7**,** 201-212.

Kashiwakura, S., Kumagai, Y., Kubo, H. & Wagatsuma, K. 2013. Dissolution of Rare Earth Elements from Coal Fly Ash Particles in a Dilute H2SO4 Solvent. *Open Journal of Physical Chemistry,* 03**,** 69-75.

Kazemian, H., Naghdali, Z., Ghaffari Kashani, T. & Farhadi, F. 2010. Conversion of high silicon fly ash to Na-P1 zeolite: Alkaline fusion followed by hydrothermal crystallization. *Advanced Powder Technology,* 21**,** 279-283.

Khanra, S., Mallick, D., Dutta, S. N. & Chaudhuri, S. K. 1998. Studies on the phase mineralogy and leaching characteristics of coal fly ash. 251-275.

Kim, J. K. & Lee, H. D. 2009. Effects of step change of heating source on synthesis of zeolite 4A from coal fly ash. *Journal of Industrial and Engineering Chemistry,* 15**,** 736-742.

Kola, H. & Perämäki, P. 2004. The study of the selection of emission lines and plasma operating conditions for efficient internal standardization in inductively coupled plasma optical emission spectrometry. *Spectrochimica Acta Part B: Atomic Spectroscopy,* 59**,** 231-242.

Komonweeraket, K., Cetin, B., Aydilek, A. H., Benson, C. H. & Edil, T. B. 2015. Effects of pH on the leaching mechanisms of elements from fly ash mixed soils. *Fuel,* 140**,** 788-802.

Kondru, A. K., Kumar, P., Teng, T. T., Chand, S. & Wasewar, K. L. 2011. Synthesis and characterization of Na-Y zeolite from coal fly ash and its effectiveness in removal of dye from aqueous solution by wet peroxide oxidation. *Archives of Environmental Science,* 5**,** 46-54.

Kruger, R. A. 1997. Fly ash beneficiation in South Africa: creating new opportunities in the market-place. *Fuel,* 76**,** 777-779.

Kumar, D., Gupta, A. & Kumar, N. 2014. Some Geotechnical Properties of Coal Fly Ash and Sand Mixtures with Different Ratio using in Highway & Embankments *Global Journal of Researches in Engineering* 14**,** 32-38.

Kutchko, B. & Kim, A. 2006. Fly ash characterization by SEM–EDS. *Fuel,* 85**,** 2537-2544.

Lee, W. & Van Deventer, J. 2003. Use of infrared spectroscopy to study geopolymerization of heterogeneous amorphous aluminosilicates. *Langmuir,* 19**,** 8726-8734.

León, G., Pérez, L. E., Linares, J. C., Hartmann, A. & Quintana, M. 2007. Genotoxic effects in wild rodents (Rattus rattus and Mus musculus) in an open coal mining area. *Mutation Research/Genetic Toxicology and Environmental Mutagenesis,* 630**,** 42-49.

Liu, B., Chen, F., Zheng, L., Ge, J., Xi, H. & Qian, Y. 2013. Synthesis and structural properties of hierarchically structured aluminosilicates with zeolite Y (FAU). *RSC Advances,* 3**,** 15075-15084.

Madzivire, G. 2012. *Chemistry and speciation of potentially toxic and radioactive elements during mine water treatment.* Ph.D: Chemistry, Unpublished Thesis, University of the Western Cape.

Madzivire, G., Gitari, W. M., Vadapalli, V. R. K. & Petrik, L. F. 2013. Jet loop reactor application for mine water treatment using fly ash, lime and aluminium hydroxide. *International Journal of Environmental Science and Technology,* 12**,** 173-182.

Mainganye, D. 2012. *Synthesis of zeolites from South African coal fly ash: Investigation of scale-up conditions.* MTech: Chemical Engineering, Unpublished thesis, Cape Peninsula Univeristy of Technology.

Mainganye, D., Ojumu, T. V. & Petrik, L. 2013. Synthesis of zeolites Na-P1 from South African coal fly ash: Effect of impeller design and agitation. *Materials,* 6**,** 2704-2089.

Marrot, B., Bebon, C., Colson, D. & Klein, J. P. 2001. Influence of the shear rate during the synthesis of zeolites. *Crystal Research and Technology,* 36**,** 269-281.

Mayfield, D. B. & Lewis, A. S. 2013. Environmental Review of Coal Ash as a Resource for Rare Earth and Strategic Elements. *2013 World of Coal Ash (WOCA) Conference.* Lexington, KY.

Miller, F. A. & Wilkins, C. H. 1952. Infrared spectra and characteristic frequencies of inorganic ions. *Analytical chemistry,* 24**,** 1253-1294.

Moholkar, V. S., Senthil Kumar, P. & Pandit, A. B. 1999. Hydrodynamic cavitation for sonochemical effects. *Ultrasonics Sonochemistry,* 6**,** 53-65.

Molina, A. & Poole, C. 2004. A comparative study using two methods to produce zeolites from fly ash. *Minerals Engineering,* 17**,** 167-173.

Moore, G. L. 2012. *Introduction to Inductively Coupled Plasma Atomic Emission Spectrometry,* Amsterdam, Elsevier Science.

Moreno, N., Querol, X., Ayora, C., Alastuey, A., Fernández-Pereira, C. & Janssen-Jurkovicová, M. 2001. Potential environmental applications of pure zeolitic material synthesized from fly ash. *Journal of environmental engineering,* 127**,** 994-1002.

Moriyama, R., Takeda, S., Onozaki, M., Katayama, Y., Shiota, K., Fukuda, T., Sugihara, H. & Tani, Y. 2005. Large-scale synthesis of artificial zeolite from coal fly ash with a small charge of alkaline solution. *Fuel,* 84**,** 1455-1461.

Murayama, N., Yamamoto, H. & Shibata, J. 2002a. Mechanism of zeolite synthesis from coal fly ash by alkali hydrothermal reaction. *International Journal of Mineral Processing,* 64**,** 1-17.

Murayama, N., Yamamoto, H. & Shibata, J. 2002b. Zeolite synthesis from coal fly ash by hydrothermal reaction using various alkali sources. *Journal of Chemical Technology and Biotechnology,* 77**,** 280-286.

Musyoka, N. M. 2009. *Hydrothermal synthesis and optimisation of zeolite Na-P1 from South African coal fly ash* Msc: Chemistry, Unpublished thesis, University of the Western Cape.

Musyoka, N. M. 2012. *Zeolite A , X and Cancrinite from South African coal fly ash : mechanism of crystallization , routes to rapid synthesis and new morphology* PhD: Chemistry, Unpublished thesis, University of the Western Cape.

Musyoka, N. M., Petrik, L. & Hums, E. 2012a. Synthesis of Zeolite A, X and P from a South African Coal Fly Ash. *Advanced Materials Research,* 512-515**,** 1757-1762.

Musyoka, N. M., Petrik, L. F., Balfour, G., Gitari, W. M. & Hums, E. 2011a. Synthesis of hydroxy sodalite from coal fly ash using waste industrial brine solution. *Journal of environmental science and health. Part A, Toxic/hazardous substances & environmental engineering,* 46**,** 1699-707.

Musyoka, N. M., Petrik, L. F., Fatoba, O. O. & Hums, E. 2013. Synthesis of zeolites from coal fly ash using mine waters. *Minerals Engineering,* 53**,** 9-15.

Musyoka, N. M., Petrik, L. F. & Hums, E. 2011b. Ultrasonic assisted synthesis of zeolite A from coal fly ash using mine waters (acid mine drainage and circumneutral mine water) as a substitute for ultra pure water. *Rüde, R. T., Freund, A. & Wolkersdorfer, Ch.: Mine Water – Managing the Challenges.* Aachen, Germany.

Musyoka, N. M., Petrik, L. F., Hums, E., Baser, H. & Schwieger, W. 2012b. In situ ultrasonic monitoring of zeolite A crystallization from coal fly ash. *Catalysis Today,* 190**,** 38-46.

Musyoka, N. M., Petrik, L. F., Hums, E., Baser, H. & Schwieger, W. 2014. In situ ultrasonic diagnostic of zeolite X crystallization with novel (hierarchical) morphology from coal fly ash. *Ultrasonics,* 54**,** 537-543.

Musyoka, N. M. A., Petrik, L. F., Gitari, W. M. B., Balfour, G. & Hums, E. C. 2012c. Optimization of hydrothermal synthesis of pure phase zeolite Na-P1 from South African coal fly ashes. *Journal of Environmental Science and Health Part A ToxicHazardous Substances and Environmental Engineering,* 47**,** 337-350.

REFERENCES

Nyale, S. M. 2014. *Geopolymers from South African Fly Ash: Synthesis and Characteristics.* Ph.D: Chemistry, Unpublished Thesis, University of the Western Cape

Nyale, S. M., Babajide, O. O., Birch, G. D., Böke, N. & Petrik, L. F. 2013. Synthesis and Characterization of Coal Fly Ash-based Foamed Geopolymer. *Procedia Environmental Sciences,* 18**,** 722-730.

Nyale, S. M., Eze, C. P., Akinyeye, R. O., Gitari, W. M., Akinyemi, S. A., Fatoba, O. O. & Petrik, L. F. 2014. The leaching behaviour and geochemical fractionation of trace elements in hydraulically disposed weathered coal fly ash. *Journal of environmental science and health. Part A, Toxic/hazardous substances & environmental engineering,* 49**,** 233-42.

Ojha, K., Pradhan, N. C. & Samanta, A. N. 2004. Zeolite from fly ash: Synthesis and characterization. *Bulletin of Materials Science,* 27**,** 555-564.

Ojumu, T., Du Plessis, P. & Petrik, L. 2016. Synthesis of zeolite A from coal fly ash using ultrasonic treatment-a replacement for fusion step. *Ultrasonics Sonochemistry,* 31**,** 342-349.

Pandian, N. S. 2004. Fly ash characterization with reference to geotechnical applications. *Journal of the Indian Institute of Science,* 84**,** 189-216.

Park, M., Choi, C. L., Lim, W. T., Kim, M. C., Choi, J. & Heo, N. H. 2000. Molten-salt method for the synthesis of zeolitic materials I. Zeolite formation in alkaline molten-salt system. *Microporous and Mesoporous Materials,* 37**,** 81-89.

Patel, D. 2011. Matrix effect in a view of LC-MS/MS: an overview. *Int J Pharm Bio Sci,* 2**,** 559-564.

Perkampus, H. H., Grinter, H. C. & Threlfall, T. L. 2013. *UV-VIS Spectroscopy and Its Applications*, Springer Berlin Heidelberg.

Praharaj, T., Powell, M. A., Hart, B. R. & Tripathy, S. 2002. Leachability of elements from sub-bituminous coal fly ash from India. *Environment International,* 27**,** 609-615.

Querol, X., Alastuey, A., Fernández-Turiel, J. & López-Soler, A. 1995. Synthesis of zeolites by alkaline activation of ferro-aluminous fly ash. *Fuel,* 74**,** 1226-1231.

Querol, X., Alastuey, A., López-Soler, A., Plana, F., Andrés, J. M., Juan, R., Ferrer, P. & Ruiz, C. R. 1997a. A fast method for recycling fly ash: Microwave-assisted zeolite synthesis. *Environmental Science and Technology,* 31**,** 2527-2533.

Querol, X., Moreno, N., Umaa, J. C., Alastuey, A., Hernández, E., López-Soler, A. & Plana, F. 2002. Synthesis of zeolites from coal fly ash: an overview. *International Journal of Coal Geology,* 50**,** 413-423.

Querol, X., Plana, F., Alastuey, A. & López-Soler, A. 1997b. Synthesis of Na-zeolites from fly ash. *Fuel,* 76**,** 793-799.

Querol, X., Umana, J. C., Plana, F., Alastuey, A., Lopez-Soler, A., Medinaceli, A., Valero, A., Domingo, M. J. & Garcia-Rojo, E. 2001. Synthesis of zeolites from fly ash at pilot plant scale. Examples of potential applications. *Fuel,* 80**,** 857-865.

Ram, L. C. & Masto, R. E. 2014. Fly ash for soil amelioration: A review on the influence of ash blending with inorganic and organic amendments. *Earth-Science Reviews,* 128**,** 52-74.

Rayalu, S., Meshram, S. & Hasan, M. 2000. Highly crystalline faujasitic zeolites from flyash. *Journal of hazardous materials,* 77**,** 123-131.

Rayalu, S., Udhoji, J., Munshi, K. & Hasan, M. 2001. Highly crystalline zeolite—a from flyash of bituminous and lignite coal combustion. *Journal of hazardous materials,* 88**,** 107-121.

Rayalu, S. S., Labhsetwar, P. & Khanna, P. 1998. *Process for production of flyash based zeolite-Y*. US patent application 6027708.

Rayalu, S. S., Udhoji, J. S., Meshram, S. U., Naidu, R. R. & Devotta, S. 2005. Estimation of crystallinity in flyash-based zeolite-A using XRD and IR spectroscopy. *Current Science,* 89**,** 2147-2151.

Ríos, R., Carlos, A., Williams, C. D. & Roberts, C. L. 2009. A comparative study of two methods for the synthesis of fly ash-based sodium and potassium type zeolites. *Fuel,* 88**,** 1403-1416.

Rungsuk, D., Apiratikul, R., Pavarajarn, V. & Pavasant, P. 2006. Zeolite Synthesis from Fly Ash from Coal-fired Power Plant by Fusion Method *Proceedings of The 2nd Joint International Conference on "Sustainable Energy and Environment (SEE 2006)"* Bangkok, Thailand.

Saha, S. & Pal, S. K. 2012. Compressibility behavior of soil and fly ash used in successive layers. *Electronic Journal of Geotechnical Engineering,* 17 T**,** 2659-2670.

Santos, F., Li, L., Li, Y. & Amini, F. 2011. Geotechnical properties of fly ash and soil mixtures for use in highway embankments. *Proceedings World of Coal Ash (WOCA) Conference, Denver, USA*.

Seredin, V. V. & Dai, S. 2012. Coal deposits as potential alternative sources for lanthanides and yttrium. *International Journal of Coal Geology,* 94**,** 67-93.

Seredin, V. V., Dai, S., Sun, Y. & Chekryzhov, I. Y. 2013. Coal deposits as promising sources of rare metals for alternative power and energy-efficient technologies. *Applied Geochemistry,* 31**,** 1-11.

Shaheen, S. M., Hooda, P. S. & Tsadilas, C. D. 2014. Opportunities and challenges in the use of coal fly ash for soil improvements--a review. *Journal of environmental management,* 145**,** 249-67.

Shigemoto, N., Hayashi, H. & Miyaura, K. 1993. Selective formation of Na-X zeolite from coal fly ash by fusion with sodium hydroxide prior to hydrothermal reaction. *Journal of Materials Science,* 28**,** 4781-4786.

Shih, W.-H. & Chang, H.-L. 1996. Conversion of fly ash into zeolites for ion-exchange applications. *Materials Letters,* 28**,** 263-268.

Siddique, R. 2004. Performance characteristics of high-volume Class F fly ash concrete. *Cement and Concrete Research,* 34**,** 487-493.

Smith, B. C. 2011. *Fundamentals of Fourier Transform Infrared Spectroscopy, Second Edition,* USA, CRC Press.

Somerset, V., Petrik, L. & Iwuoha, E. 2008. Alkaline hydrothermal conversion of fly ash precipitates into zeolites 3: the removal of mercury and lead ions from wastewater. *Journal of environmental management,* 87**,** 125-31.

Somerset, V. S., Petrik, L. F., White, R. A., Klink, M. J., Key, D. & Iwuoha, E. I. 2005. Alkaline hydrothermal zeolites synthesized from high SiO 2 and Al 2 O 3 co-disposal fly ash filtrates. *Fuel,* 84**,** 2324-2329.

Steenbruggen, G. & Hollman, G. G. 1998. The synthesis of zeolites from fly ash and the properties of the zeolite products. *Journal of Geochemical Exploration,* 62**,** 305-309.

Stone, T. 2015. The Future of Coal. *Inside Mining,* 8**,** 8-9.

Tanaka, H., Fujii, A., Fujimoto, S. & Tanaka, Y. 2008. Microwave-Assisted Two-Step Process for the Synthesis of a Single-Phase Na-A Zeolite from Coal Fly Ash. *Advanced Powder Technology,* 19**,** 83-94.

Tanaka, H., Matsumura, S., Furusawa, S. & Hino, R. 2003. Conversion of coal fly ash to Na-X zeolites. *Journal of Materials Science Letters,* 22**,** 323-325.

Treacy, M. M. & Higgins, J. B. 2007. *Collection of simulated XRD powder patterns for zeolites fourth (4th) revised edition,* Amsterdam, Elsevier.

Ugurlu, A. 2004. Leaching characteristics of fly ash. *Environmental Geology,* 46**,** 890-895.

Ukwattage, N. L., Ranjith, P. G. & Bouazza, M. 2013. The use of coal combustion fly ash as a soil amendment in agricultural lands (with comments on its potential to improve food security and sequester carbon). *Fuel,* 109**,** 400-408.

Vassilev, S., Menendez, R., Alvarez, D., Diaz-Somoano, M. & Martinez-Tarazona, M. R. 2003. Phase-mineral and chemical composition of coal fly ashes as a basis for their multicomponent utilization. 1. Characterization of feed coals and fly ashes⋆. *Fuel,* 82**,** 1793-1811.

Vassilev, S. V. & Vassileva, C. G. 1997. Geochemistry of coals, coal ashes and combustion wastes from coal-fired power stations. *Fuel Processing Technology,* 51**,** 19-45.

Vassilev, S. V. & Vassileva, C. G. 2005. Methods for Characterization of Composition of Fly Ashes from Coal-Fired Power Stations: A Critical Overview. *Energy & Fuels,* 19**,** 1084-1098.

Vassilev, S. V. & Vassileva, C. G. 2007. A new approach for the classification of coal fly ashes based on their origin, composition, properties, and behaviour. *Fuel,* 86**,** 1490-1512.

Volli, V. & Purkait, M. K. 2015. Selective Preparation of Zeolite X and A from Flyash and its use as Catalyst for Biodiesel Production. *Journal of Hazardous Materials,* 297**,** 101-111.

Wadge, A. & Hutton, M. 1987. The leachability and chemical speciation of selected trace elements in fly ash from coal combustion and refuse incineration. *Environmental Pollution,* 48**,** 85-99.

Wang, Y., Lin, F. & Pang, W. 2008. Ion exchange of ammonium in natural and synthesized zeolites. *Journal of hazardous materials,* 160**,** 371-5.

Wang, Y., Ren, D. & Zhao, F. 1999. Comparative leaching experiments for trace elements in raw coal, laboratory ash, fly ash and bottom ash. *International Journal of Coal Geology,* 40**,** 103-108.

Wdowin, M., Franus, M., Panek, R., Badura, L. & Franus, W. 2014. The conversion technology of fly ash into zeolites. *Clean Technologies and Environmental Policy,* 16**,** 1217-1223.

Windom, B. C. & Hahn, D. W. 2009. Laser ablation—laser induced breakdown spectroscopy (LA-LIBS): A means for overcoming matrix effects leading to improved analyte response. *Journal of Analytical Atomic Spectrometry,* 24**,** 1665-1675.

Xiang, W., Han, B., Zhou, D. & Nzihou, A. 2012. Physicochemical properties and heavy metals leachability of fly ash from coal-fired power plant. *International Journal of Mining Science and Technology,* 22**,** 405-409.

Xu, R., Pang, W., Yu, J., Huo, Q. & Chen, J. 2007. *Chemistry of zeolites and related porous materials: synthesis and structure,* Singapore, John Wiley & Sons.

Yao, Z. T., Ji, X. S., Sarker, P. K., Tang, J. H., Ge, L. Q., Xia, M. S. & Xi, Y. Q. 2015. A comprehensive review on the applications of coal fly ash. *Earth-Science Reviews* 141**,** 105-121.

Zhao, X. S., Lu, G. Q. & Zhu, H. Y. 1997. Effects of Ageing and Seeding on the Formation of Zeolite Y from Coal Fly Ash. *Journal of Porous Materials,* 4**,** 245-251.

Zou, L., Ding, H., Zheng, L., He, M. & Xu, Q. 2015. Synthesis of A Single-Phase Superfine Na-Y Zeolite from Coal Fly Ash. *2015 International Conference on Materials, Environmental and Biological Engineering.* Atlantis Press.